Laser Cooling and Spectroscopy of Magnetically Trapped Atoms

by

Kristian Helmerson

B.S., University of Washington, Seattle

(1984)

Submitted to the Department of Physics in

partial fulfillment of the requirements for the degree of

DOCTOR OF PHILOSOPHY

at the

MASSACHUSETTS INSTITUTE OF TECHNOLOGY

January, 1991

Signature of Author _____
Department of Physics

Certified by _____
Thesis Supervisor

Accepted by _____
Chairman, Departmental
Committee on Graduate Studies

Laser Cooling and Spectroscopy of Magnetically Trapped Atoms

by

Kristian Helmerson

Submitted to the Department of Physics
in January of 1991 in partial fulfillment
of the requirements for the degree of
Doctor of Philosophy

Abstract

Radio frequency and laser spectroscopy was performed on neutral Na atoms confined in a magnetic trap. Both laser fluorescence and absorption spectra were obtained. The temperature and number of trapped atoms was extracted from a fit of the absorption spectrum. A resonance curve of an rf transition between two trapped magnetic substates was obtained. The rf lineshape was used to determine the energy distribution of the trapped atoms.

Laser Doppler cooling of the trapped atoms was performed. A substantial narrowing of both the rf resonance and absorption lineshape was observed following the application of Doppler cooling to the trapped atoms. These showed that the trapped atoms had been cooled to 3 ±1 milliKelvin.

Thesis Supervisor: Dr. David E. Pritchard

Title: Professor of Physics

To my parents

John and Yoko Helmerson

TABLE OF CONTENTS

Chapter I

Introduction

The field of neutral atom trapping has grown remarkably during the past couple of years [PHM89 (see appendix A), JOS89]. Initially, the emphasis was on the development of new types of neutral atom traps and increasing the storage times and numbers of trapped atoms. As the field grew, the emphasis shifted from the demonstration of novel neutral atom trapping schemes to performing experiments with trapped neutral atoms. Motivated by the beautiful, precision experiments performed on trapped charged particles [IBW87, DEH90], considerable effort has been directed toward spectroscopy of trapped neutral atoms. The benefits to spectroscopy of long interaction times and reduced motional broadening associated with the confinement of cold particles has been demonstrated with trapped ions. However, with neutral atoms there is no coulomb interaction between the trapped particles, allowing higher densities with correspondingly better signal to noise. This makes neutral atom traps highly attractive as the ultimate tool in spectroscopy.

In addition to spectroscopy, the high densities and low temperatures achievable with trapped atoms is well suited in the search for quantum collective phenomena where the deBroglie wavelength of the trapped atom is comparable to the average spacing between particles. Magnetically confined atoms are being

used in the search for Bose-Einstein condensation [HKD87] and their use has been proposed for the observation of novel radiative manifestations of a degenerate Fermi gas [KSS88, HXP90 (appendix C)].

1.1 THE MAGNETIC TRAP – WHY USE ONE?

Trapping of neutral atoms was first observed in a magnetic trap by the group at NIST (formerly NBS) in Gaithersburg [MPP85]. A spherical quadrupole magnetic field configuration was used to create an absolute minimum of the magnetic field in which "weak field seeking" (a state whose energy increases with increasing field) neutral sodium atoms were confined. The following year, the first light trap for neutral atoms was demonstrated [CBA86], in which the coupling of the induced electric dipole moment of an atom to the electro-magnetic field was used to confine neutral Na atoms at the focus of a laser beam. Subsequent years witnessed the first demonstration of a spontaneous light force trap [RPC87]; and the development of two superconducting magnetic traps [BLM87, HKD87], capable of trapping large numbers of atoms (Na and H atoms respectively) for unprecedented confinement times. Since then, interest in neutral atom traps has exploded, with the emphasis shifting toward the application of traps for other experiments. Many groups are actively pursuing research utilizing neutral atoms traps [GLJ88, KRC89, CPB90, MSR90, SST89].

By far, the most popular neutral atom trap is the spontaneous force light trap, which utilize the net momentum transfer from

resonant scattering of laser light to confine atoms. They are relatively compact, simple and cheap to construct, and are easy to use [MSR90]. However, their direct use in precision spectroscopy appears to be extremely limited.

In all neutral atom traps, the coupling of the rather intense electro-magnetic fields to the atoms, required for confinement, can strongly perturb the properties of the atom that one wishes to study. With light traps, the dynamical character of atom-radiation interaction tends to make the influence of the confining potential on the atom difficult to understand. The formation of complicated filamentary structures within the trapped atom cloud has been observed in a spontaneous force light trap [RPC87,WSW90] and to date, remains not completely understood.

An alternative scheme for confining neutral atoms is to use the coupling of the atoms' magnetic moment to an applied magnetic field to "hold on" to the atom. By creating a magnetic field minimum in free space, spin polarized atoms in a state whose energy increases with magnetic field may be confined. The advantage of such a magnetic trap over that of a light trap for spectroscopy is two-fold. First, a magnetic trap is a static trap; that is, the trapped atoms are not in the presence of an intense radiation field which tends to produce a time-dependent mixture of ground and excited state atoms. Thus, although strongly perturbed by the confining magnetic field, the perturbations are well understood, making interpretation of spectra easier, and can sometimes be used to one's advantage

[PRI83]. Second, the entire sample of trapped atoms can be spin polarized, also simplifying the spectra.

1.2 EXPERIMENTS WITH TRAPPED ATOMS

Since the first demonstration of neutral atom trapping in 1985, a limited number of experiments have been performed utilizing trapped neutral atoms. Collisions of cold trapped atoms have been observed in light traps [CPB90, GLJ88, SWM89]. Evaporative cooling was demonstrated [MDS88] and the corresponding energy distributions were measured [DSM89] for Hydrogen confined in a magnetic trap. The ground state hyperfine splitting of cesium [SEW89] and sodium [KRC89] was observed using cold atoms from a spontaneous force light trap.

The experiments described in this thesis are important and unique in several respects. They are among the earliest, and in some cases the first, such experiments on trapped neutral atoms. They are the only resonance experiments on trapped neutral atoms. The techniques and analyses developed with neutral sodium atoms can be applied to other magnetically trapped species. All of the measurements in this thesis were performed on trapped atoms *in situ*, in contrast to most of the aforementioned experiments (the cold collision studies being the exception) in which the actual measurement was made on atoms outside of the trap. What follows is a brief overview of the experiments described in this thesis and their particular significance to the field of neutral atom trapping.

First, both laser fluorescence and absorption spectra of trapped atoms have been obtained. The absorption spectra presented are the first for trapped neutral atoms. Previous absorption measurements of trapped neutral atoms [RPC87] were conducted at a fixed laser frequency. The laser fluorescence and absorption measurements represent a non-destructive technique for probing trapped atoms and the information contained in the spectra can be used to obtain the temperature and number of trapped atoms.

The first rf spectroscopy of trapped neutral atoms [MHB88] was performed. In addition to being an important first step in the development of neutral atom traps as a spectroscopic tool, such experiments provide valuable information about the energy distribution of the trapped atoms. The demonstrated use of rf-induced transitions to selectively change the magnetic-sublevel population of trapped atoms, is also of importance in that its use has been proposed as part of a "cyclic" cooling scheme [PRI83], in a variation of evaporative cooling [PHM89 (see appendix A), HLS89], and in an "energy space optical pumping" scheme [PHB87 (see appendix B)], all of which should permit cooling of trapped neutral atoms to μK temperatures.

The success of neutral atom traps owes much to the development and realization of various cooling schemes for reducing the thermal energy of neutral atoms [PMP85, EBH85, CHB85]. Since the confining potentials of neutral atom traps are typically less than one kelvin deep, a substantial amount of the kinetic energy of the

atom must be removed before it can be confined. Once confined though, it is still desirable to cool the atoms even further. Both magnetic and Doppler broadening due to the motion of the atoms in the confining potential decrease as one decreases the kinetic energy of the atoms. This leads to correspondingly narrower linewidths in resonance measurements, thus making high resolution spectroscopy of the trapped atoms possible.

This thesis also describes the first laser Doppler cooling experiments on magnetically trapped atoms. A standing wave of light tuned below resonance was applied to the trapped atoms resulting in a damping of the motion of the atoms along the direction of laser beam. The motion orthogonal to the laser beam was coupled by the trap into the damped direction which reduced the total energy of the trapped atoms. A substantial narrowing of the rf and laser resonance lineshapes as well as an enhancement in the density of trapped atoms was observed following Doppler cooling of the atoms.

Although Doppler cooling of trapped atoms is designed into spontaneous force light traps, the experiments on atoms confined in a magnetic trap are unique in that many of the parameters such as laser detuning and power may be changed without affecting the character or performance of the trap.

1.3 OUTLINE OF THESIS

This thesis describes laser cooling and spectroscopy experiments performed on magnetically confined neutral sodium atoms. What follows is a chapter by chapter breakdown of the above mentioned experiments which form the main scope of this thesis.

Chapter 2 contains a review of some of the properties of the sodium atom, relevant to the understanding of the present work. It is followed by a brief description of the techniques and apparatus used for magnetic trapping of sodium atoms, including a description of the specific modifications and improvements made to the existing apparatus which permitted us to perform the experiments, described in this thesis.

In chapter 3, the laser fluorescence and absorption experiments are described. Experiments involving fluorescence measurements to determine the loss rate of atoms from the trap are presented. The fluorescence and absorption spectra obtained are then presented, followed by a general explanation of the lineshape in terms of the profile of the confining magnetic field along the axis of the trap.

A quantitative model of the fluorescence and absorption curves is constructed in chapter 4, using the measured values of the magnetic field on axis. A fit of this model to the actual data is then made, from which the temperature and number of trapped atoms are

extracted. An analysis of the contributions of the magnetic field off-axis to the laser spectra is also presented.

Experiments involving rf-induced transitions of trapped neutral atoms are described in chapter 5. The issue of saturation of the transition is considered and data addressing this question are presented. The two different methods used to obtain rf resonance curves for the trapped atoms are described and the lineshapes obtained from both methods are presented. A general description of the rf lineshape is then given in terms of a simple model containing a potential well.

In chapter 6, a model of the rf resonance lineshape is described which assumes saturation of the transition and a truncated Boltzmann distribution for the atoms in the trap. A fit of the model to the data is made from which we extract a temperature for the trapped atoms. This is followed by a description of a technique for extracting the energy distribution of the trapped atoms from the rf resonance curve.

A theoretical analysis of one-dimensional Doppler cooling of atoms in a trap in terms of a simple model is presented in chapter 7. The trap is assumed to couple the motion orthogonal to the cooling laser beam and cooling limits are given for various coupling times and detunings. The influence of the magnetic potential on the ultimate temperature achievable with Doppler cooling is also considered.

In chapter 8, the experiments on Doppler cooling of magnetically trapped atoms are described. Laser absorption spectra and an rf resonance curve of Doppler cooled atoms are presented. The dependence of the temperature of the Doppler cooled atoms on cooling laser power and application time are obtained from the resulting absorption spectra.

In addition, we include several appendices containing papers by the author of this thesis and co-workers, describing new ideas for experiments with magnetically trapped atoms. The papers in the appendices are prefaced by a brief description of their relevance to the experiments described in this thesis.

Chapter II

Experimental Set-up

The experiments described in this thesis were performed on neutral ^{23}Na atoms confined in a magnetic trap. The chapter begins with a brief description of the characteristics of the atom, the trap, and trapping process relevant to understanding of the experiments performed. This is followed by a description of the improvements and modifications of the trap and associated apparatus that enabled the experiments to be performed.

2.1 THE ATOM

Neutral sodium atoms were used in the experiments described in this thesis. The primary reason for using sodium was its strong $3S_{1/2} \rightarrow 3P_{3/2}$ (the D2 line) transitions at 589 nm. This is a particularly convenient wavelength for tunable dye lasers

The most important property of sodium for magnetic trapping experiments is the behavior of the various hyperfine levels in a magnetic field. Figure 2.1 is a plot of the relevant ground state $3S_{1/2}$, and excited state $3P_{3/2}$, hyperfine levels of sodium as a function of applied magnetic field. The experiments described in this thesis were conducted in magnetic fields between 1500 and 2300 Gauss.

The laser transition used for slowing and cooling the atoms was the $|F=2, M=2\rangle$ to $|F'=3, M'=3\rangle$ transition indicated in figure 2.1. By using circularly polarized light to excite a $\Delta M = +1$ transition, the

atom can be kept "cycling" between these two states since angular momentum conservation requires that the atom decay back to the $|F=2,\ M=2\rangle$ state, giving us effectively a "two level" atom.

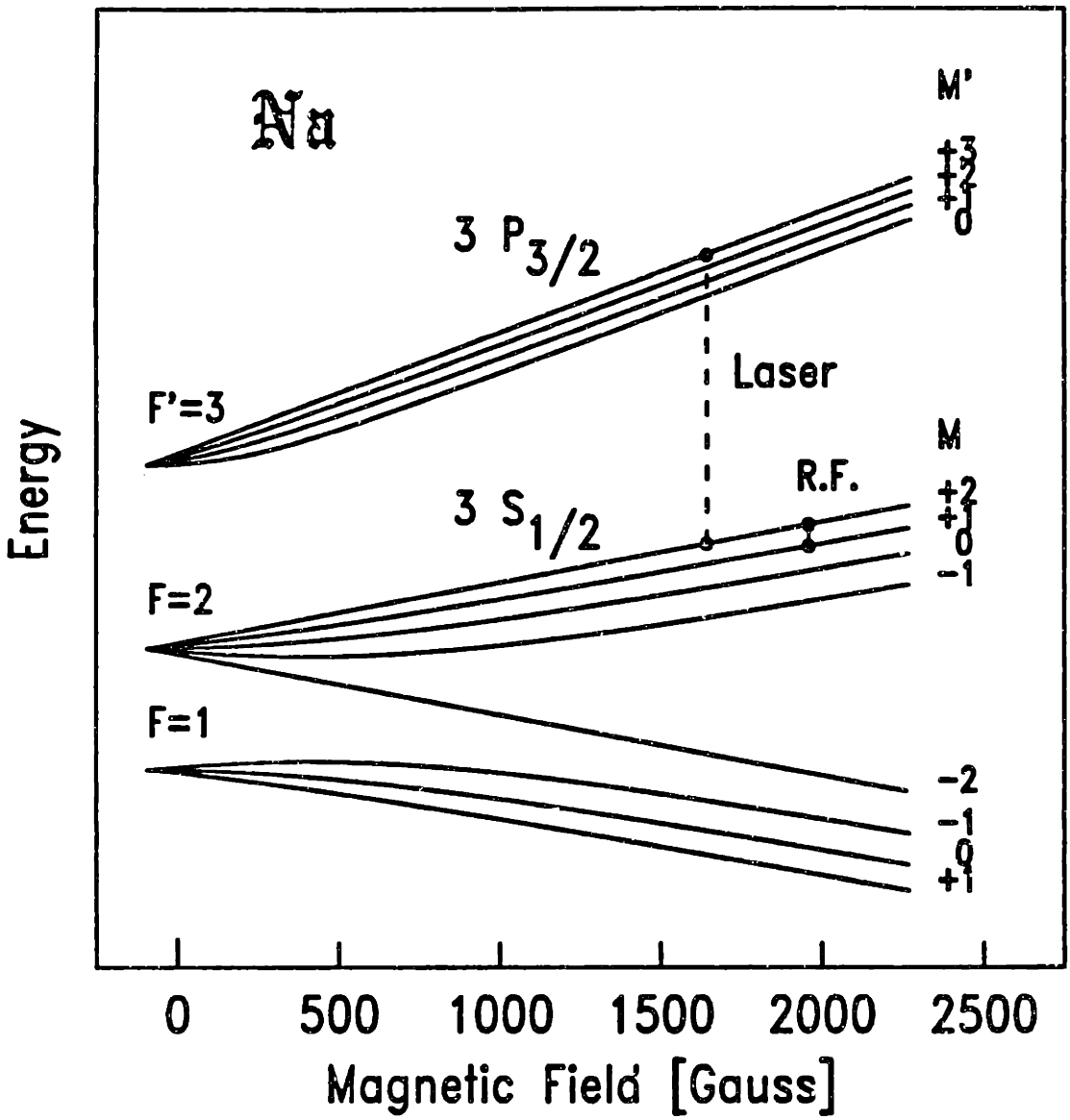

Figure 2.1: The relevant energy levels of Na $3S_{1/2}$ and $3P_{3/2}$ in a magnetic field (not to scale).

2.2 THE TRAP

Neutral sodium atoms were trapped in a magnetic field minimum via the coupling of their magnetic moment to the applied field. One can only create a magnetic field *minimum* in free space [WIN85], hence only atoms in a magnetic substate whose energy increases with magnetic field can be confined. For sodium, in a large magnetic field, this corresponds to the four magnetic substates $|F=2, M=2,1,0,-1\rangle$ shown in figure 2.1.

The trap used for this thesis work was a superconducting magnetic trap. It was constructed by Vanderlei Bagnato and co-workers, and much of the details of the construction and properties of the trap can be found in the thesis of Bagnato [BAG87].

Of particular relevance to us is the magnetic field profile of the trap. The total magnetic field along the axis of the entire apparatus is shown in figure 2.2. Typically, the currents in the magnetic trap's coils were of a value such that the minimum magnetic field in the trap was approximately 1500 gauss. This value was chosen to be large enough to Zeeman shift the trapped atoms out of resonance with the initial slowing laser which also passes through the magnetic field minimum. Radial confinement of the atoms was provided by an octopole magnet. The radial field formed by the octopole has a ρ^3 dependence which, when added in quadrature with the 1500 gauss bias field, tends to create a radial potential that has a ρ^6 dependence. The trap extends approximately 2.5 cm in the radial direction where

the magnetic field value, measured with respect to the value at the minimum, is ~850 gauss, this corresponds to a potential well depth of ~60 mK. In the longitudinal direction, the trapping potential extends about 33 cm (figure 2.3), thus the entire trapping volume is approximately 650 cm^3.

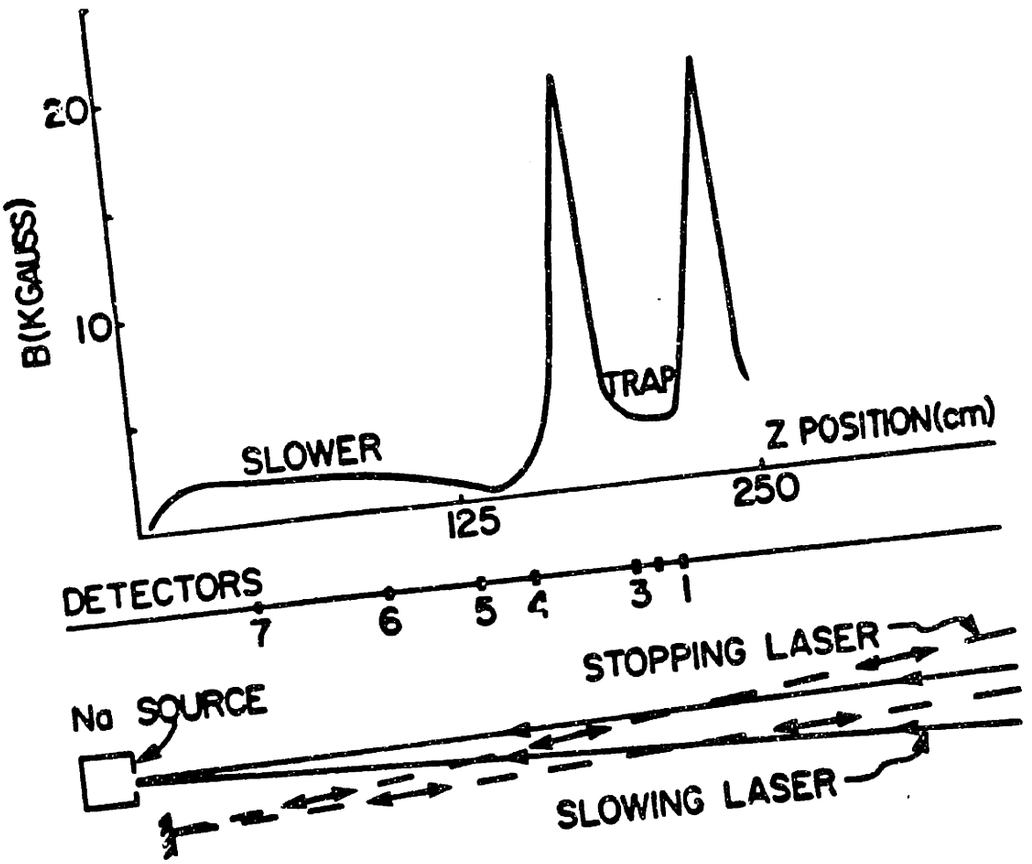

Figure 2.2: Relative longitudinal geometry of the lasers, detectors, and sodium source with respect to the axial magnetic field profile of the magnetic trap.

2.3 THE PROCESS OF LOADING THE TRAP

A thermal beam of neutral ^{23}Na atoms produced from an effusive source (typically at 550° C) is slowed down by scattering photons from a counter-propagating, travelling wave laser beam. The laser beam was circularly polarized and slightly detuned from the $3S_{1/2}(F=2, M=2)$ to $3P_{3/2}(F'=3, M'=3)$ transition in sodium. As the atoms are slowed, they are kept in resonance with the laser light by a tapered "slower" magnet (Fig. 2.2), i.e. a spatially varying magnetic field of appropriate geometry such that the resulting Zeeman shift compensates for the changing Molasses shift in the resonant frequency of the slowing atom; a technique originally conceived and demonstrated by Phillips, et.al. [PMP85]. Details of the slowing process can be found in the article by Bagnato, et.al. [BLM89].

The slowed atoms then enter a region of space containing a local magnetic field minimum formed by two axial "pinch" coils (Helmholtz's coils) for confinement in the axial direction, and an octopole field for confinement in the radial direction. Once inside this magnetic potential, the sodium atoms are brought to rest at the minimum of the magnetic field by a second laser beam (of appropriate polarization to excite the "cycling" transition) in conjunction with a second, smaller, slower magnetic field. The process of slowing and stopping the atoms to load the magnetic trap leaves the trapped atoms in the ground state $| F=2, M=2 \rangle$ magnetic substate. The second laser beam (the stopping laser), is retro-reflected back on itself to form a standing wave of light. This was

done with the intention that, tuned below resonance, the standing wave field would provide damping for the trapped atoms in the form of one-dimensional "optical molasses" [CHB85].

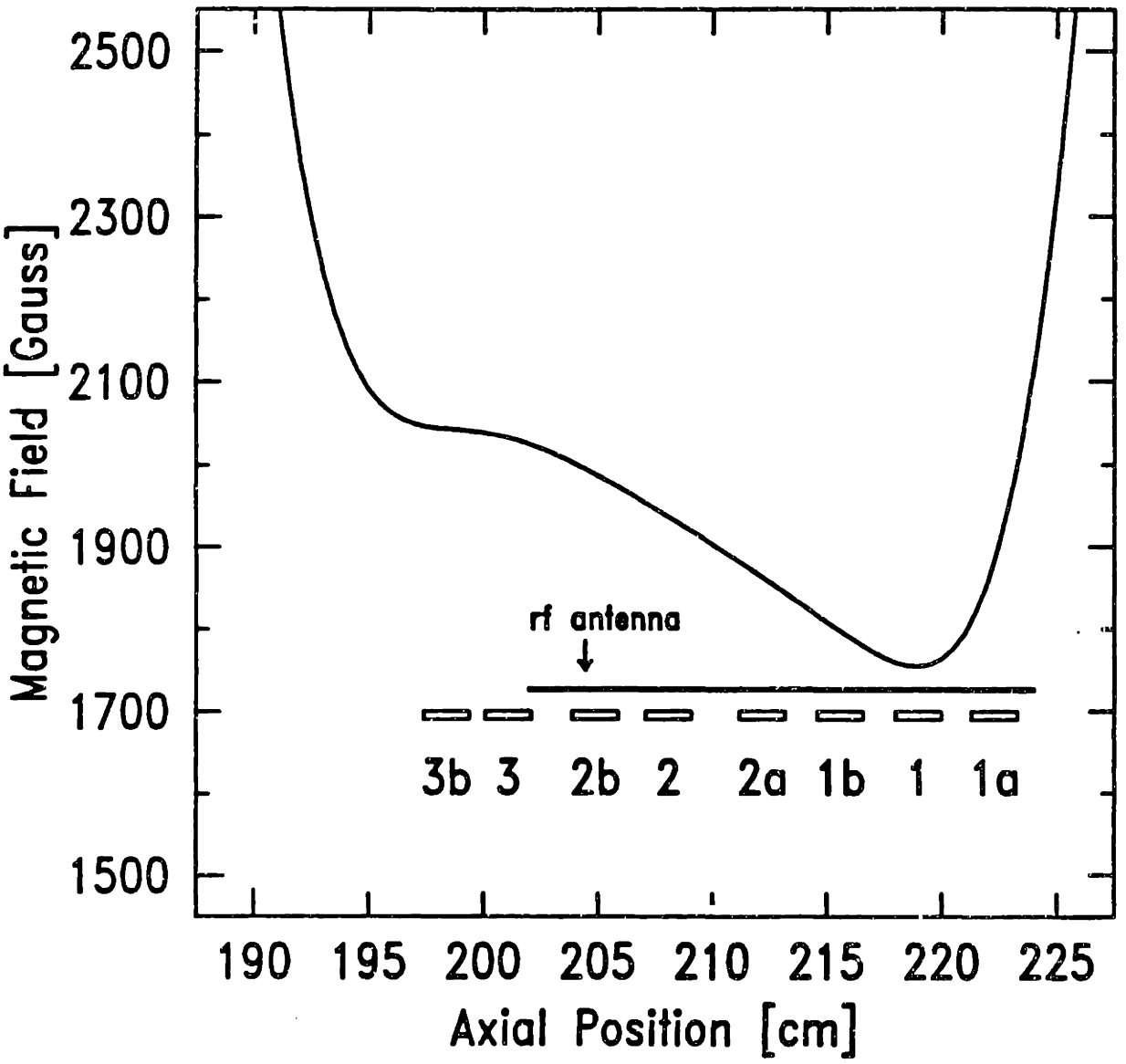

Figure 2.3: Axial magnetic field profile of the trap region. The relative axial positions of the rf antenna and various photodetectors with respect to the magnetic field profile are shown.

2.4 IMPROVEMENTS IN THE APPARATUS

Many modifications and improvements were made to the original apparatus described in the thesis of Bagnato [BAG87]. By far the most substantial modifications were in signal detection, and are as follows.

Fluorescence from the trapped atoms were detected using PIN silicon photodiodes mounted on the inside wall of the cryostat. The detectors were located longitudinally at several positions in the trap area, so that we would have limited spatial resolution of the fluorescence from the trapped atoms. Figure 2.3 indicates the positions of the detectors relative to the magnetic field. The signal from the photodiodes were carried up along wires, through a vacuum feedthrough, and into current-to-voltage amplifiers. Three changes were made to the original set-up used by Bagnato in first detecting trapped atoms.

Low noise and low drift, high gain amplifiers were constructed to convert the photodiode currents into a voltages. The first stage of these amplifiers was a high gain-bandwidth operational amplifier (op-128) configured as a current to voltage converter with feedback resistors from 100 to 600 megohms. The second stage was an instrumentation amplifier. Care was taken to minimize drift and noise pick-up by floating the input.

When it became clear that the amplifier was no longer the source of the noise in our data, we replaced the wires to the

photodiodes by low temperature coaxial cable (RMC Cryosystems, type "C1"). The signals we were looking at were basically DC (< 30 Hz), making us sensitive to acoustic noise transmitted by the cryostat and picked up by the wires moving in the large magnetic fields of the trap. The use of the coaxial cable reduced the noise by about a factor of 3.

The final improvement was to boost the signal at the source. This was done by covering as much of the inner wall of the dewar with photodiodes to increase the amount of light collected. We mounted nine UDT S200V silicon photodiodes, electrically in parallel, in a ring around each of the positions along the z-axis indicated in figure 2.3. Each photodiode measured 20mm × 10mm, resulting in 18 cm^3 of light collection area or ~1/5 of the entire solid angle. The silicon photodiodes seemed to function without any problem at 4.2K, and the only precaution necessary was in mechanically fixing the photodiodes without them breaking under thermal contraction. This was accomplished by suspending the photodiodes from the wires used to electrically hook them up in parallel.

The improvements in the light detection system and associated electronics totaled to a factor of ~100 increase in the signal to noise compared to the signals obtained previously, when trapping was first demonstrated in the apparatus.

In addition to improving the photodetection system, an antenna was added to the trap (Fig. 2.3) to transmit rf radiation to the trapped atoms. The antenna was an ~40 cm-long, shorted, two-

wire transmission line, located approximately 0.3 cm from the wall of the trap. The frequencies used in the rf spectroscopy experiments ranged from ~300 to 500 MHz, corresponding to wavelengths of ~100 to 60 cm. Since the antenna was located ~2.5 cm from the trapped atoms, the atoms were located in the near field of the rf radiation. The geometry of the antennae loop was chosen to provide the trapped atoms with an oscillating magnetic field in the plane perpendicular to the large bias field of the trap, enabling us to induce magnetic dipole transitions of the trapped atoms.. The rf signal was generated by a Fluke model 6060A frequency synthesizer followed by a 3 Watt, linear rf amplifier (ENI model 603L). The rf signal was fed to the antenna via 50 Ω, low temperature coaxial cable (RMC Cryosystems, type C).

The data acquisition system was also improved, allowing computer control via a CAMAC interface. The amplified voltage from the trapped atom signal was sent to voltage to frequency converters. The output of the voltage to frequency converters was sent to a 6 channel scaler module in the CAMAC crate. A digital to analog module in the CAMAC crate enabled us to sweep the probe laser frequency as a function of time. A CAMAC 16-bit relay module enabled us to insert neutral density filters, or shutter the lasers at a predetermined time. The Fluke synthesizer was controlled via a CAMAC GPIB interface, which allowed us computer control of the rf frequency, power and duration.

A final important modification of the experimental apparatus was to make the Helium dewar airtight to allow us to pump on the liquid helium, thereby lowering the temperature of the cryopumping surfaces in the trap to below 4.2K. The resulting improvement in the vacuum enabled us to obtain trapping times in excess of 30 minutes. A roughing pump was used to reduce the pressure in the liquid helium resevoir to less than 50 torr. The pressure was monitored by a mechanical vacuum gauge.

Chapter III

Absorption/Fluorescence Experiments

Laser absorption and fluorescence spectra have been obtained from magnetically trapped neutral sodium atoms. The absorption spectra are the first for trapped neutral atoms. A substantial broadening of the lineshape due to the confining magnetic field was observed in both the fluorescence and absorption spectra. The lineshape of the absorption spectrum can be interpreted in terms of the magnetic field profile along the axis of the trap. In addition, fluorescence measurements were used to monitor the decrease in the number of trapped atoms as a function of time.

3.1 FLUORESCENCE

Fluorescence spectra of trapped sodium atoms were obtained in the following manner. A sample of atoms was loaded into the trap using the technique described in the previous chapter. The loading lasers and atomic beam were then blocked. After a variable time delay (typically 15 seconds), the probe laser is applied to the trapped atoms and scanned through resonance (typically 2 GHz in 20 seconds). The number of photons scattered (fluorescence) by the trapped atoms was recorded as a function of laser detuning. Figure 3.1 shows a typical fluorescence spectrum from detector 1 (see figure 2.3) of trapped atoms just after loading the trap. The spectrum was taken with an ~5 μW (~1 cm diameter) probe beam, scanned from low to high frequency over a range of 2 GHz in 30 seconds.

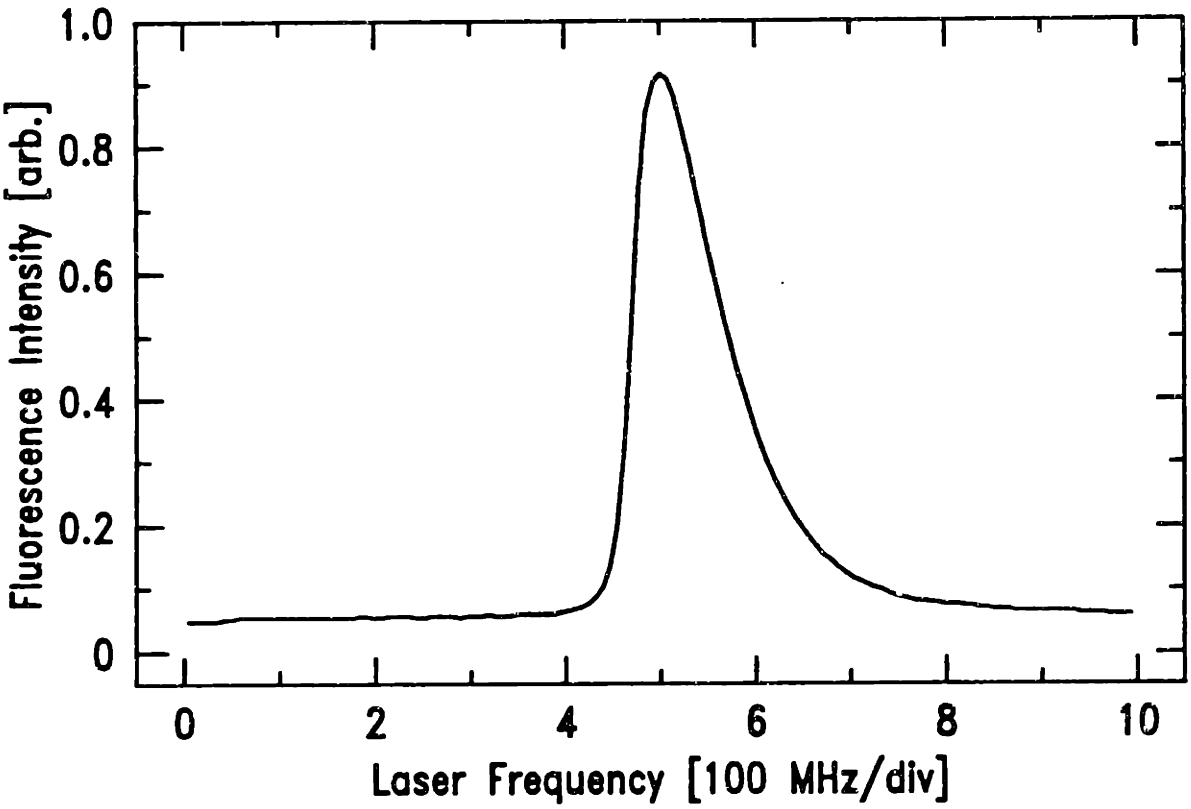

Figure 3.1: Typical laser fluorescence spectrum of trapped neutral atoms from the detector located at the minimum of the trap.

A. Confinement Time Measurements

Measurements were made of the trapping time, (i.e. how long the atoms stayed in the trap), routinely at the beginning of a run. This was accomplished by monitoring the height of the fluorescence signal as a function of time. Since the fluorescence signal is proportional to the number of trapped atoms, the decay rate of this signal is equal to the decay rate for atoms in the trap. To avoid spurious heating or optical pumping effects, the probe laser was attenuated until no noticeable change in the decay rate of the signal could be observed.

In practice, the frequency of the laser was scanned over the trapped atom resonance, rather than being kept fixed at the peak of fluorescence. This was done in order to avoid the effects of any drift of the laser frequency during the time in which measurements were made. In figure 3.2 we clearly see the decay of the height of the fluorescence peak observed by detector 1, as a function of time as the probe laser was repetitively swept over the trapped atoms resonance (with a period of ~9 seconds). The small secondary peak in the spectrum is due to the fly-back of the laser frequency over the trapped atom resonance before the next sweep. A fit of an exponential function of time to the peaks heights of the fluorescence spectra (dashed line in figure 3.2) indicates a 1/e trapping time of ~33 seconds. The exponential decay of the number of atoms with time implies that the loss rate is proportional to the number of trapped atoms. This suggests that the primary loss mechanism for

the trapped atoms is a collision between a trapped sodium atom and a background atom.

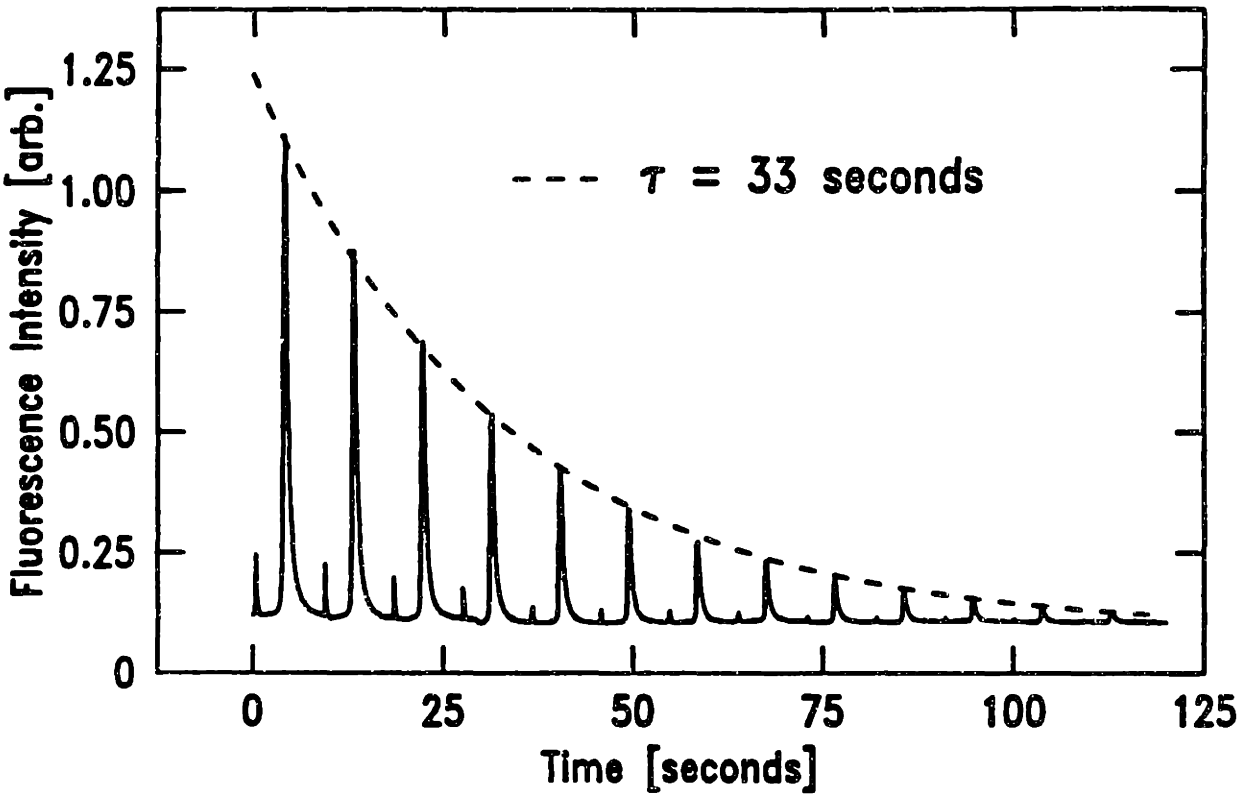

Figure 3.2: Repetitive fluorescence scan of trapped atoms (taken with the detector at the minimum of the trap) illustrating the decay of the number of trapped atoms with time. A fit of the decay to an exponential (dashed line) yields a decay time of ~33 seconds.

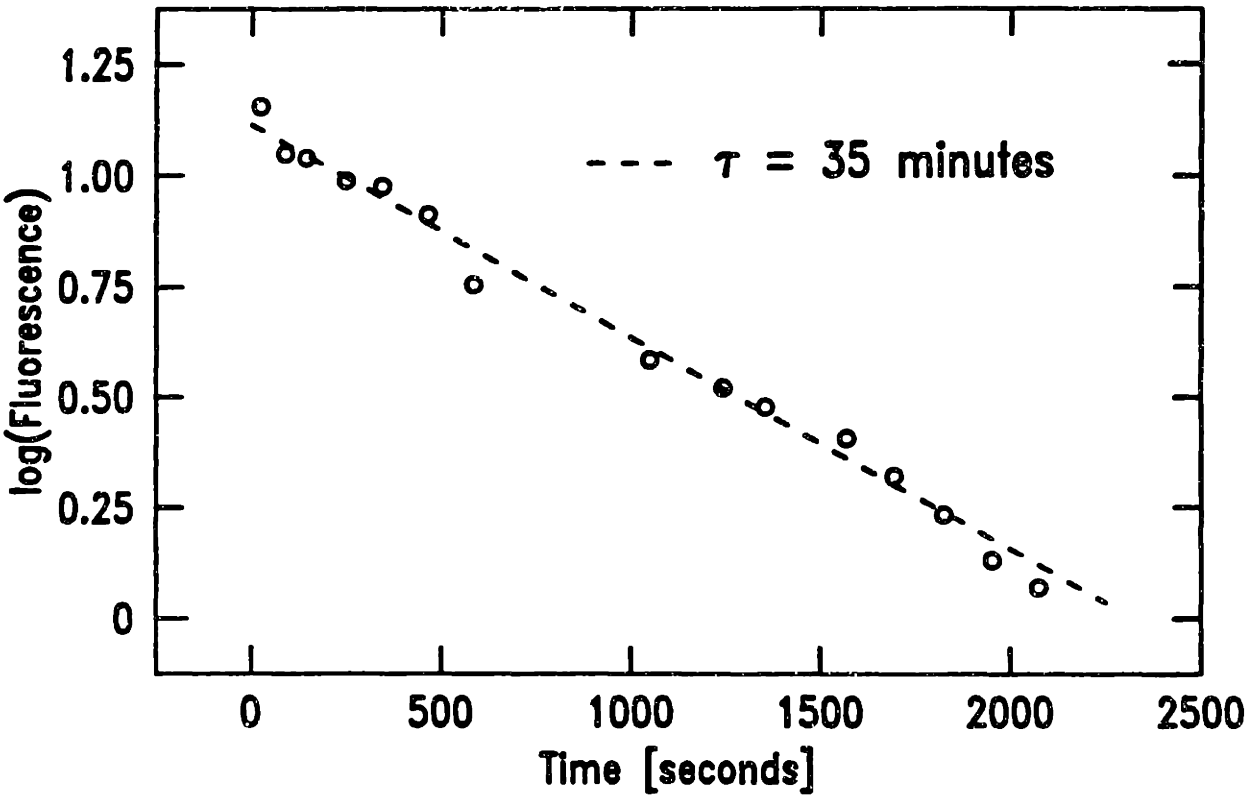

Figure 3.3: Log plot of the peak of fluorescence of trapped atoms (at the minimum of the trap) as a function of time illustrating the greatly improved trapping times achieved after pumping on the liquid He reservoir. The dashed line corresponds to an exponential decay with a decay time of ~35 minutes.

To improve the trapping time, we pumped on the liquid helium reservoir of the superconducting magnets to lower the temperature of the He bath. Below 4.2K (the boiling point of liquid He), we expect the vacuum to improve as the colder surfaces pump the residual background. The liquid helium was pumped down to ~75 torr (corresponding to a temperature of ~1.7 K) and a substantial improvement in the lifetime of the trapped atoms was observed. Figure 3.3 is a plot of the logarithm of the peak of the fluorescence spectrum of trapped atoms taken at successive times after pumping on the liquid helium reservoir. The straight line fit (dashed line in figure 3.3) indicates a 1/e trapping time of ~35 minutes. The loss of atoms from the trap is still characterized by an exponential decay. As a 30 minute trapping time was sufficient for our experiments, no attempt was made to further improve the vacuum.

B. Fluorescence Spectra at the Various Detectors

Fluorescence from the trapped atoms was also monitored on other detectors located in the trap region. Figure 3.4 is a series of four simultaneous fluorescence spectra from trapped atoms, as seen by detectors 1, 1b, 2a, and 2 (see figure 2.3). The fluorescence lineshape obtained by each detector is basically determined by the finite field of view of each detector with respect to the magnetic field profile on axis.

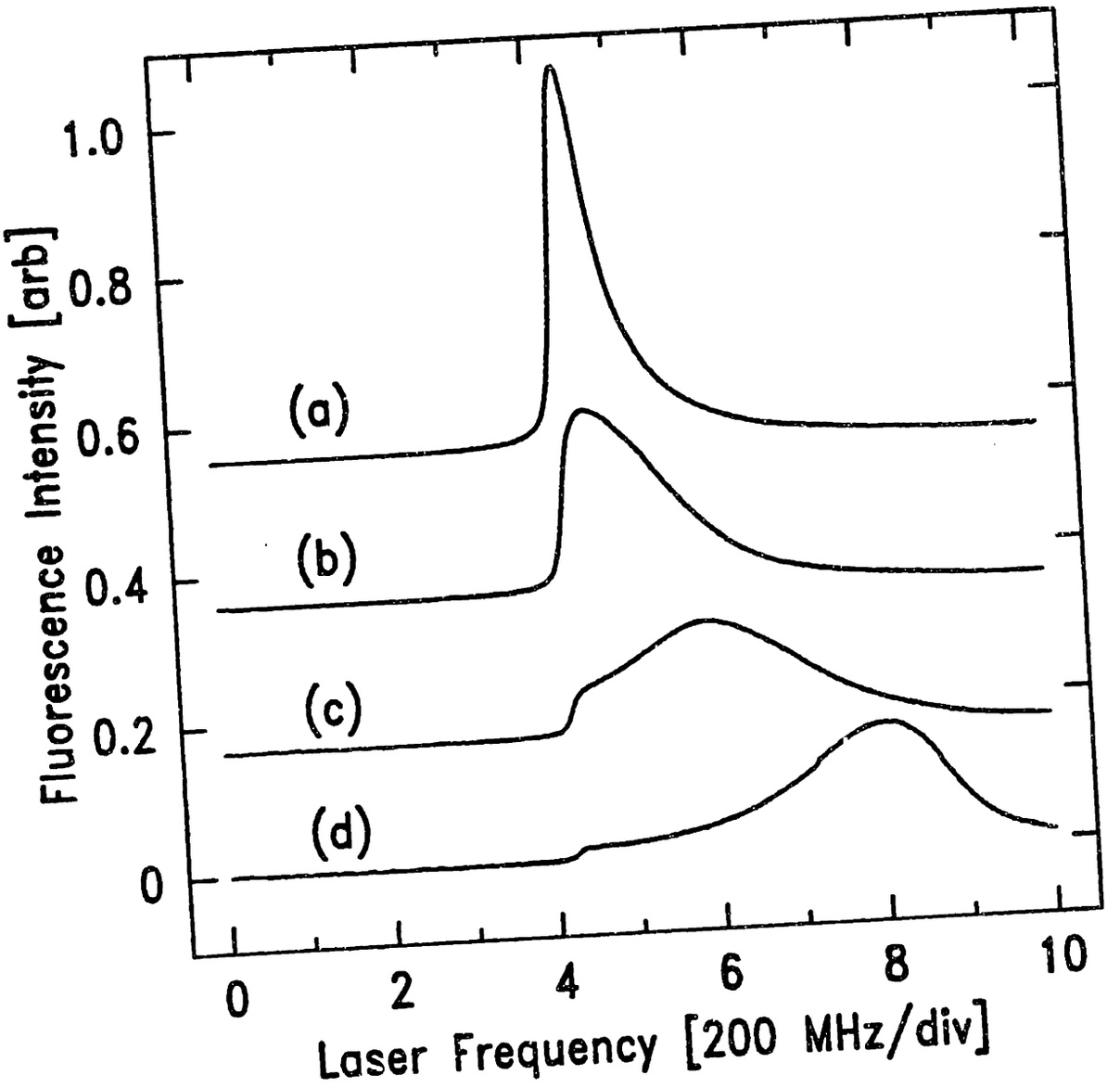

Figure 3.4: Simultaneous fluorescence spectra of trapped atoms from four detectors located at different positions in the trap. Scans (a), (b), (c), and (d) were taken with detectors 1, 1b, 2a, and 2 respectively (see figure 2.3).

Initially, the laser frequency is well below the minimum resonant frequency of the trapped atoms and the fluorescence signal obtained is essentially zero. As the probe laser comes into resonance with the trapped atoms at the minimum magnetic field of the trap, there is a rapid increase in fluorescence and we observe a peak in the fluorescence spectrum obtained with detector 1, since this detector is located at an axial position corresponding to the minimum of the trap (see figure 2.3). As the laser frequency is further increased, we come into resonance with atoms located at higher values of the magnetic field. Consequently, we observe the peak of the fluorescence spectrum from detectors 1b, 2a, and 2 [figure 3.4(b), (c), and (d), respectively] at respectively higher frequencies as these detectors are located at an axial position corresponding to higher magnetic fields, respectively.

The width of the fluorescence spectrum is determined by the variation of the magnetic field (dB/dz) within the field of view of each photodetector. Due to the frequency response of the transition, only those atoms at a magnetic field such that their resonant frequency is within a natural linewidth of the laser frequency tend to be excited. The finite field of view of the photodetector limits the spatial region from which fluorescence from the trapped atoms can be collected. Therefore we expect narrower and higher peaks when dB/dz is small. This is evident in figure 3.4 where the narrowest and tallest peak corresponds to detector 1 which is located at the magnetic field minimum where dB/dz = 0. Conversely, from figure

2.3 we see that detector 2a and 2 are located at a position where there is a fairly large variation of the magnetic field over the spatial extent of the detector, hence the fluorescence peaks obtained by these detectors are broader and lower.

The area of the fluorescence spectrum is determined by the number of atoms within the field of view of the photodetector which in turn is determined by the energy distribution of the atoms. Since the value of the magnetic field accessible by the trapped atom is determined by its energy, the area of the fluorescence lineshape obtained from detectors located at high values of the magnetic field will tend to decrease as the temperature of the distribution decreases, and there are fewer atoms with sufficient energy to reach the values of magnetic field in front of these detectors. The area of the fluorescence spectra from detectors 1, 1b, 2a, and 2 [figures 3.4 (a), (b), (c), and (d)] are approximately the same. From figure 2.3, we see that the location of these detectors spans an ~200 Gauss variation of the magnetic trap potential which corresponds to ~14 mK. Thus, the temperature of the trapped atoms appears to be higher than 14 mK.

The amount of fluorescence from atoms at the position corresponding to the minimum magnetic field seen by the other photodetectors is reduced due to their finite field of view. This is evident in figure 3.4 where the height of the rapid increase in the fluorescence signal decreases as a function of the increasing distance of the photodetector from the minimum of the trap. However,

despite being ~11 cm away from the trap minimum, detector 2 can still see fluorescence from atoms located at the bottom of the trap potential.

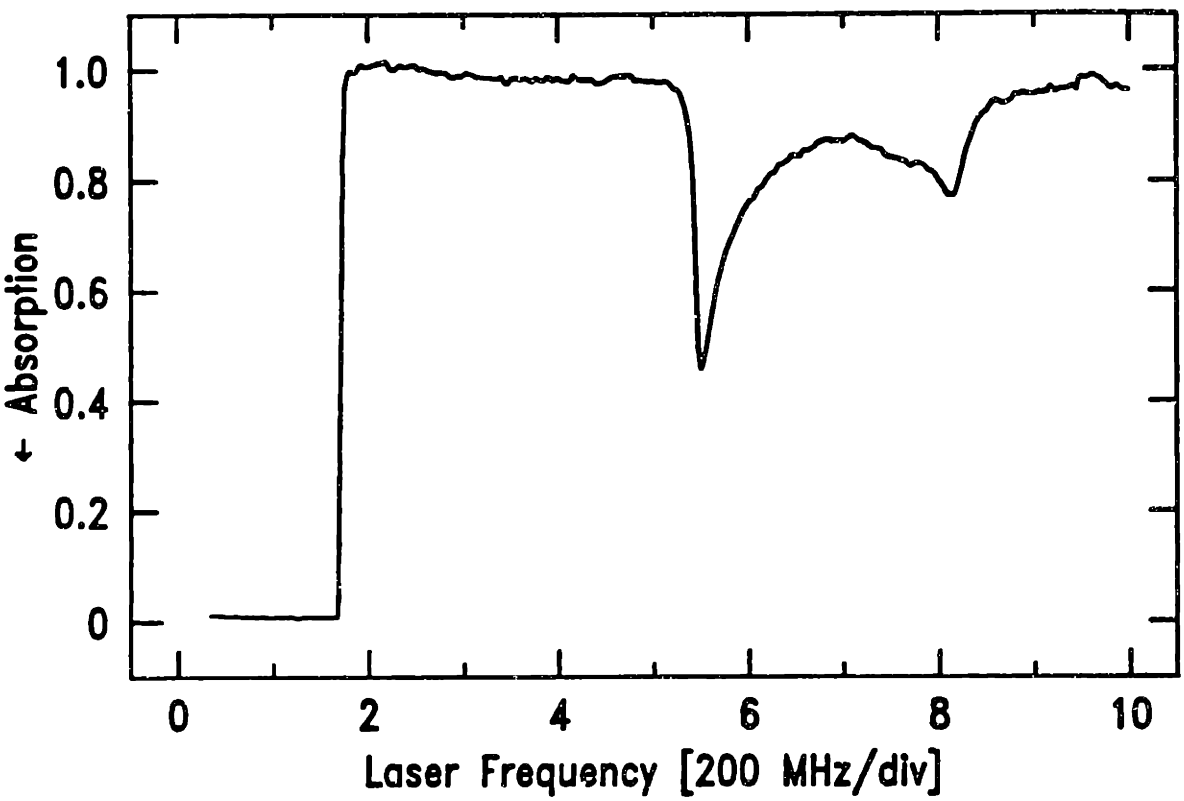

Figure 3.5: Simultaneous absorption spectrum of trapped atoms corresponding to the scan of figure 3.1. The zero intensity baseline at the beginning of the scan implies >50% absorption of the probe beam passing (twice) through the sample of trapped atoms.

3.2 ABSORPTION

Simultaneous absorption spectra of the trapped atoms were recorded for many of the fluorescence scans. The general procedure for recording these spectra was to block the laser at the beginning of the scan so that a zero intensity base line could be established, and then open the shutter allowing the weak probe beam to interact with the trapped atoms while the frequency was swept. In addition, the laser power was recorded during the scan so that any fluctuations in the intensity of the laser could be divided out later. Figure 3.5 is a typical absorption spectrum obtained from trapped atoms. From the zero intensity baseline, we see that there is ~55% absorption of the laser as it passes through the sample of trapped atoms. Since the recorded absorption spectrum is for two passes of the probe laser through the trapped atom cloud, an ~55% measured absorption implies an ~33% single pass absorption of the laser beam

The general shape of the absorption spectrum can be understood by considering the magnetic field profile along the axis of the trap and the distribution in energy of atoms in the trap. Figure 3.6, is a schematic representation of the magnetic field, or correspondingly the potential energy (since $U=\mu B$), along the axis (z direction) of the magnetic trap and the resulting absorption profile. The number of atoms with energy between E and $E+\Delta E$ is qualitatively represented by the density of dots in the trap in the interval between B and $B+\Delta B$, where $\Delta B=\Delta E/\mu$. The Lorentzian absorption profile of the transition that we are exciting selects, at the

laser frequency ω, to within the natural linewidth of the transition Γ, those atoms located at a magnetic field between B and $B+\Delta B$, where $B=\hbar\omega/\mu$ and $\Delta B=\hbar\Gamma/\mu$. The total number of atoms that will absorb photons from a laser beam at a frequency ω, is given by the number of atoms in the trap, in the region between z and $z+\Delta z$ (the region between the dashed lines in the magnetic potential of figure 3.6) where Δz is determined by $\partial B/\partial z$ at B(z). Thus we can explain the general features of the absorption spectrum as follows:

A. The sharp front edge of the absorption curve reflects the fact that below the minimum value of the magnetic field, there are no atoms available and hence no absorption.

B. We expect to see the greatest amount of absorption where $\partial B/\partial z$ is small, since $\Delta z=[\partial B/\partial z]^{-1}\Delta B$. This is well reflected by the two dips in the corresponding absorption spectrum of figure 3.6 and the actual spectrum in figure 3.5. The first and deepest dip is at a frequency which corresponds to atoms resonant at the minimum magnetic field. Since this is a local magnetic field minimum, we necessarily have $\partial B/\partial z=0$. The second dip is at a frequency which corresponds to atoms at the top of the "second slower" field in the trap (Fig. 2.3). In this region, $\partial B/\partial z\approx 0$ and there is enhanced absorption of the probe laser. The observation that there is less absorption at this frequency then at the frequency corresponding to the minimum of the trap, despite that B is flat for a longer region Δz, at the top of the second slower, is due to the energy

distribution of the trapped atoms; i.e. there are fewer atoms with sufficient energy to reach this value of the magnetic field compared to the total number of atoms, all of which can access the minimum of the trap.

C The limited extent in frequency of the absorption spectrum (~1100 MHz) reflects the finite depth of the magnetic trap (~800 Gauss).

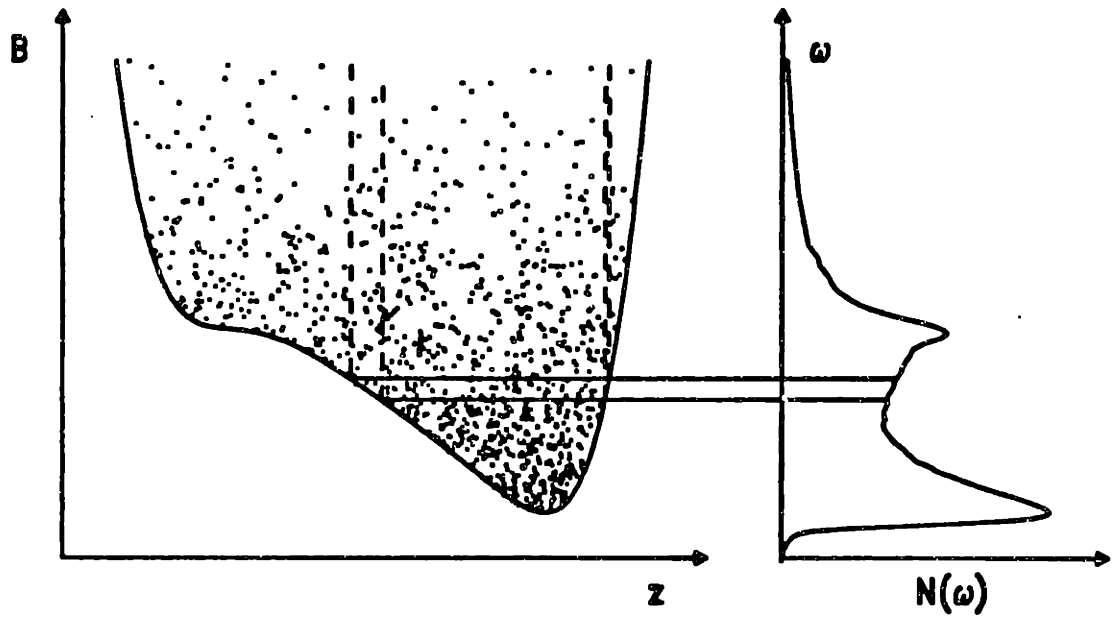

Figure 3.6: Plot of the axial magnetic field profile and the resulting absorption lineshape. The energy distribution of atoms is represented by the density of dots in the trap. The amount of absorption between ω and $\omega+\Delta\omega$ is detemined by the number of atoms resonant with the laser in this frequency interval, and is represented by the region between the dashed lines.

The qualitative agreement between the absorption spectrum obtained with magnetically trapped atoms (figure 3.5) and the lineshape predicted from the simple model based on only the axial magnetic field profile, suggests that the density of states in the radial direction is constant over the diameter of the probe laser; justification for this assumption will be deferred until chapter 4, where we construct a quantitative model for the absorption spectrum.

Simple Estimate of the Number of Trapped Atoms

A quick estimate of the total number of trapped atoms can be obtained from the absorption spectrum of figure 3.5. We approximate the absorption profile of figure 3.5 by a square profile with an average absorption α, and a width equal to the frequency span between the two dips (~525 MHz) in the absorption spectrum. The fraction of the laser intensity absorbed by the trapped atoms α, is given by $1 - \exp(-2\sigma nL)$. Where 2L is the total path length of the probe laser through the sample (the factor of 2 results from the retro-reflected beam), σ is the optical absorption cross-section, and n is the density of atoms. The trap volume is approximately $\pi\rho^2 L$, where ρ=2.5 cm, and so the total number of trapped atoms is $N = n\pi\rho^2 L$, or

$$N = -\frac{\pi\rho^2}{2\sigma}\ln(1-\alpha)$$

Since the total absorption of the transition is spread out over ~525 MHz as opposed to the natural linewidth $\Gamma/2\pi = 10$ MHz, the absorption cross-section is reduced by a factor of 10/525. Taking $\sigma = (3\lambda^2/2\pi) \times (10/525)$ (λ=589 nm), the reduced cross-section on resonance, and α ~0.2, we obtain N ~7×10^{10} for the number of atoms in the trap. A better estimate of the number of atoms in the trap will be obtained in the next chapter when we consider the frequency dependence and the energy distribution of the trapped atoms in analyzing the absorption spectrum.

Chapter IV

The Absorption/Fluorescence Model

In this chapter, we construct a quantitative model of the absorption and fluorescence lineshape assuming a Boltzmann distribution for the trapped atoms and using the measured value of the magnetic field along the axis of the trap. From a fit of the model to the experimental absorption lineshape, we obtain the temperature and total number of trapped atoms.

4.1 GENERAL DESCRIPTION OF THE MODEL

The experimental situation we are modelling is represented schematically in figure 4.1. A laser beam, of frequency ω_L and cross sectional area dS, propagates in the z direction and passes through a cloud of trapped atoms. The number of photons scattered out of the laser beam per unit time by atoms located between z and z+dz is given by the scattering rate for an atom at z multiplied by the number of atoms at z in the volume element dSdz, and is equal to,

$$\frac{\Gamma}{2}\frac{(\Gamma/2)^2}{(\omega_L-\omega_a)^2+(\Gamma/2)^2}\frac{I(\vec{r})}{I_{sat}}n(\vec{r})\,dS\,dz \qquad (4.1)$$

where $n(\vec{r})$ is the number of trapped atoms per unit volume, and Γ is the natural linewidth of the transition. $I(\vec{r})$ is the intensity of the laser beam at $\vec{r}$, I_{sat} is the intensity required to saturate the transition, and ω_a is the resonant frequency of the atoms in the volume element dSdz. We have neglected saturation broadening

since I/I_{sat} ~10^{-5} for our experimental conditions. In addition, we have assumed that there is no dependence of the number of photons scattered on the velocity distribution of atoms in the trap; that is, there is negligible Doppler broadening of the lineshape. This last assumption is justified in that for atoms with an average kinetic energy of 25 mK (~1/2 the trap depth), the corresponding Doppler shift is ~8 MHz, which is considerably smaller than the ~250 MHz shift due to a magnetic confining potential ~25 mK deep.

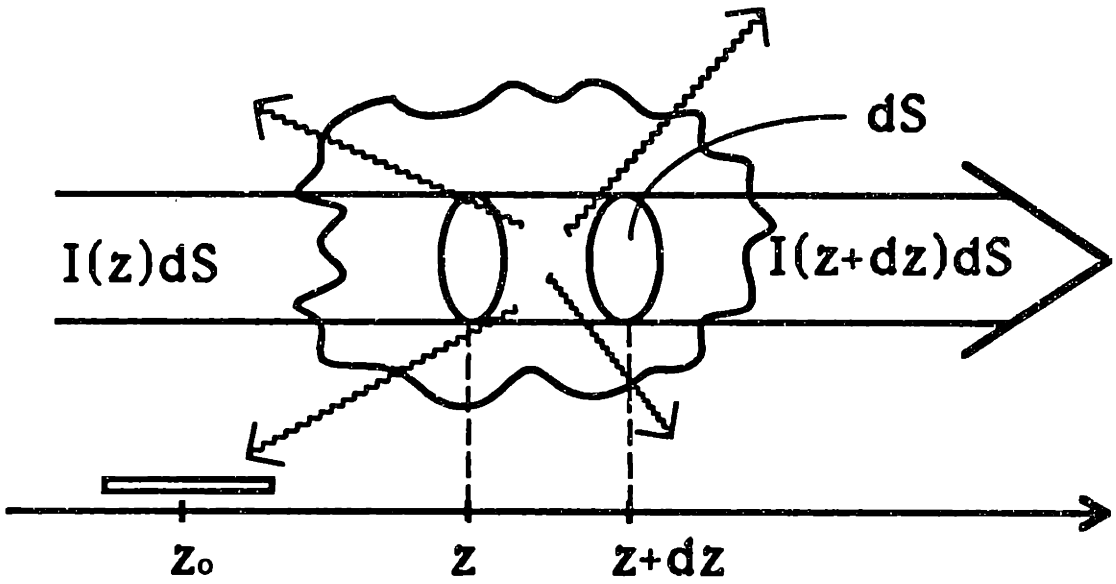

Figure 4.1: Schematic representation of the interaction of the probe laser with a cloud of trapped atoms. Absorption is represented by the decrease in intensity I(z)−I(z+dz) by a slice of atoms between z and z+dz. Fluoscence is represented by the number of photons, emitted by a slice of atoms between z and z+dz, reaching a photodetector at z_0.

The density $n(\vec{r})$, is in general a function of position. For the case of our trapped atoms, we will assume that the distribution of atoms is given by a truncated Boltzmann distribution. Thus,

$$n(\vec{r}) = \frac{N}{Z} \int d^3p \, e^{-[p^2/2m + U(\vec{r})]/k_B T} \tag{4.2}$$

where N is the total number of atoms in the trap, p and m are the momentum and mass of the atom respectively and $U(\vec{r})$ is the potential energy. Z is the partition function and is given by,

$$Z = \int d^3r \int d^3p \, e^{-[p^2/2m + U(\vec{r})]/k_B T} \tag{4.3}$$

The integration is over all trapped atoms; that is, all atoms with total energy $E_{total} = p^2/2m + U(\vec{r}) \leq E_{escape}$, the maximum energy allowed by the trap potential. Thus the integral in equation 4.2 extends from p=0 to $p=[2m(E_{escape}-U(\vec{r}))]^{1/2}$ and can be written as,

$$n(\vec{r}) = \frac{N}{Z} (2\pi m k_B T)^{3/2} \left\{ e^{-U(\vec{r})/k_B T} \, \mathrm{erf}\left(\sqrt{\frac{E_{escape} - U(\vec{r})}{k_B}} \right) - 2 \sqrt{\frac{E_{escape} - U(\vec{r})}{k_B}} \, e^{-E_{escape}/k_B T} \right\} \tag{4.4}$$

where erf(x) is the error function.

The potential energy $U(\vec{r})$, for atoms confined in a magnetic field $B(\vec{r})$, is given by $U(\vec{r}) = \mu B(\vec{r}) + mgz$, where g is the acceleration due to gravity. The resonant frequency of the atoms ω_a in the confining magnetic field is $\omega_o + \gamma B$ where $\gamma = \mu/\hbar$ and ω_o is the the unperturbed resonant frequency. For a macroscopic size laser beam, we have to integrate over the profile of the laser beam, and so the

number of photons scattered per unit time out of the slice of a laser beam between z and z+dz becomes,

$$F(\Delta, z)dz = dz \int dxdy \frac{\Gamma}{2} \frac{(\Gamma/2)^2}{(\Delta - \gamma B(\vec{r}))^2 + (\Gamma/2)^2} \frac{I(\vec{r})}{I_{sat}} n(\vec{r}) \qquad (4.5)$$

where $\Delta = \omega_L - \omega_C$ is the laser detuning from resonance at zero field, and integration is over the extent of the laser beam in the x and y direction.

To simplify equation 4.5, we assume that there are negligible variations of the magnetic field (and hence, the potential energy) across the limited profile of the laser beam. By negligible variation, we mean that the Lorentzian absorption profile of the atom essentially cannot distinguish the field variations and so the off axis field variations are less than $\hbar\Gamma/\mu$. The validity of this assumption, with respect to the actual experimental conditions, will be discussed in section 4.2B, where we shall estimate the radial dependence of the magnetic field in the trap.

Under the assumption that the variations of the field off axis are negligible, over the region in which the atoms are being probed, we can replace $B(\vec{r})$ by the value of the magnetic field on axis B(z), and so $U(\vec{r}) \rightarrow U(z) = \mu B(z) + mgz$. Thus, the only radial dependence in the integral is from the profile of the laser beam, and we re-express the integration over the profile of the laser beam as,

$$\int dxdy\, I(\vec{r}) = \pi R^2 I(z) \qquad (4.6)$$

where R is an effective radius for the laser beam and I(z) is the intensity of the laser beam on axis. For our experimental conditions, the laser beam was very nearly a parallel gaussian beam with a 1 cm waist, hence R~0.5 cm. With these approximations, the number of photons scattered per unit time out of the slice, between z and z+dz, of a laser beam of cross sectional area πR^2 is,

$$F(\Delta, z)dz = \pi R^2 \frac{\Gamma}{2} \frac{(\Gamma/2)^2}{(\Delta - \gamma B(z))^2 + (\Gamma/2)^2} \frac{I(z)}{I_{sat}} n(z)\, dz \qquad (4.7)$$

A. Absorption Line Shape

The absorption line shape was obtained experimentally by recording the decrease in the intensity of a laser beam that passed through a cloud of trapped atoms of finite extent L, as a function of laser detuning Δ. The decrease in the laser intensity I(z)−I(z+dz), by a slice of atoms between z and z+dz, is equal to the energy of the photon $\hbar\omega$ multiplied by the number of photons scattered out of the laser beam per unit time by the slice of atoms, divided by the cross sectional area of the laser beam. Thus, I(z)−I(z+dz) = dI = $\hbar\omega \times F(\Delta,z)dz/\pi R^2$, which can be solved for I(z) to yield,

$$I = I_o e^{-\alpha(\Delta,z)L} \qquad (4.8)$$

where,

$$\alpha(\Delta,z) = \frac{1}{L}\frac{\Gamma}{2}\frac{\hbar\omega}{I_{sat}}\int_{z_{min}}^{z} \frac{(\Gamma/2)^2}{(\Delta - \gamma\, B(z'))^2 + (\Gamma/2)^2}\, n(z')\, dz' \tag{4.9}$$

I_0 is the incident laser intensity and z_{min} is the point along the axis of the trap where the laser beam first encounters trapped atoms. We note that the size of the laser beam, R, cancels out for the absorption measurements as only the column density is measured.

Equations 4.8 and 4.9 are then the basic equations for the absorption lineshape.

B. Fluorescence Line Shape

The fluorescence line shape was obtained experimentally by counting the number of photons that hit a photodetector during a time interval Δt, as a function of laser detuning Δ. In general, the photodetector can only receive photons emitted into some fraction of the total solid angle 4π, because of its small size relative to the trapped atom cloud. This fraction of the total solid angle will be some function $D(z-z_0)$, of the axial distance from the detector. The number of photons seen by a photodetector at position z_0, during the time interval Δt, is $N_{fluor}(\Delta, z_0)$, and is obtained by integrating, over the extent of the trapped atom cloud, the detector response function $D(z-z_0)$ multiplied by the number of photons emitted by the atoms in a slice of the laser beam between z and z+dz.

$$N_{fluor}(\Delta, z_0) = \Delta t \int dz\, D(z - z_0)\, F(\Delta, z) \tag{4.10}$$

Where $I(z) = I_0 \exp[-\alpha(\Delta, z)L]$, is used in $F(\Delta, z)dz$ to included the possible attenuation of the intensity of the laser beam due to absorption as it passes through the trapped atom cloud.

Equation 4.10 with 4.7 and the appropriate detector response function are then the basic equations for the fluorescence lineshape.

4.2 ANALYSIS OF THE MAGNETIC FIELDS

A. The Magnetic Field On Axis

The calculation of the fluorescence and absorption lineshape explicitly requires the magnetic field profile along the axis of the trap. To get a decent fit of the model to the data, we needed to measure a magnetic field on axis that was equivalent to the field present when the spectra was taken. The magnetic field on axis is composed of the fields produced from three sets of coils. The axial "pinch" coils, used for axial confinement of the atoms; the second slower field, used for stopping atoms in the trap; and the octopole field, used for radial confinement of the atoms (see chapter 2).

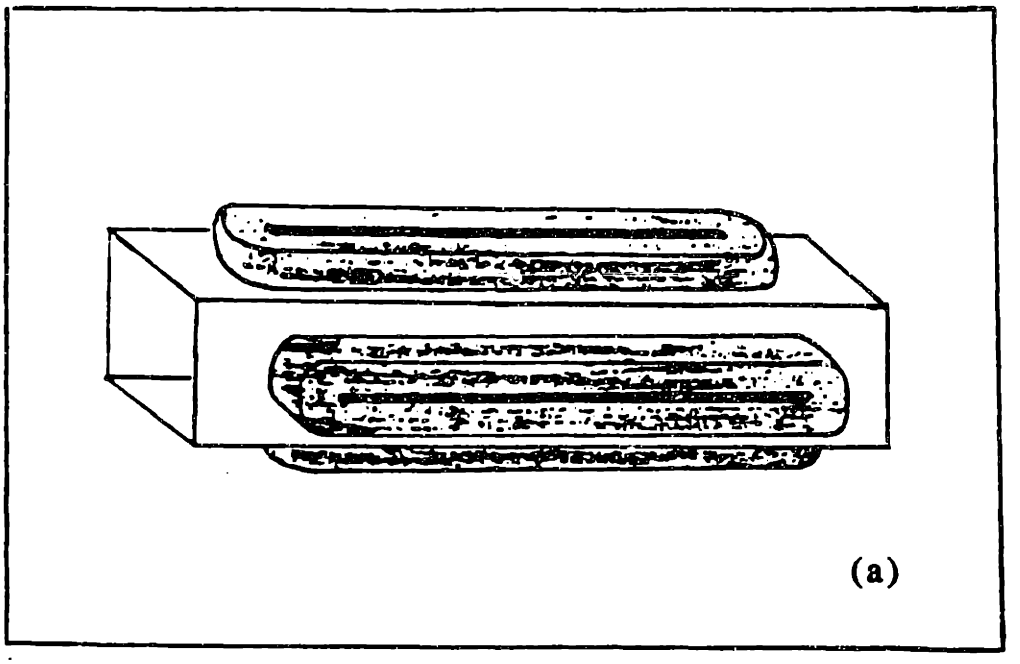

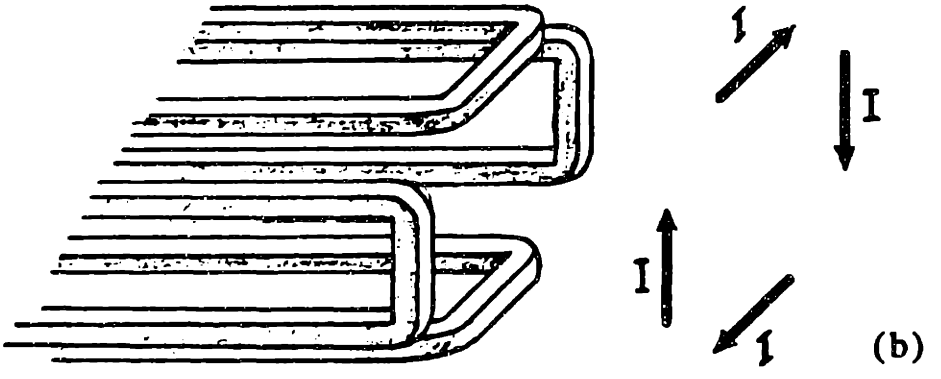

Figure 4.2: (a) Configuration of coils comprising the octopole magnet in the magnetic trap. (b) Schematic representation of the end of the octopole magnet of (a), illustrating how such a current configuration can give rise to an "effective" current loop thereby creating an axial magnetic field.

The Influence of the Octopole Field on the Axial Field Profile

A finite length octopole magnet gives rise to an axial magnetic field. The octopole magnet used for radial confinement in the magnetic trap had a coil configuration similar to figure 4.2(a). Figure 4.2(b) illustrates how the configuration of the wires at the end of this octopole magnet can give rise to an "effective" current loop that results in a field along the axis of the trap. We can obtain an estimate of the end effect by considering the end of the octopole as loops of wire with the same number of amp-turns as the octopole magnet (~72,000 amp-turns). We take the radius of the loop R, as half the distance between the poles of the magnet (R~6 cm), and the axial location of the loop as being at the end of the octopole, which is ~30 cm from the trap minimum. The axial field from this loop at the trap minimum is then ~60 Gauss. Thus, in estimating the actual magnetic field profile along the axis of the trap under which the absorption and fluorescence spectra were obtained, we must consider the influence of the octopole magnet.

Measuring the Magnetic Field on Axis

Measurement of the field produced by superconducting magnet coils is accomplished by measuring, at a reduced current, the field the coils produce when they are in a normal state. The measurements made are then scaled by the appropriate value of the current to obtain the field present when the magnet wires are superconducting. In principle this procedure will give an exact result

for the fields present when the magnets are superconducting provided that, when one is making the measurement of the axial field at reduced current, any stray magnetic fields present are small in comparison, or subtracted out with a background measurement. The only major complication that could arise and undermine the measurement procedure would be the presence of non-superconducting shorts through the insulation between some of the turns of the magnet coils. This would result in a lower value of the magnetic field measured while the magnets are normal than when the magnets are superconducting.

The axial magnetic field profile in the magnetic trap was measured for various magnet configurations. Magnetic field measurements were taken with a Hall probe every 1 cm, over the region in which atoms were confined. The axial field under the following conditions were recorded.

1. Axial "pinch" coils at 0.5 Amp; all other coils at 0 Amp.
2. Second slower coil at 1 Amp; all other coils at 0 Amp.
3. Octopole coils at 1 Amp; all other coils at 0 Amp.
4. All coils at 0 Amp (background measurement).

The last measurement was made to eliminate the influence of stray fields (such as the earth's field), during the measurement of the magnetic field from the coils. Figure 4.3(a), (b), and (c) are plots of the resulting field measurements under conditions 1, 2, and 3 respectively after having subtracted the background measurement.

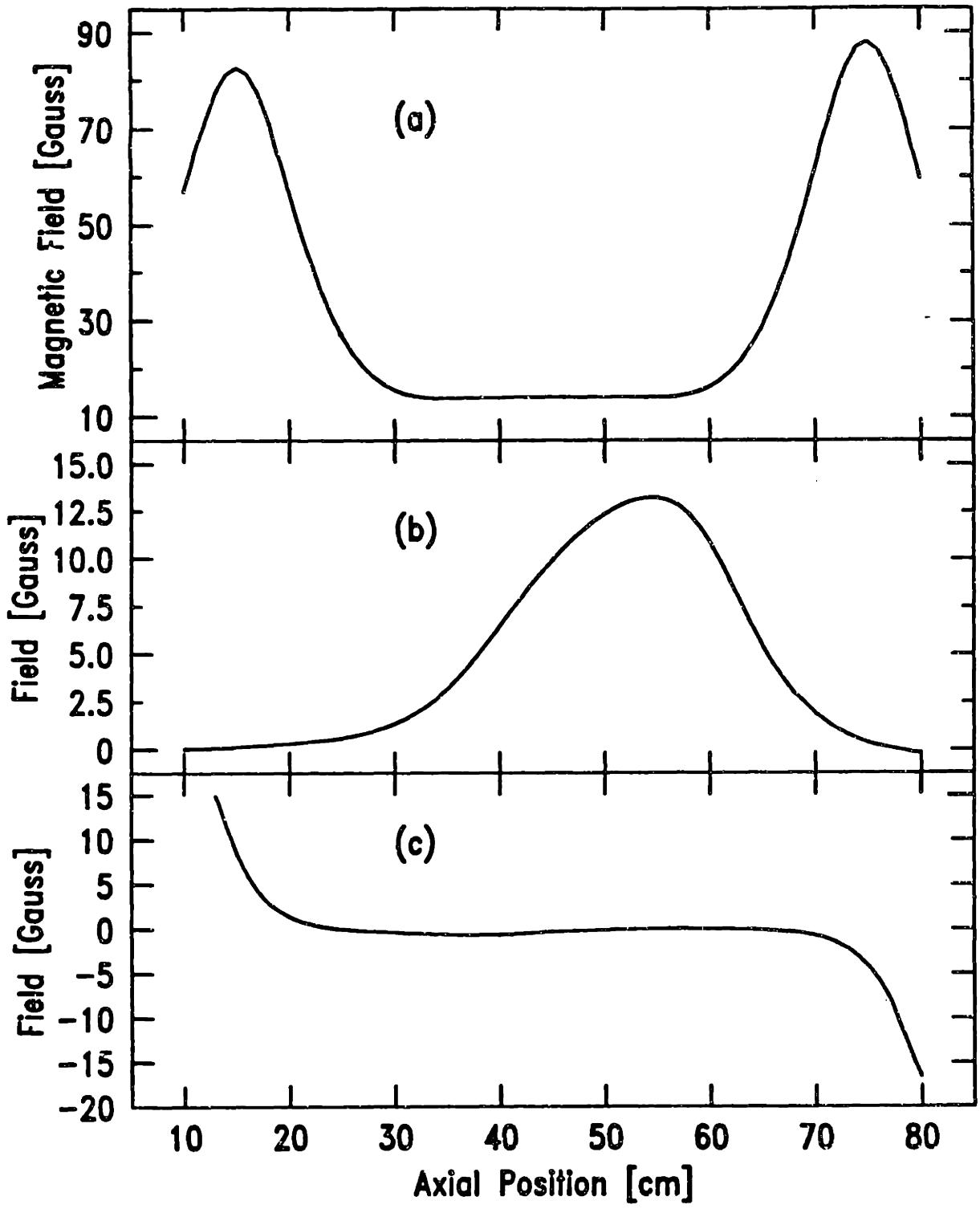

Figure 4.3: Measurement of the magnetic field profile on axis for, (a) axial "pinch" coils at 0.5 amps, (b) second slower coil at 1 amp, and (c) octopole coil at 1 amp.

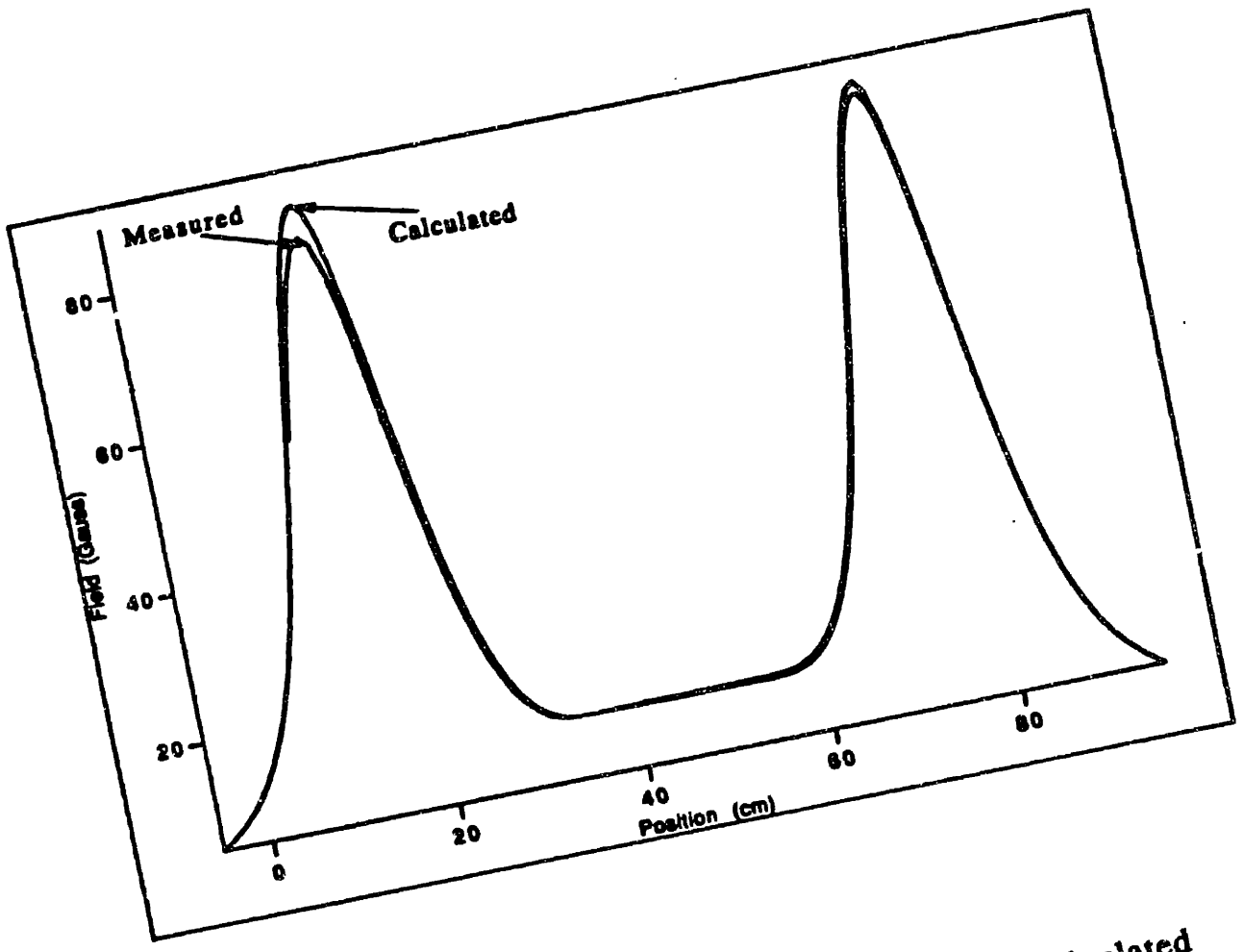

Figure 4.4: Comparison of the measured and calculated magnetic field profile on axis due to the axial "pinch" coil, emphasizing an electrical short between some of the wires comprising the left coil.

A complication arises when figure 4.3(a) is examined closely; the heights of the two peaks due to the axial "pinch" coils are not equal. This is most likely due to a short between some of the turns comprising the left "pinch" coil. To check if this is a reasonable explanation for the difference in heights, a comparison was made of the measured axial field with a numerical calculation of the field produced by the equivalent current configuration for the axial "pinch" coils. Figure 4.4 is plot of the measured and calculated magnetic field on axis produced by the "pinch" coils. The agreement between the peaks on the right is quite good, supporting the hypothesis that there is a short between some of the turn windings in the left "pinch" coil. In order to get around the problem of the partially shorted coil, we will use the calculated axial field profile due to the axial "pinch" coils in our calculation of the absorption and fluorescence line shape.

Our Best Estimate of the Magnetic Field on Axis

Our best estimate of the magnetic field profile on axis, is comprised of the measured second slower field, the measured octopole field and the calculated axial "pinch" coil field. In order to reproduce the axial magnetic field profile that we had when the fluorescence and absorption spectra were taken, we need to scale the measured or calculated magnetic fields by the appropriate currents and sum up the contribution of each individual set of magnets to obtain the overall field profile. The only uncertainty in this procedure is when we add in the contribution due to the octopole.

Since the primary role of the octopole field was to provide radial confinement there is some ambiguity in the sign of the current used as either sign will give rise to basically the same radial confinement field; the radial fields are added in quadrature with the axial fields hence there is no dependence on the sign of the current. Figure 4.5 is plot of the field along the axis of the trap over the range in which atoms are confined. The currents used ("pinch" coil 60 A, second slower 28 A, octopole ±120 A) in scaling the field correspond to those used during the experiment. A zero current, octopole field plot is included in figure 4.5 to emphasize the end effects of the finite length octopole coils.

The dependence of the magnetic field profile on the direction of the current in the octopole magnet is quite significant. The difference, from figure 4.5, between the top of the second slower and the minimum of the magnetic field is ~470 and ~280 Gauss with +120 Amps and −120 Amps in the octopole magnet respectively. From the discussion of the absorption lineshape in the previous chapter, these differences would correspond to a separation of the two dips in the absorption spectrum of ~660 and ~390 MHz respectively. This difference is easily detectable in the absorption spectra obtained thus lifting the ambiguity in the sign of the octopole current.

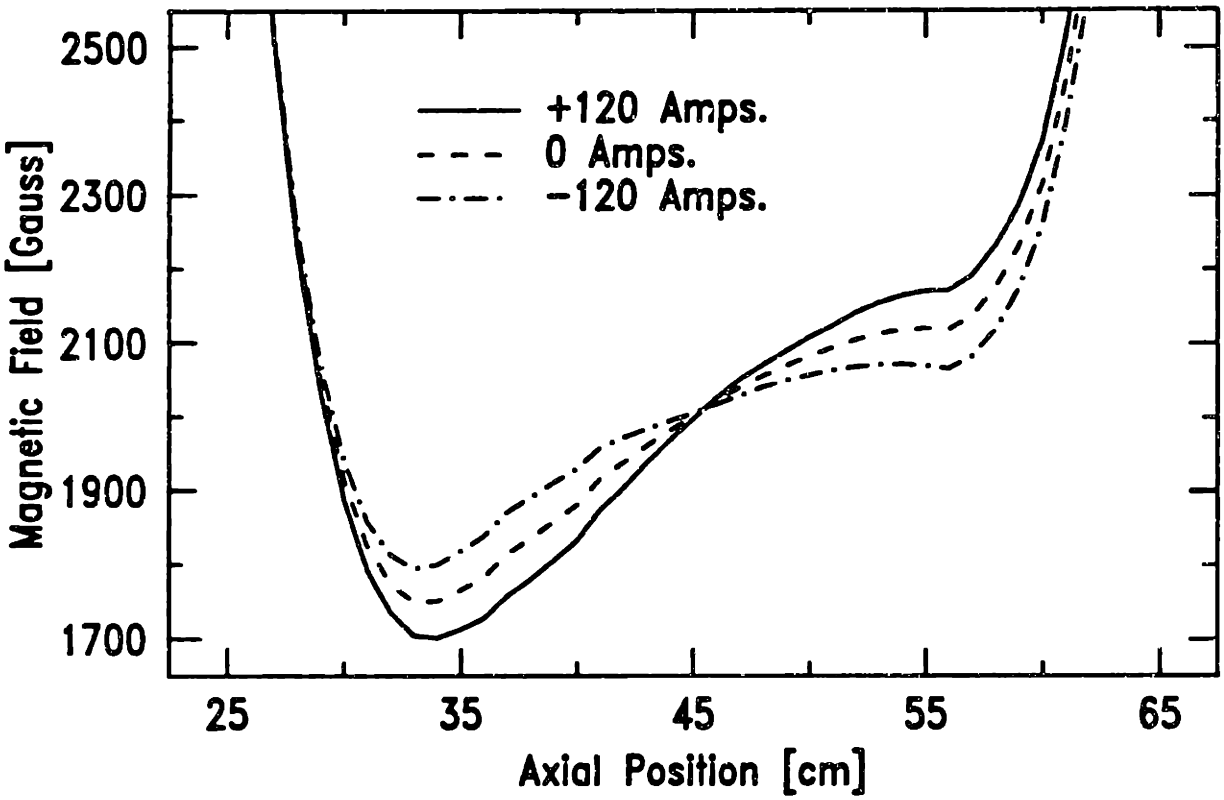

Figure 4.5: The resulting magnetic field profile on axis for the calculated axial "pinch" coils at 60 amps, the second slower coil at 28 amps, and the octopole magnet at +120, 0, and −120 amps.

B. Estimate of the Radial Dependence of the Magnetic Field

In deriving the expressions for the absorption and fluorescence line shapes (Eqs. 4.8, 4.9 and 4.10), we made the assumption that the magnetic field was essentially constant over the diameter of the probe laser beam. This, we said, was equivalent to having the frequency shift due to the field variations off axis, small compared to natural linewidth of the transition we are using to probe the atoms. In order to verify this hypothesis, we need to estimate the magnetic field off axis.

We estimate the radial dependence of the magnetic field in the trap by calculating the field off axis resulting from the measured value of the magnetic field on axis, and adding this calculated field to a pure octopole field. This estimate assumes that the field on axis arises purely from magnets with axial symmetry. This is certainly an excellent approximation for estimating the radial dependence of the magnetic field resulting from the second slower and axial "pinch" coils. Corrections to the radial field will be of the order $(B_z/B_\rho)^2$, where B_z is the axial field due to the octopole and B_ρ is the radial field due to one of the poles of the octopole magnet. At +120 Amps, the largest B_z in the trap region is ~60 Gauss. Approximating a pole of the octopole magnet as an infinite wire ~6 cm from the axis, we obtain B_ρ= 2400 Gauss at ρ=0, and so the correction is on the order of 0.1%.

Quantitatively, the procedure for estimating the magnetic field off axis is:

1. Fit the measured field (equivalent to the field on axis during the experiments) to a polynomial of order n.
2. Assuming axial symmetry, solve the source free Maxwell equations, using the polynomial fit, to obtain the radial dependence of the magnetic field that produced the measured field on axis.
3. Add in a pure octopole field.

A sixth order polynomial fit was made to the measured field of figure 4.5 with +120 amps in the octopole magnet. Thus, the magnetic field $\vec{B}_a(\rho,z)$ is described on axis by,

$$\vec{B}_a(0,z) = \sum_{n=0}^{6} d_n z^n \hat{z}$$

Solving the source free Maxwell equations for an axially symmetric field, we obtain the magnetic field,

$$\vec{B}_a(\rho,z) = B_{az}(\rho,z)\hat{z} + B_{a\rho}(\rho,z)\hat{\rho}$$

with,

$$B_{az}(\rho,z) = \sum_{n=0}^{6} c_n(\rho) z^n$$

and

$$B_{a\rho}(\rho,z) = \sum_{n=0}^{4} \frac{1}{n+1}\frac{\partial c_n}{\partial \rho} z^{n+1}\hat{z} - \frac{5}{16}d_5\rho^5 + \frac{3}{8}d_3\rho^3 - \frac{1}{2}d_1\rho$$

where,

$$c_0 = -(5/16)d_6\rho^6 + (3/8)d_4\rho^4 - (1/2)d_2\rho^2 + d_0$$
$$c_1 = (15/8)d_5\rho^4 - (3/2)d_3\rho^2 + d_1$$

$$c_2 = (45/8)d_6\rho^4 - 3d_4\rho^2 + d_2$$
$$c_3 = -5d_5\rho^2 + d_3$$
$$c_4 = -(15/2)d_6\rho^2 + d_4$$
$$c_5 = d_5$$
$$c_6 = d_6$$

We add a pure octopole field $\vec{B}_o(\rho,\phi) = b_o\rho^3(\cos 4\phi\hat{\rho} - \sin 4\phi\hat{\phi})$ to $\vec{B}_a(\rho,z)$ to obtain the estimate of the magnetic field $\vec{B}(\rho,z)$ in the trap.

$$\vec{B}(\rho,z) = \vec{B}_a(\rho,z) + \vec{B}_o(\rho,\phi)$$

In our magnetic trap, the atoms are confined in regions of large (>1500 Gauss) magnetic field and the Larmor frequency of the trapped atom is much larger than the oscillation frequency of the atom in the trap, thus the spin of the trapped atoms adiabatically follow the magnetic field direction [PMP85] thus we need only concern ourselves with the magnitude of the magnetic field.

$$B(\rho,z) = \sqrt{B_a^2 + B_o^2 + 2\vec{B}_a \cdot \vec{B}_o}$$

Figure 4.6 is a contour plot of this equation for the magnitude of the magnetic field as a function of ρ and z (with $\phi = 0$) over the region in which the atoms are confined in the magnetic trap. Each constant field line differs from the adjacent one by 30 gauss. The dashed line in figure 4.6 indicates the approximate radial extent of the probe laser beam. The most striking feature of this plot is how it resembles a piece of toast! Excuse me. At this resolution, one can see that the trap potential is relatively constant across the probe laser and out to a radial distance of ~1 cm. A closer examination of the region accessed by the probe laser reveals that the magnetic field variations

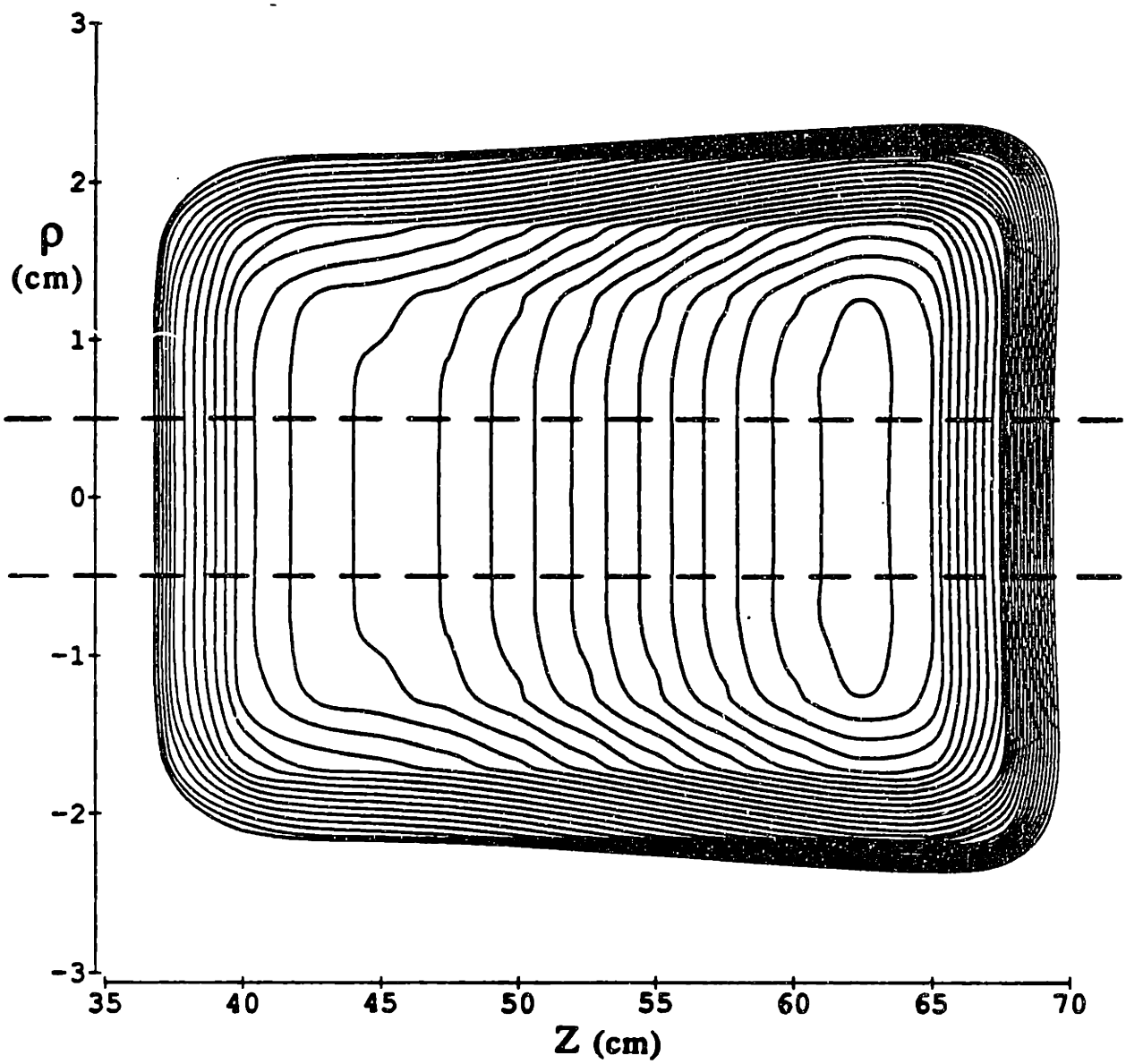

Figure 4.6: Contour plot of magnetic field as a function of radial ρ, and axial position z. Each constant field line differs from the adjacent one by 30 Gauss. The minimum of the field in the axial direction is at z=62.5 cm. The region between the dashed lines corresponds to the extent of the probe laser beam.

in this region are less than $\hbar\Gamma/\mu$ ~7 Gauss for $36 < z < 70$ cm, and are less than 3 Gauss for a range along the z axis ±3 cm from the minimum of the potential. With this estimate of the magnetic field in the trap, it appears that one is justified in neglecting the variations of the magnetic field across the profile of the probe laser.

4.3 A FIT OF THE MODEL TO THE DATA

A numerical calculation of the absorption line shape was performed using the estimated values of the magnetic field on axis ("pinch" coils 60A, second slower 28A, octopole +120A), obtained in the manner described in section B of this chapter. The function α from equation 4.9 was multiplied by a factor of 2, to account for two passes of the laser beam through the sample of trapped atoms, and then integrated over all axial position z such that $U(z) \leq E_{escape}$. The resulting absorption spectrum (Eq. 4.8) has two adjustable parameters, the number of atoms N, and the temperature T. Both of which enter equation 4.8 through the density term (Eq. 4.4) in α (Eq. 4.9). In computing the partition function Z, the trap potential in the radial direction was approximated as a square well with a minimum value U(z) and maximum value E_{escape}. This was done to speed up the calculation and, for a ρ^6 radial potential, results in an ~15% over estimate of the volume of the trap, which is comparable to the uncertainty in our knowledge of the effective diameter of the trap and laser beam. However, in a fit of the calculation to the experimentally obtained lineshape, the error in computing Z can be absorbed in the total number of atoms N.

A fit of the calculated absorption lineshape to the experimentally obtained absorption spectrum of figure 3.5 was performed. The temperature T, was adjusted until the calculated absorption lineshape gave the same relative sizes for the two dips observed in the spectrum of figure 3.5. The total number of atoms N, was then adjusted until the absolute value for the absorption at the frequency corresponding to the minimum of the trap coincided. In this manner, the best fit of the absorption model to the data was achieved. Figure 4.7 is a plot of the absorption spectrum in figure 3.5 and the best fit of the calculated lineshape to the data.

A value of $N=2\times10^{11}$ for the total number of atoms in the trap was used in the fit. This compares favorably to the quick estimate of the total number of atoms, performed at the end of chapter 3. A temperature T=500 mK, was used in the calculation of the lineshape. We found that basically any temperature greater than the trap depth (~50 mK) provided a comparable fit to the absorption spectrum. This implies that all states in the trap potential are occupied with nearly equal probability.

The high temperature of the trapped atoms is most likely the result of heating in the transverse direction by the intense (>10 mW/cm^2) standing-wave laser beam used to slow and stop atoms in the trap. This laser beam rapidly cools the longitudinal motion of the atoms in the trap, but simultaneously heats the transverse motion due to the random nature of the spontaneously emitted photons. Cooling of the transverse motion is only achieved indirectly through

the coupling of the transverse and longitudinal motions of the atoms by the trap which occurs over much longer time scales. A more detailed explanation of this phenomena will be given in chapter 7, when we consider Doppler cooling of atoms in the trap.

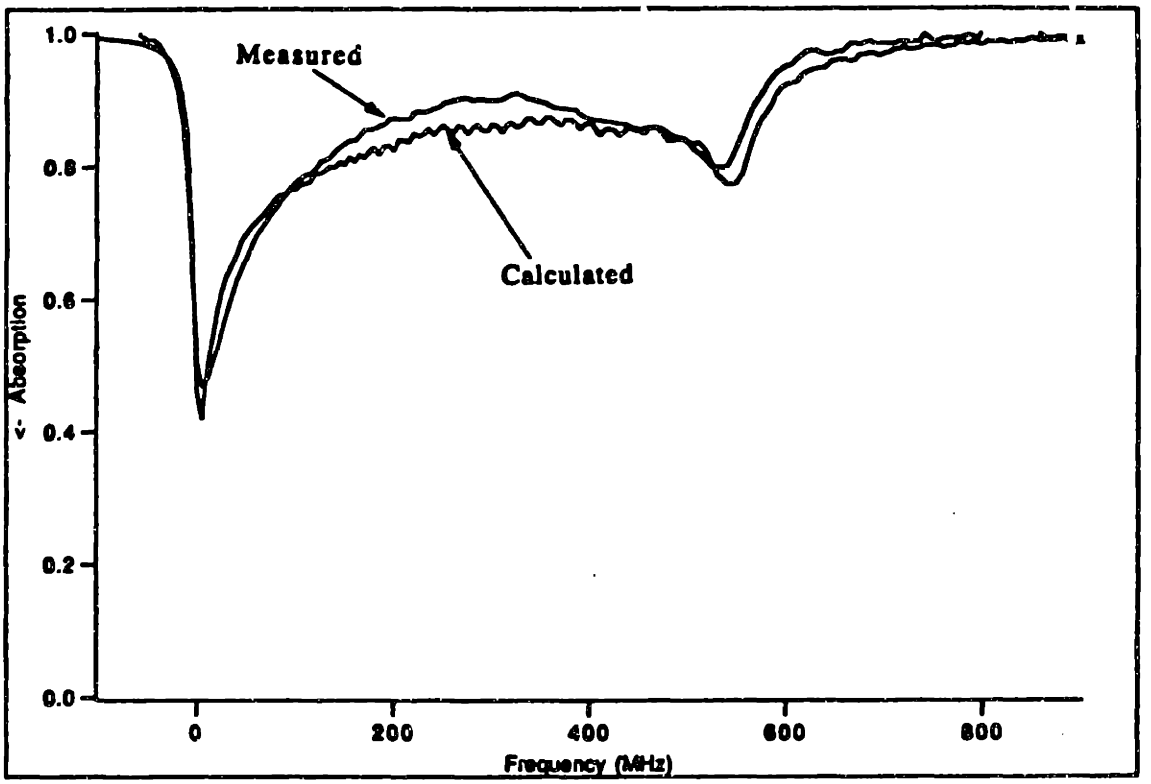

Figure 4.7: Measured and calculated absorption spectra. A value of $N=2\times10^{11}$ for the number of trapped atoms and T=500 mK for the temperature was used in the calculated lineshape.

A numerical calculation of the fluorescence lineshape, equation 4.10, was performed using the previously calculated absorption profile of the laser intensity and the estimated magnetic field on axis. Equation 4.10 was integrated over the sample of the trapped atoms with a detector response function for the detector located at the minimum of the trap potential. A gaussian function, centered at the location of the photodetector, with the width as an adjustable parameter, was used as the detector response function. Our simple calculations of the angular response of the photodetector showed that it was closely approximated by the gaussian function.

A fit was made of the fluorescence spectrum obtained with detector 1, corresponding to the absorption spectrum of figure 3.5. A best fit of the calculated fluorescence lineshape was obtained by adjusting the "effective width" of the detector response function and rescaling the height of the calculated lineshape to coincide with the height of the experimentally obtained fluorescence spectrum. Figure 4.8 shows the fluorescence spectrum and fit with an effective width of ~8 cm for the photodetectors.

Possible explanations for the deviations of the calculated lineshapes from the experimentally obtained spectra are: The estimated magnetic field on axis does not represent the actual magnetic field present when the data were taken. The distribution of atoms in the trap may not be entirely described by a Boltzmann distribution. The angular response of the photodetector, in the case of the fluorescence spectrum, may not be entirely characterized by a

gaussian function due to the radial spatial extent of the trapped atoms.

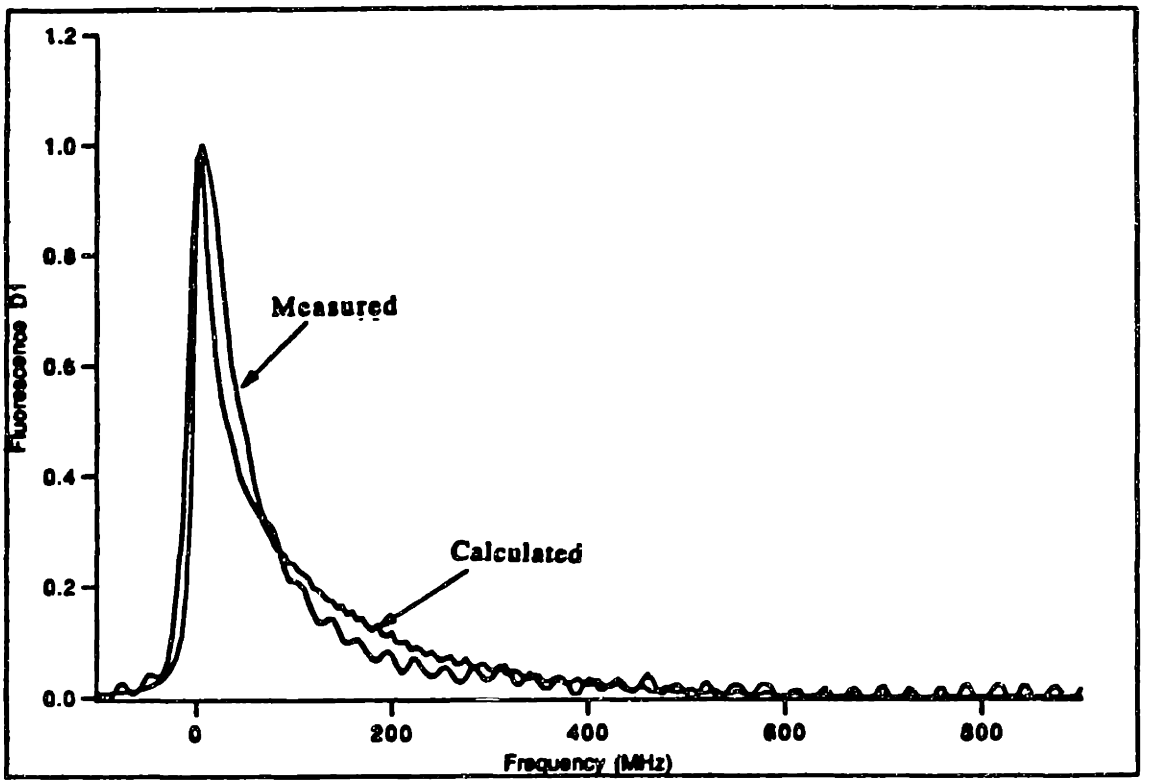

Figure 4.8: Measured and calculated fluorescence spectra corresponding to the detector at the minimum of the trap potential.

CHAPTER V

rf Spectroscopy Experiments

The observation of rf-induced transitions of trapped neutral atoms is described. An rf resonance curve for a sample of trapped Na atoms was obtained by measuring the relative population of two trapped magnetic substates as a function of applied rf frequency, and the general shape of the curve is explained. These rf experiments constitute the first rf resonance experiments on trapped neutral particles.

5.1 OBSERVATION OF RF-INDUCED TRANSITIONS

Resonant radio-frequency (rf) pulses were applied, using the antenna located in the trap region, to a sample of trapped Na atoms to induce Zeeman transitions between the four trapped ground state hyperfine levels, $|F=2, M=2,1,0,-1\rangle$ (see figure 2.1). The transfer of population between the four trapped magnetic sublevels was monitored by the variation in the laser induced fluorescence spectrum of the trapped atoms, as observed by the photodetector located at the minimum of the trap (fig. 2.3, detector 1). At a magnetic field of ~1500 gauss, corresponding to the value at the minimum of the trap, the fluorescence spectrum displays well resolved peaks corresponding to the various $|F=2, M\rangle \rightarrow |F'=3, M'=M+1\rangle$ optical transitions induced by the weak, circularly polarized probe laser beam.

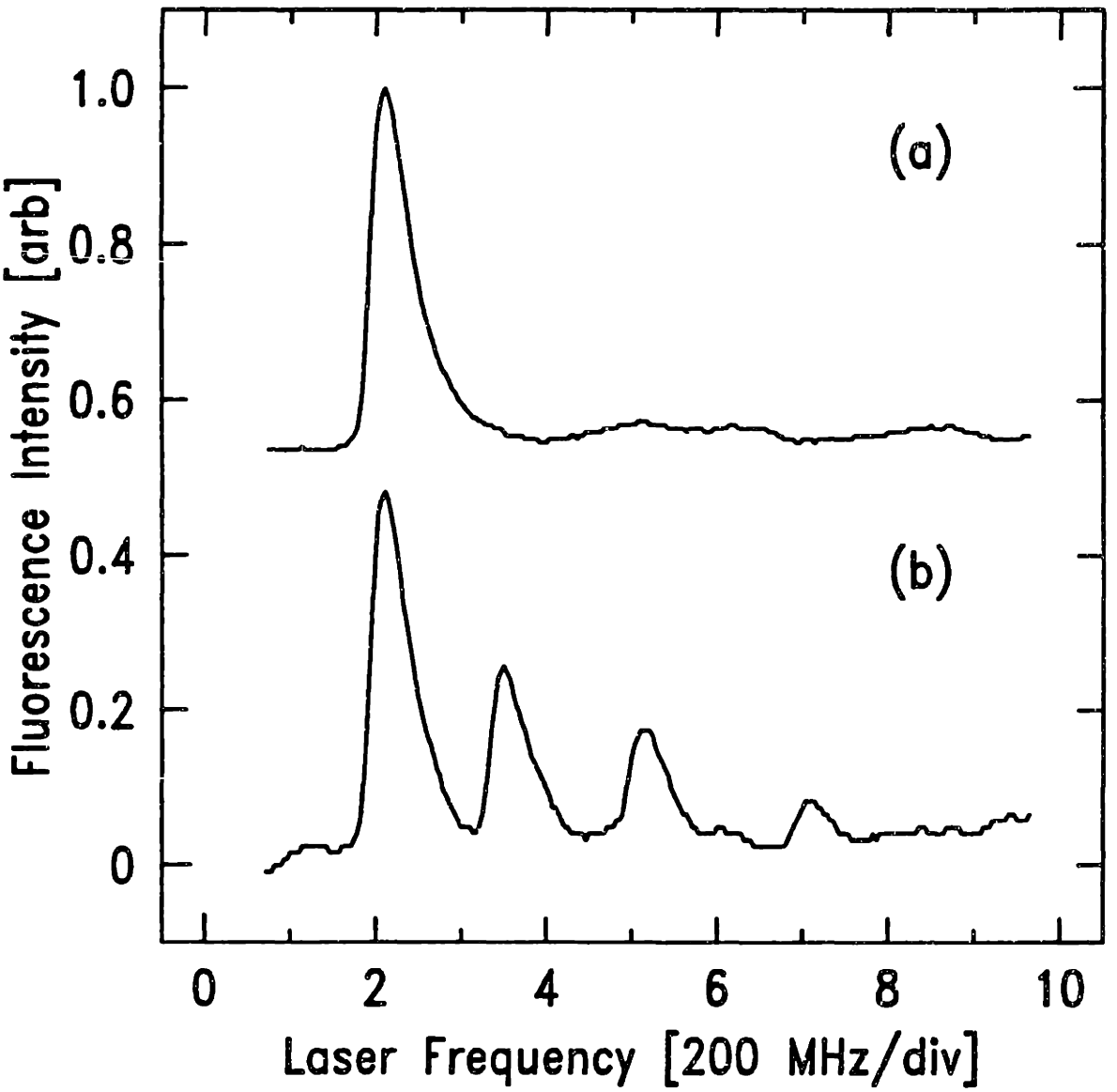

Figure 5.1: Fluorescence spectrum for trapped Na atoms induced by a weak circularly polarized probe laser beam. Scan a, before the application of the rf pulse, with all the atoms in the $|F=2, M=2\rangle$ state; scan b, after a series of rf pulses, showing population in all four trapped magnetic substates, $|F=2, M=1,1,0,-1\rangle$.

Figure 5.1, shows fluorescence spectra from the trapped atoms before (scan a), and after (scan b), repeated application of rf pulses at 330, 378 and 455 MHz. These frequencies correspond to the three possible $\Delta M = \pm 1$ magnetic dipole transitions among the four trapped substates at close to the minimum magnetic field in the trap. These frequencies are the most effective for transferring population, as all the trapped atoms, regardless of their total energy, eventually pass close to the field minimum during their motion in the trap (fig. 2.3). The four peaks observed in the fluorescence spectrum (scanning from red to blue) correspond to the $|F=2,\ M=2,1,0,-1\rangle \rightarrow |F'=3,\ M'=3,2,1,0\rangle$ transitions respectively, and the differences in frequency of adjacent peaks are approximately equal to the frequency of the applied rf pulses (330, 378 and 455 MHz) minus the corresponding excited state hyperfine splitting of ~30 MHz at ~1500 gauss.

5.2 SATURATION OF THE RF TRANSITION

The power level of the rf signal produced an ~10 mgauss rf magnetic field in the trap region, which should induce magnetic dipole transitions amongst the trapped magnetic substates with a Rabi frequency $\Omega_R/2\pi$ of ~2 kHz, at a magnetic field of ~1500 Gauss. The duration of the applied rf pulses was ~5 seconds, long enough to ensure that the populations of the four magnetic substates were approximately equalized. The difference in the peak heights in Fig. 5.1(b) is primarily due to optical pumping effects produced by the circularly polarized probe laser. The branching ratios for decay of the various excited states back to the original M level, determine the

number of times atoms in each magnetic substate can be cycled, and therefore the height of the peaks. Table 5.1 shows the various branching ratios for the sodium D lines at a magnetic field of 1520 Gauss, corresponding to its value at the minimum of the trap.

Figure 5.2 is a sequence of fluorescence spectra from two different runs where the transfer of population between the ground state $|F=2, M=2\rangle$ and $|F=2, M=1\rangle$ trapped magnetic substates is observed after applying an rf pulse ($\Omega_R/2\pi \approx 2$ kHz, $\tau = 5$ sec.) of the appropriate frequency to maximize population transfer. The two peaks in each spectrum (going from red to blue laser detuning) correspond to the $|F=2, M=2\rangle \rightarrow |F'=3, M'=3\rangle$ and $|F=2, M=1\rangle \rightarrow |F'=3, M'=2\rangle$ optical transitions respectively. The first three fluorescence spectra [figures 5.2(a), (b) and (c)] are from the same run and differ only in the intensity of the probe beam used to observe population transfer. One can see that the fluorescence peak corresponding to the $|F=2, M=1\rangle \rightarrow |F'=3, M'=2\rangle$ transition increases with respect to the peak corresponding to the $|F=2, M=2\rangle \rightarrow |F'=3, M'=3\rangle$ transition, with decreasing probe laser intensity. Improvements in signal to noise of our fluorescence detection system, for a subsequent run, allowed us to use a probe laser, for the fluorescence scan of figure 5.2(d), that was ~40 times weaker than the one used for scan c.

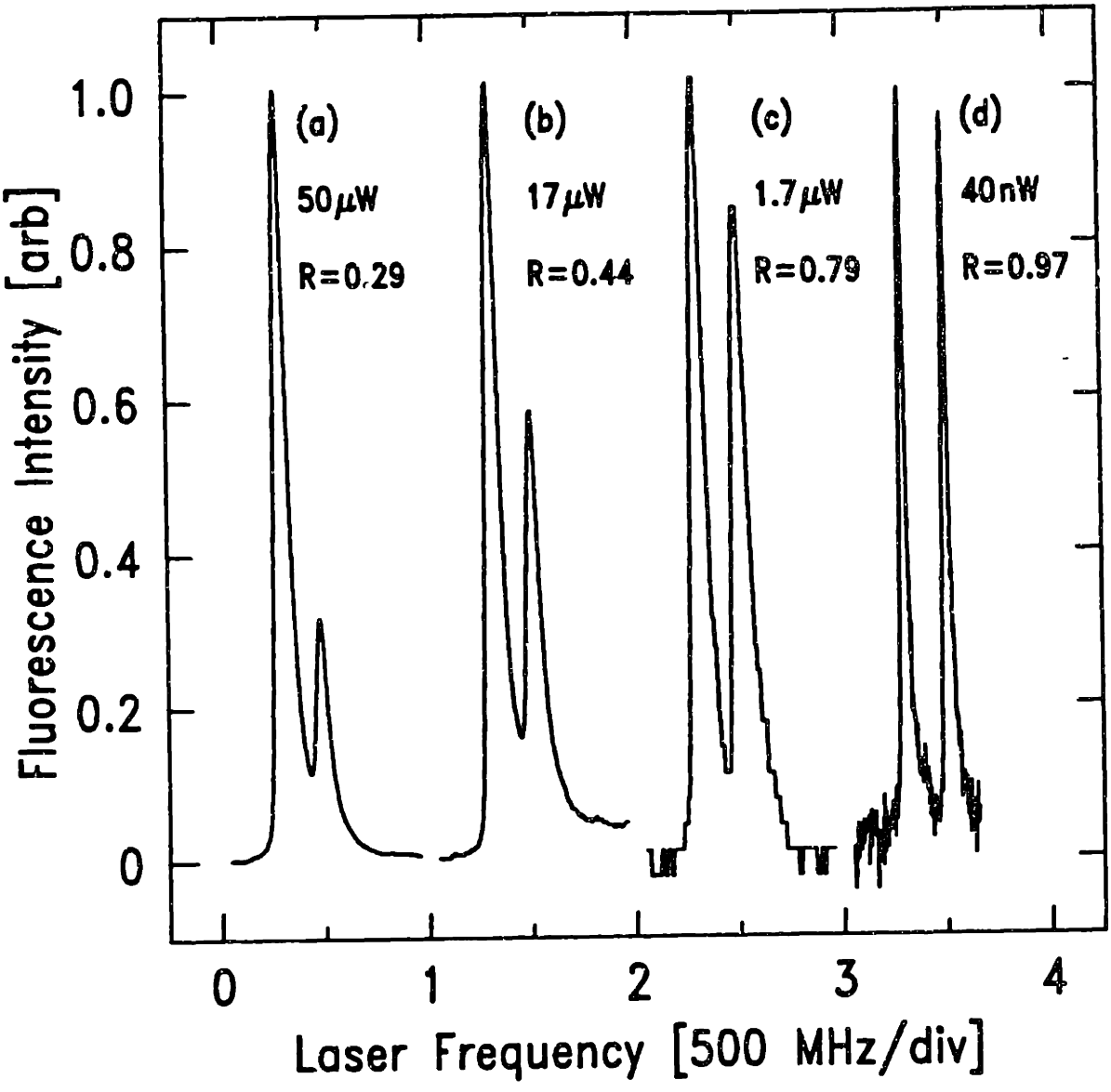

Figure 5.2: Four fluorescence spectra with two peaks corresponding (from left to right) to the $|F=2, M=2\rangle \rightarrow |F'=3, M'=3\rangle$ and $|F=2, M=1\rangle \rightarrow |F'=3, M'=2\rangle$ optical transitions. These four spectra illustrate the effect of optical pumping on the ratio of the peak heights R. $R \rightarrow 0.98$ as the laser power approaches zero implies saturation of the rf transition used to transfer population between the $|F=2, M=2\rangle$ and $|F=2, M=1\rangle$ trapped substates. [(a), (b), and (c) are data from the same run.]

		$3S_{1/2}$							
		|2.0, 2.0>	|2.0, 1.0>	|2.0, 0.0>	|2.0,-1.0>	|2.0,-2.0>	|1.0,-1.0>	|1.0, 0.0>	|1.0, 1.0>
	|3.0, 3.0>	1.0000000	0.0000000	0.0000000	0.0000000	0.0000000	0.0000000	0.0000000	0.0000000
	|3.0, 2.0>	0.0000704	0.9807367	0.0000000	0.0000000	0.0000000	0.0000000	0.0000000	0.0191930
	|3.0, 1.0>	0.0000000	0.0000876	0.9640798	0.0000000	0.0000000	0.0000000	0.0358311	0.0000014
	|3.0, 0.0>	0.0000000	0.0000000	0.0000612	0.9573570	0.0000000	0.0425799	0.0000019	0.0000000
	|2.0, 2.0>	0.6665963	0.0053594	0.0000000	0.0000000	0.0000000	0.0000000	0.0000000	0.3280444
	|2.0, 1.0>	0.0000432	0.6547621	0.0103481	0.0000000	0.0000000	0.0000000	0.3230310	0.0118156
	|2.0, 0.0>	0.0000000	0.0000577	0.6443184	0.0127209	0.0000000	0.3206170	0.0222851	0.0000008
$3P_{3/2}$	|3.0,-1.0>	0.0000000	0.0000000	0.0000434	0.6398554	0.3332888	0.0268112	0.0000012	0.0000000
	|3.0,-2.0>	0.0000000	0.0000000	0.0000000	0.3208010	0.6665963	0.0126027	0.0000000	0.0000000
	|2.0,-1.0>	0.0000000	0.0000000	0.3229937	0.0268070	0.0000445	0.6397732	0.0103815	0.0000000
	|1.0, 0.0>	0.0000000	0.3278581	0.0222845	0.0000030	0.0000000	0.0000555	0.6443225	0.0054765
	|1.0, 1.0>	0.3332901	0.0118170	0.0000019	0.0000000	0.0000000	0.0000000	0.0000413	0.6548497
	|3.0,-3.0>	0.0000000	0.0000000	0.0000000	0.0000000	1.0000000	0.0000000	0.0000000	0.0000000
	|2.0,-2.0>	0.0000000	0.0000000	0.0000000	0.0424514	0.0000704	0.9574782	0.0000000	0.0000000
	|1.0,-1.0>	0.0000000	0.0000000	0.0358664	0.0000042	0.0000000	0.0000823	0.9640472	0.0000000
	|0.0, 0.0>	0.0000000	0.0193215	0.0000026	0.0000000	0.0000000	0.0000000	0.0000572	0.9806188
	|2.0, 2.0>	0.3333333	0.0139040	0.0000000	0.0000000	0.0000000	0.0000000	0.0000000	0.6527627
	|2.0, 1.0>	0.0019254	0.3203463	0.0254963	0.0000000	0.0000000	0.0000000	0.6392449	0.0129870
	|2.0, 0.0>	0.0000000	0.0028464	0.3107699	0.0297887	0.0000000	0.6339709	0.0225634	0.0000606
$3P_{1/2}$	|2.0,-1.0>	0.0000000	0.0000000	0.0024101	0.3087862	0.6641604	0.0245471	0.0000961	0.0000000
	|2.0,-2.0>	0.0000000	0.0000000	0.0000000	0.6367475	0.3333333	0.0299191	0.0000000	0.0000000
	|1.0,-1.0>	0.0000000	0.0000000	0.6386864	0.0245471	0.0025062	0.3087862	0.0254740	0.0000000
	|1.0, 0.0>	0.0000000	0.6499163	0.0225634	0.0001305	0.0000000	0.0027766	0.3107699	0.0138433
	|1.0, 1.0>	0.6647412	0.0129870	0.0000739	0.0000000	0.0000000	0.0000000	0.0018516	0.3203463

Table 5.1: Relative strengths for the Sodium $3S_{1/2} \rightarrow 3P_{3/2}$ and $3S_{1/2} \rightarrow 3P_{1/2}$ transition at 1520 Gauss.

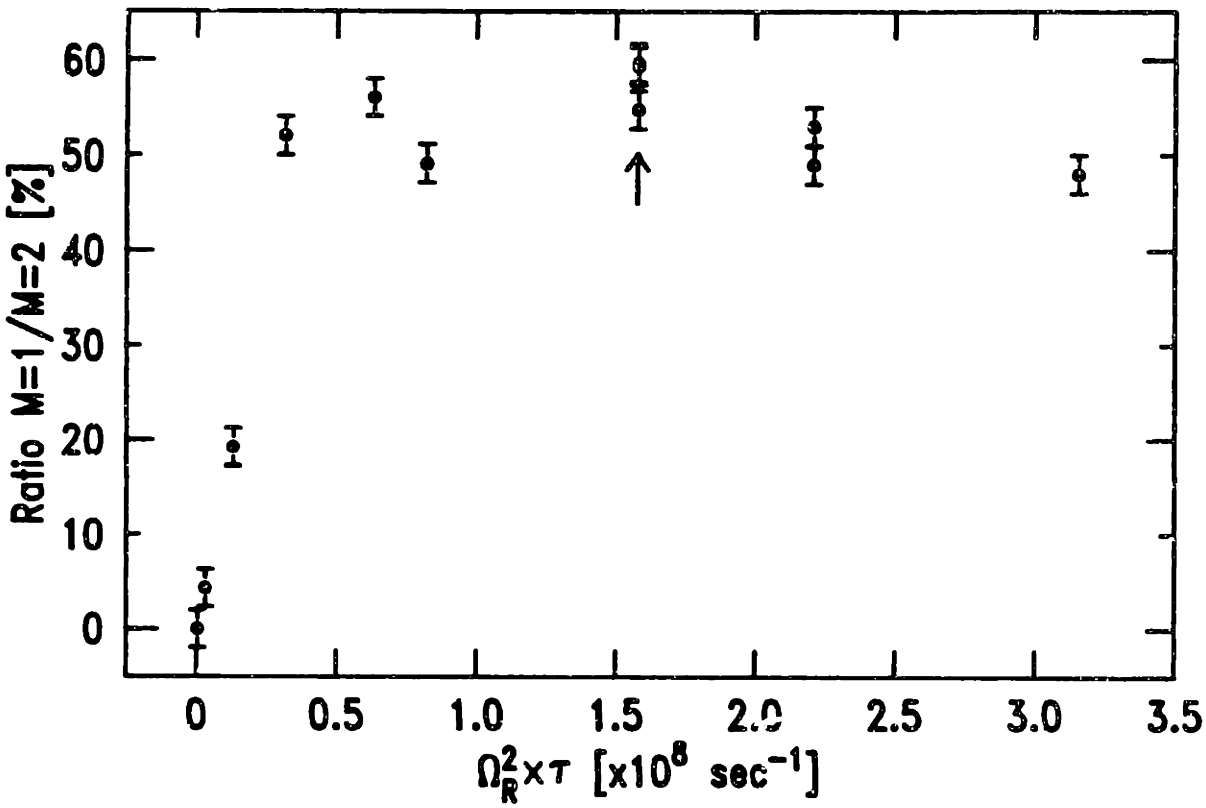

Figure 5.3: Saturation of the transfer of population between $|F=2, M=2\rangle$ and $|F=2, M=1\rangle$ trapped substates as a function of the power($\Omega_R{}^2$)×duration(τ) of the applied rf pulse. The applied rf pulse was at the frequency corresponding to maximum transfer of population. The arrow indicates where we typically performed the rf experiments.

From table 5.1, we see that the branching ratio for the excited $|F'=3,\ M'=2\rangle$ state to decay to the ground state $|F=2,\ M=1\rangle$ is 0.98 hence as the laser power decreases to zero we would expect the ratio of the peak height of the $|F=2,\ M=1\rangle \rightarrow |F'=3,\ M'=2\rangle$ to that of the $|F=2,\ M=2\rangle \rightarrow |F'=3,\ M'=3\rangle$ transition to approach 0.98, if the initial population in each of the ground state magnetic sublevels were equal. The ratio of the two peak heights in the final fluorescence scan of figure 5.2 is 0.97, very close to 0.98, indicating near perfect saturation of the rf transition at the applied rf frequency. In addition, the ratio being very close to 0.98 implies that, at this low probe intensity, we were scattering less than one photon per atom and the effects of heating and/or optical pumping from the probe laser were negligible (since each scattering event, involving two photons, imparts only ~2 μK of recoil energy to the trapped atom) during the scan period in which the laser frequency increased from its initial value to the value corresponding to the peak of the resonance for the $|F=2,\ M=1\rangle \rightarrow |F'=3,\ M'=2\rangle$ transition, [a time interval of 18 sec for the scan of figure 5.2(c)].

The question, "How far above saturation are we?" was addressed by the following experiment. Again, an rf pulse was applied to the trapped atoms at a frequency allowing maximum equilibration of population between the $|F=2,\ M=1\rangle$ and $|F=2,\ M=2\rangle$ ground state, and the ratio of the corresponding peak heights in the fluorescence scan was then determined. This procedure was repeated as a function of varying rf power (or correspondingly,

varying Ω_R) and the rf pulse duration τ. Figure 5.3 is a plot of the ratio of the peak heights of the fluorescence spectra from atoms in the $|F=2, M=1\rangle$ and $|F=2, M=2\rangle$ magnetic substates as a function of $\Omega_R{}^2 \times \tau$, which is proportional to the number of rf photons in the pulse. From the location of the arrow on figure 5.3, which indicates where we typically performed rf resonance measurements, we see that we were saturating the rf transition. Our inability to operate significantly further within the saturation zone of figure 5.3 was limited by experimental considerations: in the case of Ω_R, by the maximum output from the rf generating electronics, and in the case of τ, by the maximum storage time of the trapped atoms.

5.3 RF RESONANCE CURVE

An rf resonance curve for a sample of trapped atoms for the $|F=2, M=2\rangle$ to $|F=2, M=1\rangle$ transition was obtained by inducing rf transitions, and subsequently measuring the relative peak heights for the two states in the fluorescence spectrum as a function of the frequency of the applied rf pulse. As the height of each peak in the fluorescence spectrum depends linearly on the number of trapped atoms in that state, by measuring the relative peak heights we obtain an rf resonance curve that is insensitive to variations in the number of trapped atoms. Two different implementations of this optical-double resonance technique were used in obtaining an rf resonance curve.

A. Load and Pulse Method

The first implementation, which we will call the "load and pulse" method, involves the following sequence of events.

1. A sample of atoms is loaded into the trap.
2. An rf pulse, of fixed power and duration, and frequency is applied to the trapped atoms.
3. A fluorescence spectrum is then taken from which the relative peak heights for the two states is obtained.

The procedure is then repeated on a new sample of trapped atoms with an rf pulse of same power and duration but at a different frequency. In this manner, we obtained the rf resonance curves of figure 5.4(a) and (b).

This method has the advantage of not requiring very long confinement times for the trapped atoms (the rf scan of figure 5.4 required ~30 seconds per point), and, more importantly, the sample of atoms one starts with is in only one magnetic substate hence one is sensitive to any population transfer from the initial magnetic substate to another magnetic substate due to the applied rf pulse (provided of course, that one can detect the fluorescence from atoms in the other magnetic substate) and not just a monotonically increasing population transfer which would result from an rf scan on the same sample of trapped atoms. On the other hand, this method has the disadvantage that it is sensitive to load to load variations in the energy distribution of the trapped atoms.

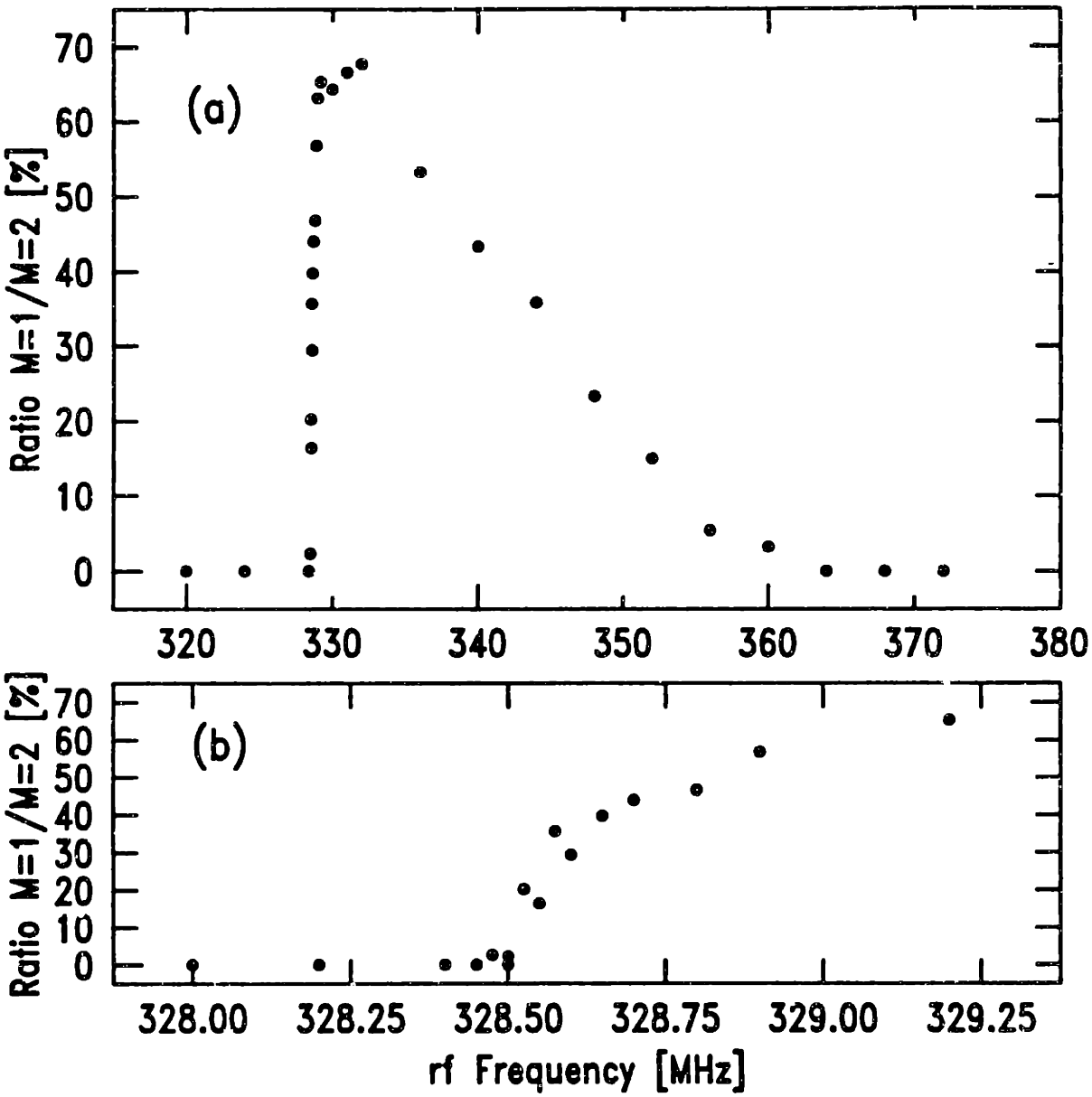

Figure 5.4: rf resonance lineshape for the |F=2, M=2⟩ to |F=2, M=1⟩ transition using the "load and pulse" method. The sharp rise at 328.5 MHz, expanded in (b), corresponds to atoms at the minimum magnetic field of the trap (error bars are about the size of the points).

B. Semi-Continuous Scan Method

The second implementation, which we will call the "semi-continuous scan" method, requires the following sequence of steps to obtain an rf resonance curve.

1. A sample of atoms is loaded into the trap.
2. An rf pulse, of fixed power and duration, and frequency is applied to the trapped atoms.
3. A fluorescence spectrum is then taken from which the relative peak heights for the two states is obtained.
4. Another rf pulse of same power and duration but at a different rf frequency is applied to the trapped atoms and a fluorescence spectrum is subsequently taken.

The procedure is repeated on the *same sample* of trapped atoms, each time monotonically varying the rf frequency (eg. low to high frequency). After the rf frequency has been monotonically scanned to cover the entire extent of the rf resonance curve, a new sample of atoms is loaded into the trap and the procedure of applying rf pulses followed by fluorescence measurements is repeated except that the rf frequency is monotonically scanned in the other direction (eg. high to low frequency). The result is the rf resonance curve of figure 5.5, where the monotonically increasing portion of the curve was obtained by scanning the rf frequency from low to high on a sample of trapped atoms and the monotonically decreasing portion of the curve was obtained by scanning the rf frequency from high to low on a second sample of trapped atoms.

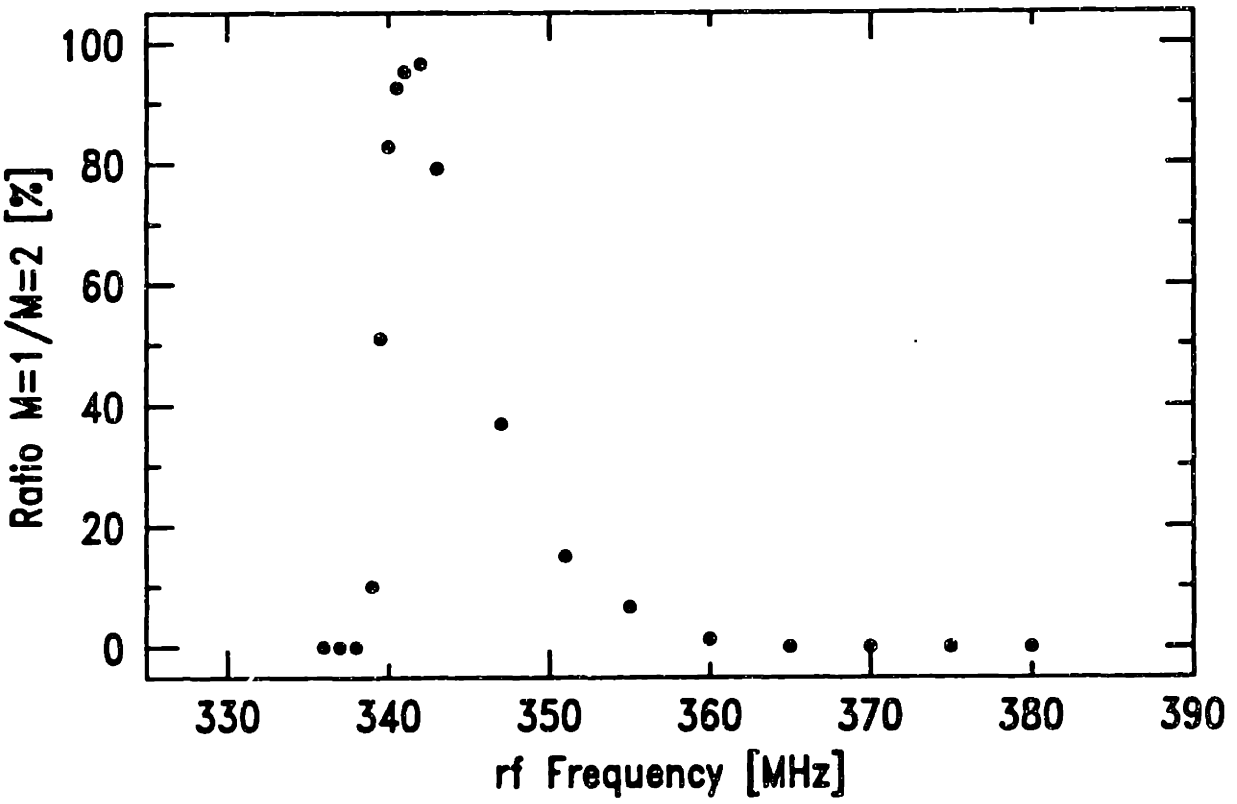

Figure 5.5: rf resonance lineshape for |F=2, M=2⟩ to |F=2, M=1⟩ transition using the "continuous scan" method (error bars are about the size of the points).

This method has the obvious advantage that there will be considerably less point to point scatter due to load to load variations in the energy distributions of the trapped atoms since the entire rf resonance curve is obtained from only two samples of trapped atoms. However, since this method is only sensitive to a monotonically increasing transfer of population from the initial magnetic substate to the other magnetic substate, to resolve any structure of the rf lineshape (possibly due to several local minimums in the trap), one would need more than two samples of trapped atoms.

The major disadvantage of this method is that it requires sufficiently long trapping times (the rf scan of figure 5.5 took ~20 minutes per sample of atoms). Therefore the rf scan is much more sensitive to perturbations that modify the energy distribution of the trapped atoms. If the collision rate of the trapped atoms is sufficiently high we would expect the rf resonance curve, for a scan decreasing in rf frequency, to indicate a net population transfer greater than the actual population transfer at a particular rf frequency. The reason for this is that collisions will redistribute atoms which have already undergone an rf transition into energy states which have yet to be addressed by the rf and vice versa; however, a measurement of the population transfer will display all atoms that have undergone an rf transition sometime in their history, regardless of whether the atom is currently being addressed by the rf. This results in an over indication of the amount of

population transfer by the rf frequency currently being applied to the trapped atoms.

We estimate the collision time for our trapped atoms to be greater than 40 seconds [PRI86], which is approximately the length of time between points. No effects of collisions are observed in a comparison of the rf scan taken with the "semi-continuous scan" method to the rf scan taken with the "load and pulse" method. As the energy change addressed by the rf from point to point is ~1 mK, no noticeable effect of collisions implies that the average energy transfer per collision during the time interval from point to point is less than 1 mK.

In addition to collisions, this method is more sensitive to heating and cooling effects from the probe laser, as the same sample of trapped atoms is probed many times, compared to only once with the "load and pulse" method. However, at the probe laser intensities used for the measurements in figure 5.5, we were scattering ~1 photon per atom per point and the ~20 μK of heating resulting from 10 scans of one sample of trapped atoms, is negligible compared to the several mK average temperature of the sample.

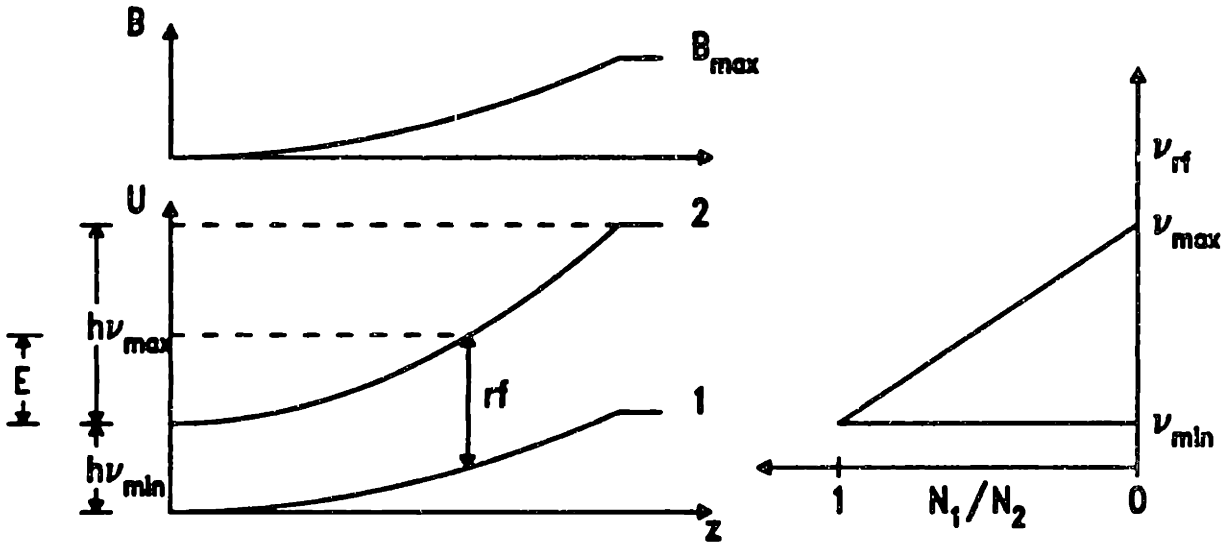

Figure 5.6: A schematic representation of a harmonic magnetic field of finite depth, the corresponding trap potentials for an atom in magnetic substate 1 and 2, and the resulting rf lineshape from the transfer of population from state 1 to state 2 for a uniform distribution of atoms in the trap.

5.4 GENERAL EXPLANATION OF THE RF RESONANCE LINESHAPE

The general features of the rf resonance curve can be explained by considering the simple, picture of a magnetic trap shown in figure 5.6. The confining magnetic field is of finite depth and is symmetric about its one minimum point. The two trapped magnetic substates, designated 1 and 2, have different magnetic moments and hence correspondingly different energies in the magnetic potential. As the energy difference between the two levels increases monotonically with magnetic field, the rf frequency is resonant only with atoms at one value of the magnetic field, and the applied rf (being a reversible process), transfers half of those atoms in the initial substate, *that have sufficient total energy to reach this value of magnetic field*, into the other substate. Thus the resulting rf lineshape has the following general form:

1. At low rf frequencies, the signal is zero as no transitions are induced since no trapped atoms can be in a magnetic field below the trap minimum.
2. At an rf frequency corresponding exactly to the trap minimum, the curve should have a sharp rise to the maximum value since all atoms eventually pass through the minimum magnetic field region and undergo rf transitions.
3. As the frequency is further increased, the rf resonates with atoms at correspondingly higher magnetic fields. Since the number of atoms with sufficient energy to reach this value of the magnetic field decreases with increasing

magnetic field, the height of the curve decreases monotonically with increasing fields or correspondingly, increasing rf frequency.

4. At an rf frequency corresponding to the maximum magnetic field, the signal is zero and remains zero for all rf frequencies above this value; since the magnetic trap cannot contain atoms with energy greater than this value there are no atoms available to undergo an rf transition, hence no transfer of population is observed.

The rf resonance curves of figure 5.4(a) and 5.5 clearly display the features predicted from this simple model. The curve of figure 5.4(a) starts out at zero for low rf frequencies and at ~328.5 MHz there is a sharp rise of the curve where the rf is resonant with atoms at the trap minimum (B_{min}=1520 Gauss). For the values of magnetic field used to confine the atoms (~1500-2300 Gauss), the energy difference between the two levels increases monotonically with magnetic field [d(E/h)/dB ~60 kHz/G; see figure 2.1] and since the rf is resonant only with atoms at one value of the magnetic field, as the rf frequency is further increased, the height of the curve decreases monotonically as there are fewer atoms available to undergo rf transitions. At approximately 360 MHz, the lowest saddle point on the lip of the trap is reached (~2300 Gauss); nearly all atoms energetic enough to reach this value of the field escape from the trap within the time scale of these measurements, and so the signal is essentially zero above this value.

A detailed scan of the rising edge of the rf resonance curve, of figure 5.4(a) was also performed using the "load and pulse" method and is shown in figure 5.4(b). The width of the rising edge is ~250 kHz and may be a reflection of the lack of saturation in the process of population transfer in this region of the curve: The atoms may not have had sufficient time during the application of the rf pulse to find the region of magnetic field where they would be resonant with the rf radiation and undergo an rf transition. This effect should be most pronounced at low rf frequencies, since the spatial region where the atoms are resonant with the rf decreases with decreasing magnetic field, possibly approaching a point for the magnetic field minimum. In addition, the motion of the trapped atoms may not be sufficiently ergodic. That is, there may be states of well defined angular momentum about the axis of the trap which does not allow the atom to access the region near the axis. If these atoms are detected in a fluorescence scan, this would result in a decrease in the ratio of population between the two substates for rf frequencies resonant with atoms near the axis of the trap. The apparent structure in the leading edge of the curve may also reflect the magnetic field irregularities resulting from the use of an octopole field for radial confinement, which as mentioned earlier, results in an off-axis annular magnetic field minimum.

CHAPTER VI

rf Lineshape Model

A simple model of the rf lineshape is described which assumes a truncated Boltzmann distribution for the atoms in the trap. From a fit of this model to the measured rf resonance curve, we extract a temperature for the trapped atoms. In addition, we present a method by which the lineshape may be "inverted" to yield the energy distribution of the trapped atoms.

6.1 SIMPLE MODEL OF THE RF LINESHAPE

The extremely small natural linewidth of the ground state hyperfine levels makes rf spectroscopy of these levels a sensitive probe of the magnetic field in which the transition took place, and therefore a high-resolution probe of the energy distribution of atoms in a magnetic trap. For this reason, it is desirable to construct a model of the rf lineshape from which the energy distribution of trapped atoms can be obtained.

The rf resonance lineshape was obtained by inducing rf transitions from the $|F=2, M=2\rangle$ to $|F=2, M=1\rangle$ magnetic substate, and subsequently measuring the relative peak heights for the two states in the fluorescence spectrum as a function of the frequency of the applied rf pulse. Any other transition could be used, but the process of loading the trap produced a sample of trapped atoms initially in the $|F=2, M=2\rangle$ magnetic substate.

We shall construct a simple model of the rf resonance lineshape in which we assume a truncated Boltzmann distribution for the atoms in the trap, and saturation in the transfer of population between the two magnetic substates. In addition, we shall make the following assumptions about the fluorescence detected when measuring the relative number of atoms in each magnetic substate:

1. Doppler shifts are negligible.
2. The effect of gravity is negligible.
3. We detect fluorescence only from atoms located at the minimum of the trap.

We shall begin by considering the assumptions in regard to the fluorescence detected and then the assumptions about the rf transitions

A. Assumptions About the Fluorescence Detected

The number of photons emitted N_M, by the trapped atoms in a magnetic substate M, during a fixed time interval is proportional to the number of atoms at a magnetic field B multiplied by the Zeeman absorption profile of an atom at that magnetic field, integrated over all trapped atoms. Thus,

$$N_M \propto \int d^3x \int d^3p \frac{1}{(\mu_M B/\hbar)^2 + (\Gamma/2)^2} P_M(E) \qquad (6.1)$$

where $B(\vec{r})$ is the magnetic field, Γ is the natural linewidth of the laser transition, E is the energy of an atom, and $P_M(E)$ and μ_M are respectively, the energy distribution and magnetic moment of an atom in substate M of the trap. Since we are only interested in the

amount of fluorescence at the peak of the spectrum, we have taken the laser frequency to be resonant with atoms at the minimum magnetic field. Hence the detuning in the denominator becomes $\mu_M B/\hbar$, where B is measured with respect to the minimum value of the magnetic field in the trap.

We have assumed that the motion of the atoms in the trap is ergodic so that their distribution in the trap is characterized by only their total energy. The geometry of the trapping fields is such that there is no perfect rotational symmetry; angular momentum is not conserved on some time scale. Thus given enough time, the trapped atoms will access all energy allowed states of the trap.

We now make the assumption that we only detect fluorescence coming from atoms at the minimum magnetic field. For a fixed laser frequency, the width of the atomic transition restricts the variation of the magnetic field over which atoms will be excited. That is, most of the fluorescence will come from atoms located in a region of magnetic field where the Zeeman shift is less than or comparable to the natural linewidth of the transition. For the $|F=2, M=2,1\rangle \rightarrow |F'=3, M'=3,2\rangle$ optical transitions in sodium, with a natural linewidth of 10 MHz, this corresponds to a variation of approximately ± 7 Gauss. Thus, we can consider the fluorescence as coming entirely from atoms located at the minimum of the trap if there are no appreciable changes in the occupation of the spatial states of the trap within 7 Gauss of the minimum magnetic field. For a Boltzmann distribution, this translates to a variation of the trapping potential $\Delta U=\mu\Delta B << k_B T$,

or $T >> \mu\Delta B/k_B$ ~0.5 mK for a ΔB of 7 Gauss. From the model of the absorption lineshape in chapter 4, we obtained a temperature for the atoms greater than the depth of the trap (~60 mK) implying that this assumption is valid.

Under this assumption, the integration over positions in equation 6.1 returns a non-zero value only at the point corresponding to the minimum of the magnetic field and so equation 6.1 reduces to,

$$N_M \propto \int_0^{E_{escape}} dE \sqrt{E}\, P_M(E) \tag{6.2}$$

Where we have converted the integration over momenta to an integration over energy, assuming an isotropic velocity distribution. E=0 is the minimum energy of the trap, and E_{escape} is the depth of the trap.

The ratio R, of the heights of the peak in the fluorescence spectrum of the $|F=2, M=1\rangle$ to the $|F=2, M=2\rangle$ state, for a given rf frequency is then,

$$R = \frac{N_1}{N_2} = \frac{\int_0^{E_{escape}} dE \sqrt{E}\, P_1(E)}{\int_0^{E_{escape}} dE \sqrt{E}\, P_2(E)} \tag{6.3}$$

B. Assumptions About the RF Transitions

In constructing the model of the rf lineshape, we make the following assumptions about the process of rf induced transitions:

1. The rf transition is saturated.

2. The rf frequency is resonant with atoms at only one value of the magnetic field.

3. The effect of gravity on the trapped atoms is negligible.

Saturation of the rf transition implies that half the number of atoms in the initial magnetic substate $|F=2, M=2\rangle$, with total energy sufficient to reach the value of magnetic field which is resonant with rf radiation, will be transferred to the other magnetic substate $|F=2, M=1\rangle$. As was shown in the previous chapter, the rf transition appears to have been saturated except possibly near the front edge of the rf curve.

The second assumption is necessarily satisfied since the energy difference, between the two levels in which we are inducing population transfer, increases monotonically with magnetic field (~60 kHz/Gauss) for the values of magnetic field used in these experiments.

The effect of gravity is to displace the minimum of the mechanical confining potential with respect to the minimum of the magnetic field, to a position were the force provided by the magnetic field balances the force due to gravity. This displacement was ~0.5 cm, resulting in an ~1 Gauss change in magnetic field for the

experimental conditions in which the rf resonance curves were obtained. This ~1 Gauss shift due to gravity is negligible compared to the ~375 Gauss broadening of the absorption spectrum (figure 3.5) due to the motion of the atoms in the trap. The assumption that gravity is negligible appears to be valid. With the absence of gravity, there is then a one to one correspondence between potential energy and magnetic field for the trapped atoms and under the second assumption, a one to one correspondence between potential energy and rf frequency.

With these assumptions, we can predict how the application of the rf to the trapped atoms modifies the distribution function $P_M(E)$, for each magnetic substate M, involved. This is represented schematically in figure 6.1. Figure 6.1(a) and (b) shows $P_M(E)$, for the $|F=2, M=2\rangle$ and $|F=2, M=1\rangle$ substates respectively, prior to the application of an rf pulse. The finite depth of the trap is characterized by the truncation of the distribution at E_{escape}. After application of an rf pulse resonant with atoms at a magnetic field corresponding to energy E_{res}, the distribution functions are modified in a manner such that, if P(E) is the initial distribution function for atoms in the $|F=2, M=2\rangle$ state prior to the application of rf, then after the rf pulse, the modified distribution function for the $|F=2, M=2\rangle$ magnetic substate is,

$$P_2(E) = P(E) \quad \text{for } 0 \le E \le E_{res},$$

$$P_2(E) = P(E)/2 \quad \text{for } E_{res} \le E,$$

and for the $|F=2, M=1\rangle$ substate is,

$$P_1(E) = 0 \quad \text{for } 0 \le E \le E_{res},$$

$$P_1(E) = P(E)/2 \quad \text{for } E_{res} \le E.$$

This is represented schematically in figures 6.1(c) and (d).

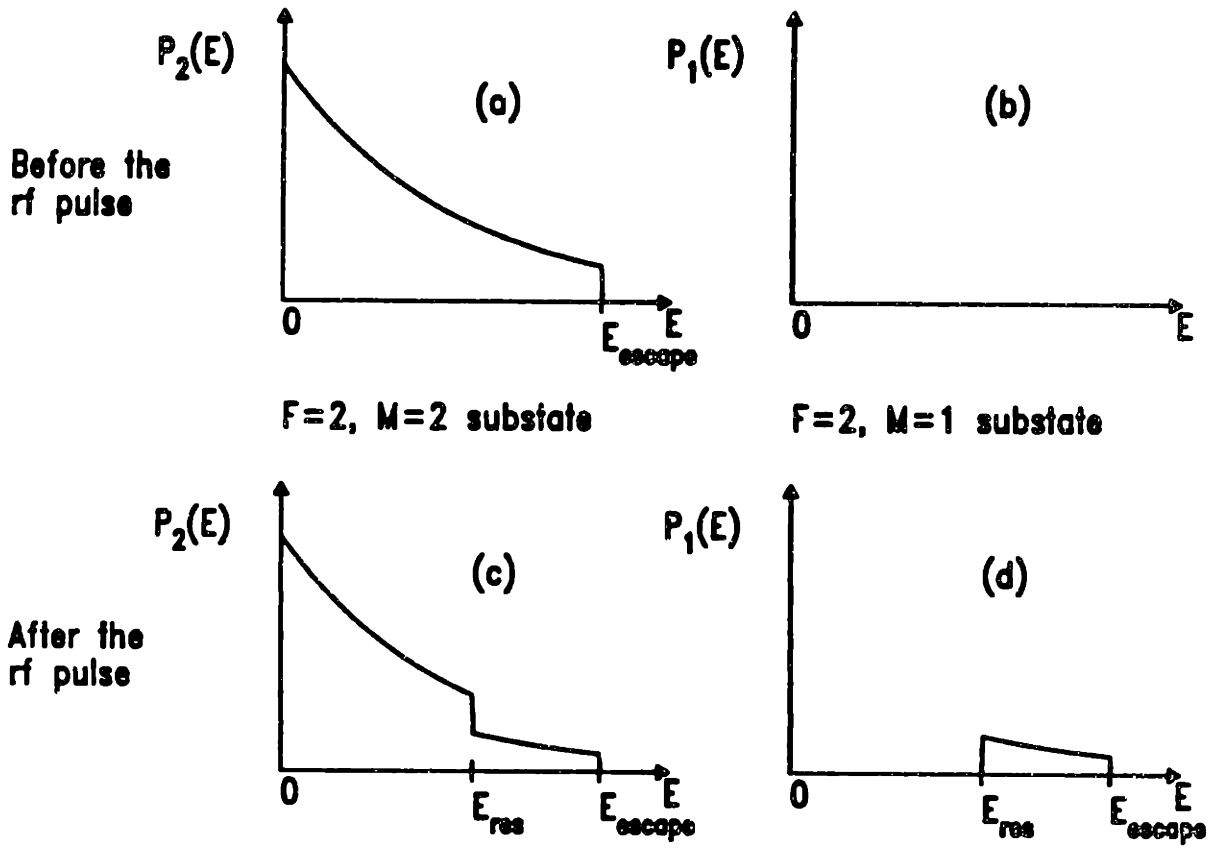

Figure 6.1: Schematic representation of the modification of the distribution function P(E), before and after the rf pulse to transfer population between the $|F=2, M=2\rangle$ and $|F=2, M=1\rangle$ magnetic substates of the trap. (a) before rf, $|F=2, M=2\rangle$; (b) before rf, $|F=2, M=1\rangle$; (c) after rf, $|F=2, M=2\rangle$; (d) after rf, $|F=2, M=1\rangle$.

Using the simple model of the change in $P_M(E)$, shown diagrammatically in figure 6.1, the ratio $R = R(E_{res}, E_{escape})$ of the peak of the fluorescence signal of the $|F=2, M=1\rangle \rightarrow |F'=3, M'=2\rangle$ transition to that of the $|F=2, M=2\rangle \rightarrow |F'=3, M'=3\rangle$ transition, after the application of an rf pulse becomes,

$$R(E_{res}, E_{escape}) = \frac{\frac{1}{2}\int_{E_{res}}^{E_{escape}} \sqrt{E}P(E)dE}{\int_0^{E_{res}} \sqrt{E}P(E)dE + \frac{1}{2}\int_{E_{res}}^{E_{escape}} \sqrt{E}P(E)dE} \qquad (6.4)$$

This function $R(E_{res}, E_{escape})$ for $0 \leq E_{res} \leq E_{escape}$, together with $R \equiv 0$ for $E_{res} < 0$ and $E_{res} > E_{escape}$, is the rf lineshape predicted by our model.

6.2 FIT OF THE SIMPLE MODEL

In order to fit equation 6.4 to the measured rf lineshape, we need to specify the initial energy distribution of the trapped atoms. In view of the reasonable fit, in chapter 4, of the absorption lineshape using a Boltzmann distribution for the trapped atoms, we shall use a Boltzmann distribution as a "trial" function for $P_M(E)$, then equation 6.4 becomes,

$$R(E_{res}, k_BT, E_{escape}) = \frac{\frac{1}{2}\int_{E_{res}}^{E_{escape}} \sqrt{E}e^{-E/k_BT}dE}{\int_0^{E_{res}} \sqrt{E}e^{-E/k_BT}dE + \frac{1}{2}\int_{E_{res}}^{E_{escape}} \sqrt{E}e^{-E/k_BT}dE} \qquad (6.5)$$

A fit of equation 6.5 was made to the data of figures 5.4(a) and 5.5. The applied rf frequency ν_{rf}, is related to E_{res} by the expressions, $E_{res} = \mu(B-B_{min})$ and $h\nu_{rf} = h\nu_{min} + \Delta\mu(B-B_{min})$, where μ is the magnetic moment of the $|F=2, M=2\rangle$ substate (μ/h ~1.4 MHz/Gauss), $\Delta\mu$ is the difference in magnetic moments of the $|F=2, M=1\rangle$ and $|F=2, M=2\rangle$ substates ($\Delta\mu$ ~60 kHz/Gauss), and h is Planck's constant. B is the magnetic field at which atoms are resonant with the rf, B_{min} is the minimum magnetic field of the trap and $h\nu_{min}$ is the energy difference between the $|F=2, M=1\rangle$ and $|F=2, M=2\rangle$ magnetic substates at B_{min}. For the data of figure 5.4(a), B_{min}=1520 Gauss, ν_{min} = 328.5 MHz and E_{escape} = 60 mK. Figure 6.2 shows a fit of the model (rescaled by a factor of 0.7 to account for optical pumping in the fluorescence spectra; see section 5.2) to the data of figure 5.4(a) for three different temperatures (100, 60, 40 mK), from which we obtained an estimate of 60^{+40}_{-20} mK for the temperature of the atoms in the trap. Thus we were justified in neglecting the effect of gravity. In addition, we show rf lineshapes for 2, 5, and 10 mK to demonstrate the substantial narrowing of the width of the rf resonance curve that occurs with decreasing temperature of the trapped atoms.

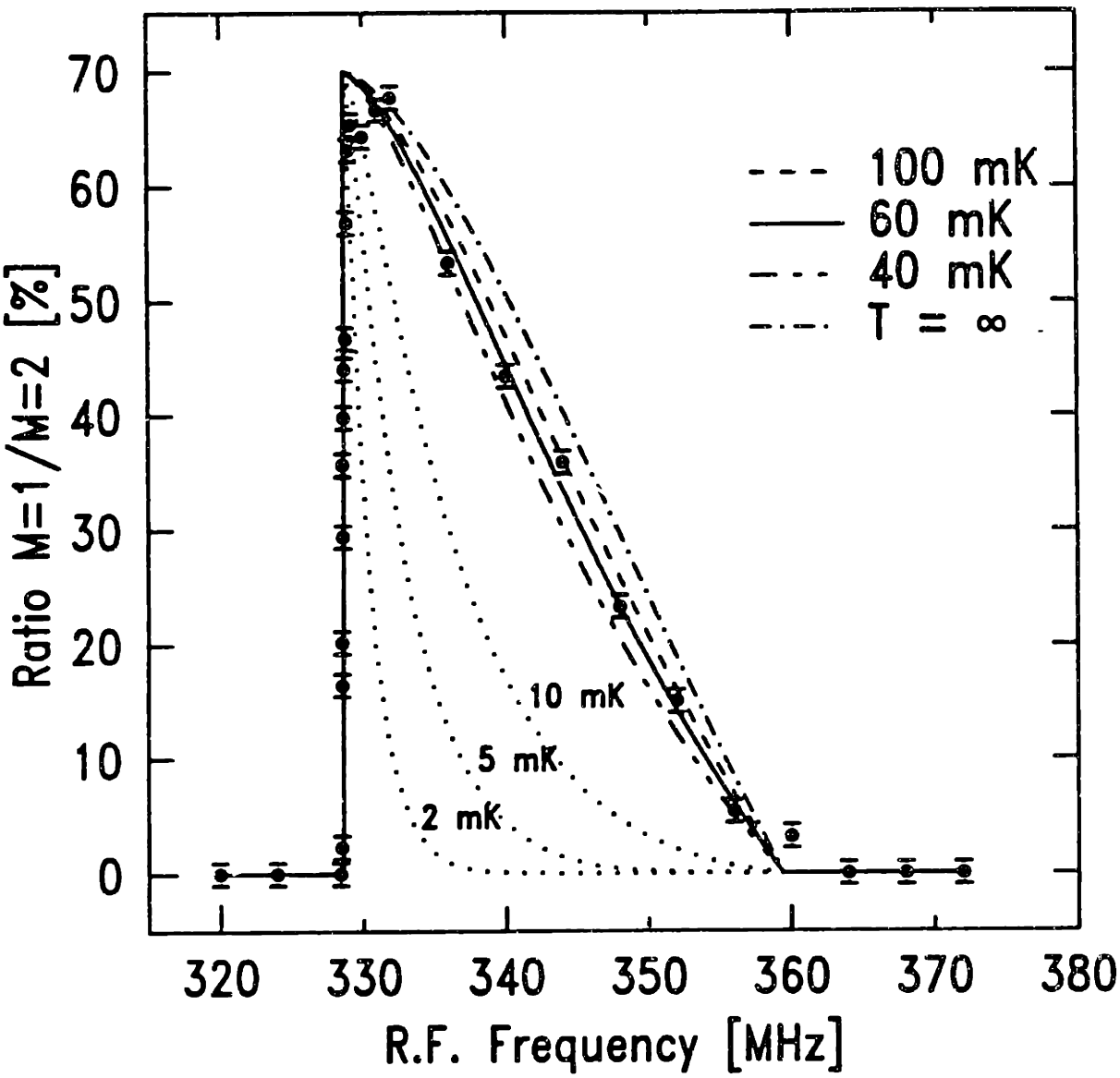

Figure 6.2: Calculated lineshape (curves) fit to the data of figure 5.4(a) taken by the "load and pulse" technique, yielding an estimated temperature for the trapped atoms of 60^{+40}_{-20} mK. A T=∞ curve is also included for comparison. The calculations for 2, 5, and 10 mK show the greatly increased sensitivity to temperature for colder samples.

The most striking result of the fit is the high temperature of the trapped atoms. The result $k_B T \sim E_{escape}$ implies that the atoms are close to being uniformly spread over all possible states within the trap, and like the simple one-dimensional model of chapter 5, the energy distribution is mainly characterized by the truncation at E_{escape} (as is evident by the $T = \infty$ curve of Fig. 6.2). This result confirms the high temperature obtained in the fit of the absorption spectrum in chapter 4. As was mentioned in chapter 4, the high temperature of the trapped atoms is most likely the result of heating in the transverse direction by the intense (>10 mW/cm^2) standing-wave laser beam used to slow and stop atoms in the trap. A more detailed explanation of this phenomena will be given in chapter 7, when we consider Doppler cooling of atoms in the trap.

Figure 6.3 is a best fit of the model to the data of figure 5.5. For this fit, we have taken B_{min}=1710 Gauss, ν_{min}=339 MHz, E_{escape}=48 mK, and T=10 mK. The temperature of the trapped atoms in this case, is substantially lower than the temperature extracted from figure 5.4. A possible explanation for the difference in temperature is that the two different runs differed in the configuration of the octopole field. As was explained in chapter 4, the end effects, due to the finite length of the octopole magnets, can either add to, or subtract (depending on the direction of the current in the magnets) from the field of the longitudinal trap coils thereby raising or lowering the minimum field of the trap. As is evident by the difference in ν_{min}, the octopole field appears to have been

reversed for the two runs (this was also seen in the absorption spectra from the runs). The axial field from the octopole magnet will also modify the field produced by the second slower magnet, used for stopping atoms in the trap (see figures 4.2-5 and the associated explanation in chapter 4). Since the final velocity of atoms being slowed into the trap strongly depends on the "effective" slower magnet profile [BLM J], it is not unreasonable to expect a different temperature for the trapped atoms for the two different octopole magnet configurations.

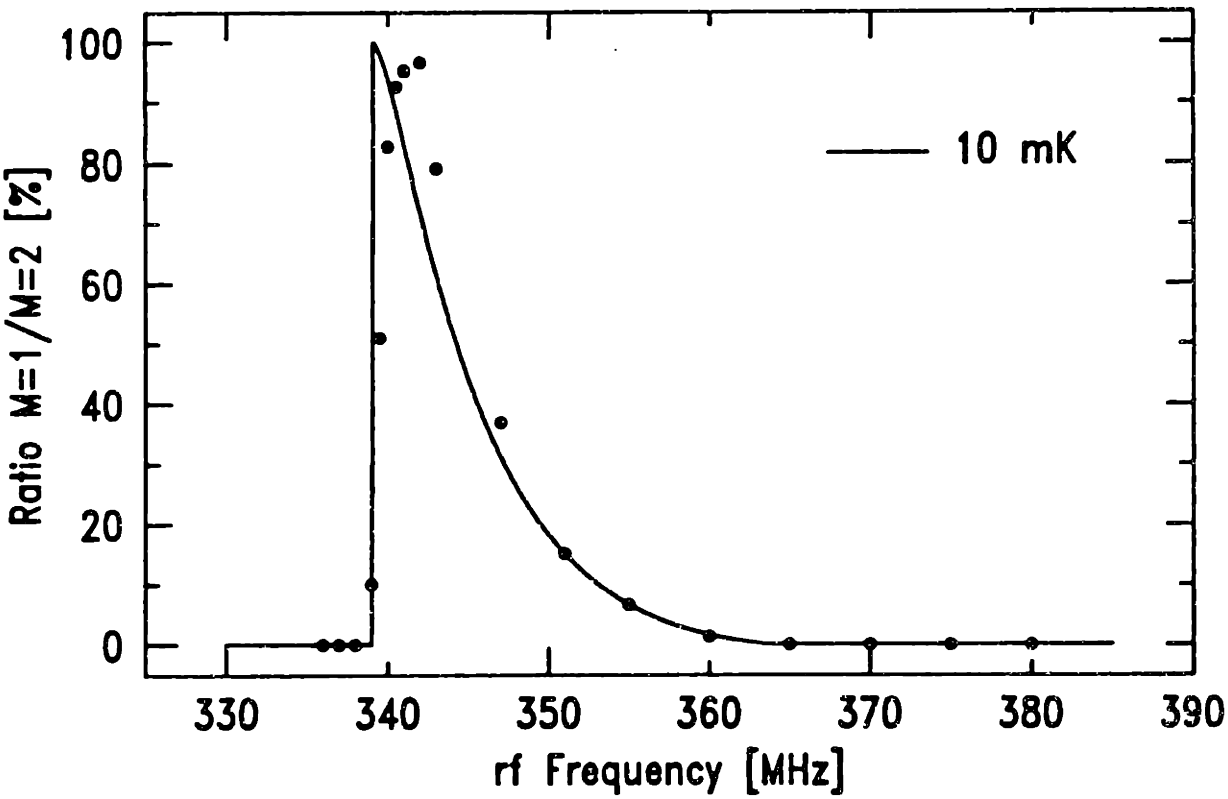

Figure 6.3: Calculated lineshape (curve) fit to the data of figure 5.5 taken by the "continuous scan" technique, yielding an estimated temperature of 10 mK.

The fit of the model to the data of figure 5.4 is much better than the fit to the data of figure 5.5. This is expected since the assumption that the fluorescence, used to determine population differences, comes entirely from atoms at the minimum of the trap becomes a better approximation with increasing temperature. Similarly, one would expect the model to be a better approximation at the high rf frequencies where the energy of the atom in the field of view of the photodetector is mostly translational energy. A better fit of the lineshape, especially at the low frequency end of the curve, might be accomplished by explicitly including the density-of-states as determined by the shape of the confining potential. Another possibility is that the distribution of trapped atoms is not a truncated Boltzmann distribution, but some other more complicated distribution function.

6.3 EXTRACTION OF THE ENERGY DISTRIBUTION

The absence in the simple model of the rf lineshape, of any dependence on the confining potential (Eq. 6.4) implies that it should be possible to extract the form of the energy distribution function from the measured lineshape. More specifically, although we assumed a truncated Boltzmann distribution in fitting the rf lineshape, the assumptions made in constructing the model are valid for any distribution $P_M(E)$; our viewpoint that the process of population transfer by the rf pulse modifies the distribution function does not depend on the explicit form of the distribution function

We start with equation 6.4, the general equation for the rf lineshape and re-express it as,

$$R = \frac{\int_0^{E_{escape}} \sqrt{E}P(E)dE - \int_0^{E_{res}} \sqrt{E}P(E)dE}{\int_0^{E_{res}} \sqrt{E}P(E)dE + \int_0^{E_{escape}} \sqrt{E}P(E)dE} \qquad (6.6)$$

This equation can be manipulated to yield,

$$\int_0^{E_{res}} \sqrt{E}P(E)dE = N\frac{1-R}{1+R} \qquad (6.7)$$

where,

$$N = \int_0^{E_{escape}} \sqrt{E}P(E)dE \qquad (6.8)$$

and so the energy distribution P(E), up to an overall normalization constant is given by,

$$P(E_{res}) = \frac{-2N}{\sqrt{E_{res}}(1+R)^2}\frac{\partial R}{\partial E_{res}} \qquad (6.9)$$

where R is evaluated at E_{res}.

The procedure for generating $P(E_{res})$ from the rf resonance curve $R(E_{res})$ was performed for the data of figures 5.4(a) and 5.5 in the region where R decreases with increasing rf frequency. This was accomplished by approximating $\partial R/\partial E_{res}$ as $(R_1-R_2)/(E_1-E_2)$ where R_1 and R_2 are the ratios of the height of the fluorescence peaks for two consecutive data points at the corresponding energies E_1 and E_2. E_{res}

was taken to be the energy between E_1 and E_2, i.e. $E_{res}=(E_1+E_2)/2$. The error in computing $\partial R/\partial E_{res}$ was taken as the limiting cases for R_1-R_2 due to the uncertainty in R_1 and R_2.

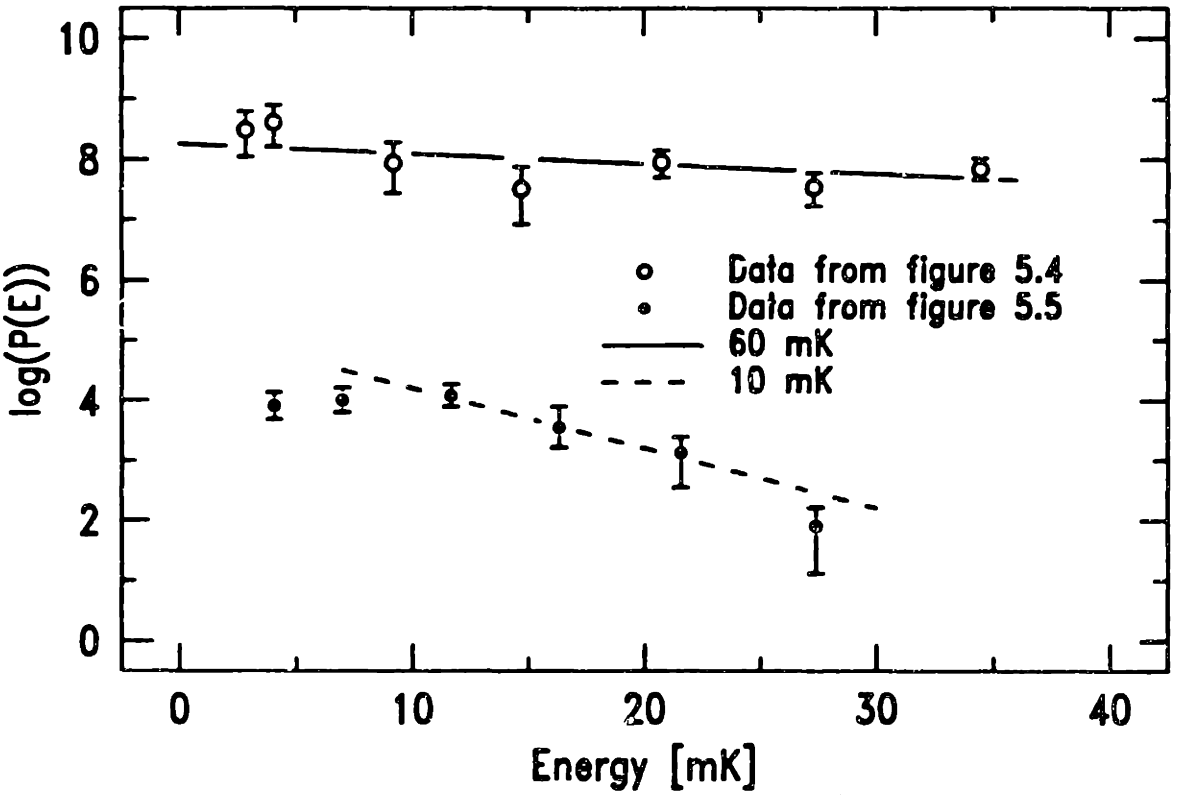

Figure 6.4: Logarithm of the energy distribution P(E), extracted from the rf resonance curves of figures 5.4(a) and 5.5. The corresponding Boltzmann distributions for 60 and 10 mK are shown by the solid and dashed lines respectively.

Figure 6.4 is a plot of the logarithm of the resulting distribution function for the data of figures 5.4(a) and 5.5. In addition, the lines corresponding to a Boltzmann distribution for a temperature of 10 and 60 mK are included for reference. Once again, the rf resonance curve of figure 5.4(a) is well described by a Boltzmann distribution (T=60 mK); the curve of figure 5.5 is fairly well described by a Boltzmann distribution (T=10 mK) for large energies but deviates from this at low energies. This is probably a reflection that there is a significant change in the density-of-states due to the confining potential, over the spatial extent of our fluorescence detection, or that the distribution function is not given by a truncated Boltzmann distribution, or both.

Chapter VII

Doppler Cooling of Atoms in a Magnetic Trap - Theory

A simple model of Doppler cooling of atoms in a trap is described. The cooling laser acts in only one-dimension. The motions in the other dimensions are coupled into the cooling laser by the trap. The ultimate temperature achievable with Doppler cooling for atoms in a harmonic, magnetic trap is also considered.

7.1 DOPPLER COOLING IN OUR MAGNETIC TRAP

An atom moving in a standing wave laser field tuned below the transition frequency of the atom will tend to scatter photons preferentially from the counter-propagating laser beam, which is Doppler shifted closer to resonance. The net momentum transfer from the scattering process results in a velocity dependent force that tends to damp the motion of the atom; this is the essence of Doppler cooling.

Doppler cooling was independently suggested in 1975, for neutral atoms by Hansch and Schawlow [HAS75], and for trapped ions by Wineland and Dehmelt [WID75]. Experimentally, three dimensional Doppler cooling was first demonstrated by Chu et.al. [CHB85]. The resulting viscous force led Chu and co-workers to call three dimensional Doppler cooling, "optical molasses." Subsequent studies of optical molasses [LWW88] has shown that, for multi-level atoms, other velocity dependent processes can occur which can result

in substantial additional cooling of the translational energy of the atoms. For a two-level atom, such processes do not occur [CWD89] and the cooling mechanism in optical molasses is that of Doppler cooling.

In our magnetic trap, the atoms are confined in a region containing a large bias field (~1500 Gauss; see figure 2.2). In this large magnetic field, the various hyperfine levels of the trapped atoms are no longer degenerate and the laser transition used to Doppler cool the trapped atoms was essentially between one ground state hyperfine level and one excited state hyperfine level (see figure 2.1). Therefore, in analyzing Doppler cooling of atoms in a magnetic trap, we will treat the system as a two-level atom.

Optical access in our magnetic trap was limited to the longitudinal direction defined by the large bias field [BAG87]. Thus, we are only capable of directly laser cooling the longitudinal motion. Cooling of the motion in the other directions was accomplished via the transfer of energy between the translational degrees of freedom by the trap.

The axial "pinch" coils, second slower coil and the octopole magnets combine to create a complicated magnetic field that mixes the radial and longitudinal directions such that angular momentum along the axis of the trap is not perfectly conserved. (A more detailed discussion of the magnetic field profile was given in chapter 4.) Thus on some time scale τ_{trap}, the motion of the atom in the longitudinal direction will be transferred into the transverse

direction. Because of the complicated structure of the magnetic fields, there could be several coupling times τ_{trap}, which which would also depend on the energy of the atom. For the analysis that follows, we will assume that the coupling of the transverse and longitudinal motion occurs on only one time scale τ_{trap}. The analysis can be generalized for several different τ_{trap}, and in the limit that the cooling rate is much smaller than the coupling rate, τ_{trap} will be determined by the longest coupling time.

This is then the situation we have when we Doppler cool atoms in our magnetic trap: Neutral atoms are confined in a magnetic trap. The longitudinal and transverse motions in the trap are coupled on a time scale τ_{trap}. Doppler cooling is applied to the trapped atoms along the longitudinal direction.

The question of interest is, "how does the energy of the trapped atoms change with time."

7.2 1-D DOPPLER COOLING OF TRAPPED ATOMS-A SIMPLE MODEL

In order to understand the process of Doppler cooling in a magnetic trap, we present a simple model of weakly confined atoms in the presence of one dimensional standing wave laser beam.

In the model, the role of the trap is simplified in that it only serves to confine the atom and couple the motion orthogonal to the cooling laser to that in the direction of the laser beam. We neglect any shift of the resonant frequency of the atom due to the confining potential. In addition, we consider the motion of the atom in the trap

as that of a free atom, and we examine the change in kinetic energy of the atom averaged over its oscillation in the confining potential. Therefore, we assume that the cooling rate is small compared to the oscillation frequency of the particle in the trap. We shall see later in this chapter that this condition implies that the cooling laser is detuned several linewidths from resonance and attenuated to very low intensities. These are in fact the conditions under which Doppler cooling of trapped atoms was performed and will be presented in chapter 8. In addition, in the experiments to be described in chapter 8, the diameter of the cooling laser was much smaller than the radial extent of the trapped atom cloud, hence only a fraction of the cloud was irradiated. This will result in a longer effective cooling time.

While these approximations are not strictly valid for an atom confined in a magnetic trap (where the frequency shift $\mu B/h$, can be comparable to the energy of the atom $k_B T$), the model does reproduce qualitatively the important experimentally observed results suggesting that those features incorporated into the model correctly characterize the process of Doppler cooling in a magnetic trap. The approximations made will be reflected in the quantitative predictions of the simple model, affecting the ultimate temperature achievable with laser Doppler cooling in a magnetic trap. This issue will be addressed in section 7.3 where we include both the frequency shift and oscillation of the energy of the atom between kinetic and potential energy in a calculation of the minimum energy achievable with Doppler cooling for atoms confined in a harmonic magnetic trap potential.

A. The Effect of the Cooling Laser

We adopt an approach similar to Wineland and Itano [WII79] in calculating the effect of the cooling laser on the atom.

Consider a free atom with velocity $\vec{v}$, in the presence of a travelling wave laser beam of frequency ω and wave vector $k\hat{z}$. The atom absorbs, from the laser, a photon of momentum $\hbar k\hat{z}$ and spontaneously emits a photon of momentum $\hbar k\hat{k}$. Averaged over the direction of the spontaneously emitted photon, the change in the kinetic energy of the atom ΔE, in the x, y, and z direction per scattering event (absorption followed by spontaneous emission) can be derived by considering conservation of energy and momentum during the scattering process.

$$\Delta E_x = \frac{1}{3}E_R \tag{7.1a}$$

$$\Delta E_y = \frac{1}{3}E_R \tag{7.1b}$$

$$\Delta E_z = \hbar k v_z + \frac{4}{3}E_R \tag{7.1c}$$

Where $E_R = \hbar^2 k^2/2m$ is the single photon recoil energy. As we are concerned with the qualitative behavior of the Doppler cooling process for trapped atoms, we make the simplifying assumption that the recoil upon reemission is isotropic. However, we note that isotropic emission is violated for the sodium transition we are using [MAN79].

The average rate of change of the kinetic energy of the atom can be obtained by multiplying the average energy change per scattering event by the rate of absorption of a photon.

$$\frac{dE_i}{dt} = \Gamma \frac{(\omega_R/2)^2}{(\Delta_L - kv_z)^2 + \omega_R^2/2 + (\Gamma/2)^2} \Delta E_i \qquad (7.2)$$

for i=x, y, z. Γ is the natural linewidth of the transition, ω_R is the Rabi frequency and $\Delta_L = \omega - \omega_0$ is the detuning of the laser from the resonant frequency ω_0, of the atom. In addition, we have included the Doppler shift of the laser beam due to the motion of the atom.

Consider the regime where $kv_z << \Gamma$, ie: where the Doppler shift is much less than the natural linewidth. For the sodium D2 line, with $\Gamma = 2\pi \times 10$ MHz, the requirement is $v << 6$ m/s which corresponds to a temperature of ~0.1 K. Since our magnetic trap is ~50 mK deep, we are mostly in this regime. Expanding equation 7.2 in powers of kv_z/Γ, we obtain,

$$\frac{dE_i}{dt} = \Gamma \frac{(\omega_R/2)^2}{\Delta_L^2 + \omega_R^2/2 + (\Gamma/2)^2} \left[1 + \frac{2\Delta_L kv_z}{\Delta_L^2 + \omega_R^2/2 + (\Gamma/2)^2} \right] \Delta E_i \qquad (7.3)$$

We now retro-reflect the laser beam back onto itself to form a standing wave. The atom moving with velocity $\vec{v}$, "sees" a second travelling wave laser beam coming from the opposite direction with respect to the first beam and correspondingly with the opposite Doppler shift. The average rate of change of the kinetic energy of the atom in the presence of the one dimensional Doppler cooling is now (to lowest order in kv_z/Γ),

$$\frac{dE_x}{dt} = 2\Gamma \frac{(\omega_R/2)^2}{\Delta_L^2 + \omega_R^2/2 + (\Gamma/2)^2} \frac{E_R}{3} \tag{7.4a}$$

$$\frac{dE_y}{dt} = 2\Gamma \frac{(\omega_R/2)^2}{\Delta_L^2 + \omega_R^2/2 + (\Gamma/2)^2} \frac{E_R}{3} \tag{7.4b}$$

$$\frac{dE_z}{dt} = 2\Gamma \frac{(\omega_R/2)^2}{\Delta_L^2 + \omega_R^2/2 + (\Gamma/2)^2} \left[\frac{8\Delta_L}{\Delta_L^2 + \omega_R^2/2 + (\Gamma/2)^2} \frac{E_R}{\hbar} E_z + \frac{4}{3} E_R \right] \tag{7.4c}$$

or more compactly,

$$\frac{dE_x}{dt} = \frac{E_R}{\tau_{heat}} \tag{7.5a}$$

$$\frac{dE_y}{dt} = \frac{E_R}{\tau_{heat}} \tag{7.5b}$$

$$\frac{dE_z}{dt} = -\frac{E_z}{\tau_{cool}} + \frac{4E_R}{\tau_{heat}} \tag{7.5c}$$

with

$$\frac{1}{\tau_{heat}} = \frac{2}{3}\Gamma \frac{I/I_{sat}}{\delta^2 + 2I/I_{sat} + 1} \tag{7.6a}$$

$$\frac{1}{\tau_{cool}} = -\Gamma \frac{32\delta(I/I_{sat})}{(\delta^2 + 2I/I_{sat} + 1)^2} \frac{E_R}{\hbar\Gamma} \tag{7.6b}$$

Where we have defined $(\omega_R/\Gamma)^2 = I/I_{sat}$ and the dimensionless detuning $\delta = \Delta_L/(\Gamma/2)$.

The effect of the cooling laser on the kinetic energy of the atom is described by equations 7.5 and 7.6. For $\delta<0$, the laser provides damping of the motion.

B. Thermalization by the Trap

Clouds of trapped ions are routinely cooled by a single laser beam [LBB86]. Collisions between the trapped ions give rise to the transfer of energy between the various degrees of freedom, allowing the entire distribution of trapped ions to be cooled. Wineland and Itano [WII79] considered the situation where a single laser beam is used to cool a collection of bound atoms, and the rate of transfer of the kinetic energy between the x, y, and z directions occurs at a characteristic collision rate γ_c. They specifically considered the case where the laser is detuned a half linewidth below resonance. We generalize this approach for arbitrary detuning, and use $1/\tau_{trap}$ as the characteristic rate for the transfer of energy from one direction into another direction. Thus equation 7.5a, b, and c are modified to,

$$\frac{dE_x}{dt} = \frac{E_R}{\tau_{heat}} + \frac{1}{\tau_{trap}}\left(\frac{E_y}{2} + \frac{E_z}{2} - E_x\right) \qquad (7.7a)$$

$$\frac{dE_y}{dt} = \frac{E_R}{\tau_{heat}} + \frac{1}{\tau_{trap}}\left(\frac{E_x}{2} + \frac{E_z}{2} - E_y\right) \qquad (7.7b)$$

$$\frac{dE_z}{dt} = -\frac{E_z}{\tau_{cool}} + \frac{4E_R}{\tau_{heat}} + \frac{1}{\tau_{trap}}\left(\frac{E_x}{2} + \frac{E_y}{2} - E_z\right) \qquad (7.7c)$$

With τ_{heat} and τ_{cool} given by equations 7.6a and b, respectively.

C. The Cooling Limit

The minimum energy achievable can be estimated by considering the cooling process to be in steady state so that the average change in the kinetic energy is zero. Setting $dE_i/dt = 0$ in

equation 7.7a, b, and c, we solve for the steady state energies $(E_i)_{min}$ and obtain

$$(E_z)_{min} = 6\frac{\tau_{cool}}{\tau_{heat}} E_R \qquad (7.8a)$$

$$(E_x)_{min} = (E_y)_{min} = 6\frac{\tau_{cool}}{\tau_{heat}} E_R\left[1 + \frac{\tau_{trap}}{3\tau_{cool}}\right] \qquad (7.8b)$$

For $\delta<0$, the motion along the cooling laser is damped. However, if $\tau_{trap} >> \tau_{cool}$, the other directions will be substantially heated by photon recoil. This is the process that we alluded to, in chapters 4 and 6, to explain the high temperature of the atoms just after loading of the trap.

The standing wave laser used for stopping atoms in the trap typically had an intensity of $\sim I_{sat}$, and was detuned ~80 MHz to the red of resonance for atoms at the bottom of the trap. According to equation 7.6a and b, this would give a $\tau_{heat}=6\times10^{-6}$ sec and $\tau_{cool}=2\times10^{-3}$ sec respectively. If we take τ_{trap} to be ~1 sec, which is several times the oscillation period of the atom in the trap, then we find, from Eq. 7.8b that the minimum energy in the motion orthogonal to the cooling laser is ~300 mK. This shows how substantial heating of the trapped atom sample could occur while loading atoms into the trap. However, since the laser beam does not irradiate the entire trap, the atoms may eventually leave before their energy reaches this value.

In general, we are only interested in the total energy of the atom. Hence we can combine equations 7.8a, and b to obtain the total minimum energy $E_{min} = (E_x)_{min} + (E_y)_{min} + (E_z)_{min}$,

$$E_{min} = 6\frac{\tau_{cool}}{\tau_{heat}} E_R \left[3 + \frac{2\tau_{trap}}{3\tau_{cool}}\right] \qquad (7.9)$$

Figure 7.1 is a plot of E_{min} vs. laser detuning for 4 different laser intensities. A value of τ_{trap}=1 sec was used in the plot. The main result of this plot is that to achieve mK temperatures ($\hbar\Gamma$ ~1 mK), one has to go to very low cooling laser intensities even for modest detunings of several times the natural linewidth.

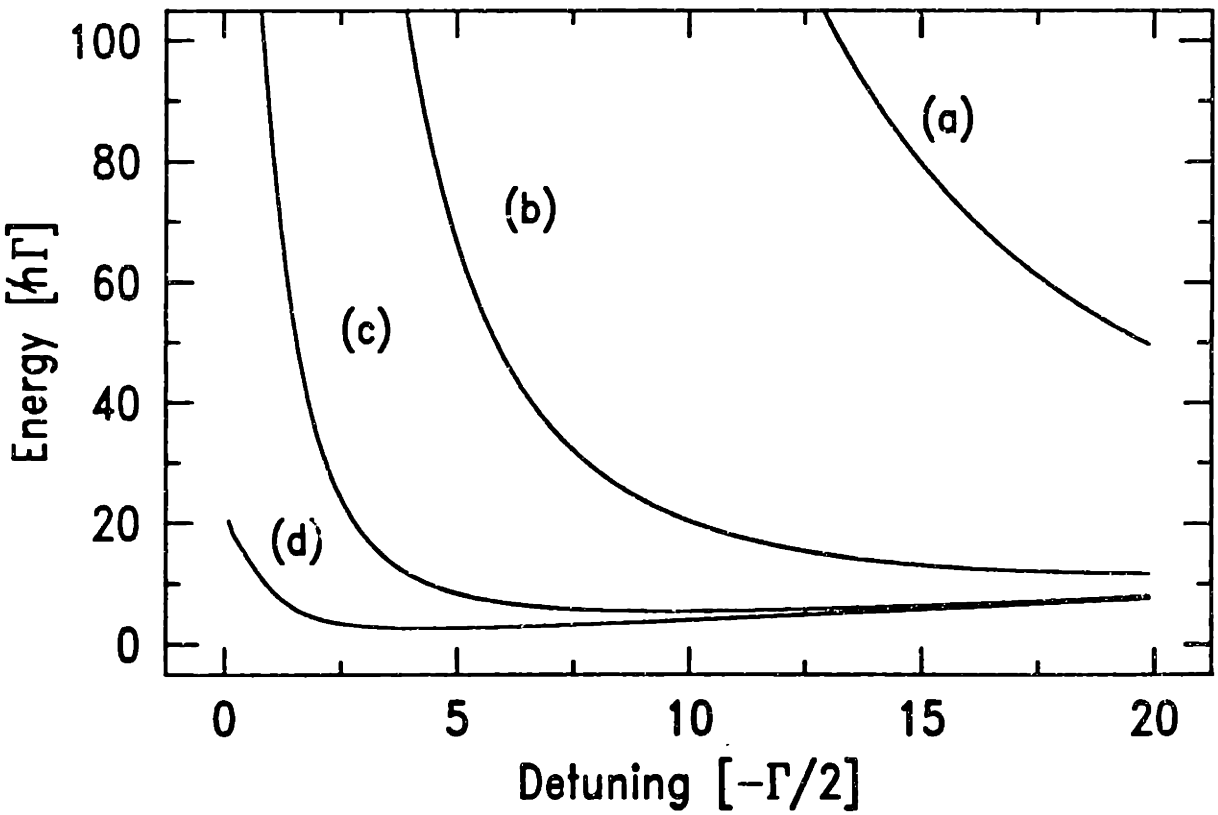

Figure 7.1: Plot of the minimum energy E_{min}, vs. laser detuning predicted for I/I_{sat} equal to (a) 10^{-1}, (b) 10^{-2}, (c) 10^{-3}, and (d) 10^{-4}, and a coupling time of 1 second.

D. Toward the Cooling Limit

We can also examine the time dependence of the energy of the atom by solving equation 7.5a, b, and c directly. For an initial energy E_{init}, and dE/dt=0 before the cooling laser is turned on at time t=0, we obtain for all t>0 while the cooling laser is on,

$$E = (E_{init} - E_{min})\, e^{-t/2\tau} \cosh\left[\frac{t}{2\tau}\sqrt{1-\frac{2\tau^2}{\tau_{cool}\tau_{trap}}}\right] + E_{min} \qquad (7.10a)$$

with

$$\frac{1}{\tau} = \frac{1}{\tau_{trap}}\left[\frac{3}{2} + \frac{\tau_{trap}}{\tau_{cool}}\right] \qquad (7.10b)$$

and E_{min} defined by equation 7.9.

The dimensionless quantity $(E-E_{min})/(E_{init}-E_{min})$ as a function of the dimensionless time t/τ_{trap} for different values of τ_{trap}/τ_{cool} is shown in figure 7.2. To achieve the lowest E_{min}, we want $\tau_{trap}/\tau_{cool} << 1$, and from figure 7.2, we see that this requires correspondingly longer application times of the cooling laser beam to the trapped atoms. That is, several mixing times are required to achieve the lowest temperatures. Hence, the general prescription for achieving the lowest temperatures with Doppler cooling for atoms in a trap is to go to very low cooling rates and apply the cooling for a long time compared to the characteristic coupling time of the trap.

A final comment on figure 7.2; for $\tau_{cool} \leq \tau_{trap}$, the energy at some time is less than E_{min}. This corresponds to cooling the atom in

one-dimension with the minimum amount of transverse heating. Since the direction along the cooling laser is completely damped, there will be no further reduction in the total energy of the atom and only heating will occur while the energy in the transverse direction is being transferred into the longitudinal direction.

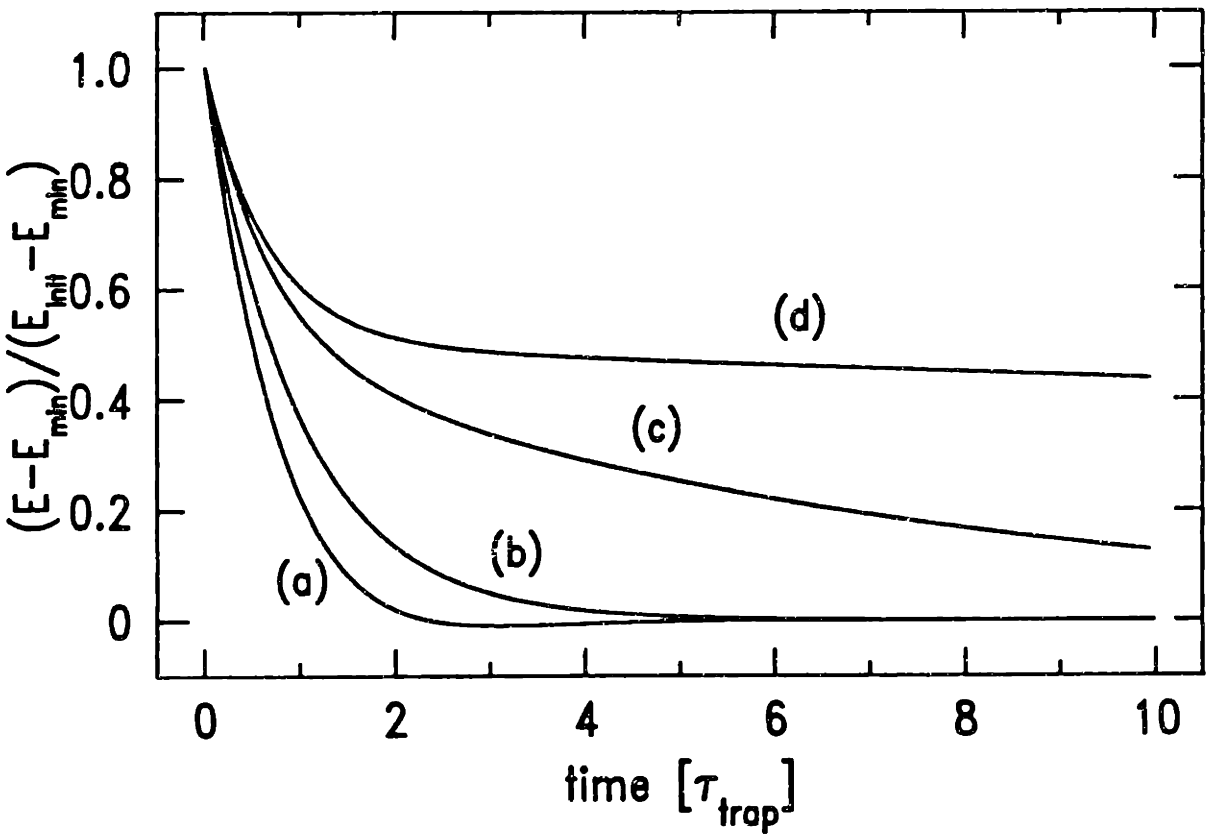

Figure 7.2: Plot of $(E-E_{min})/(E_{init}-E_{min})$ vs. time for t_{trap}/t_c equal to (a) 1, (b) 0.5, (c) 0.1, and (d) 0.01.

7.3 ULTIMATE COOLING LIMIT IN A MAGNETIC TRAP

We now consider the ultimate cooling limit of an atom subject to three-dimensional Doppler cooling in a spherically symmetric, harmonic magnetic trap.

In the trap, the atoms are no longer free atoms and thus their total energy E, is given by the sum of kinetic T, and potential U, energy. In addition, we now include the shift of the resonant frequency of the atom by the confining potential $U=\mu B$. Starting with equation 7.3, we have,

$$\frac{dE}{dt} = 2\Gamma \frac{(\omega_R/2)^2}{(\Delta_L - U/\hbar)^2 + (\Gamma/2)^2}\left[\frac{8(\Delta_L - U/\hbar)}{(\Delta_L - U/\hbar)^2 + (\Gamma/2)^2}\frac{E_R}{\hbar}T + 2E_R\right] \qquad (7.11)$$

We have taken the low intensity limit since we wish to consider the case where the cooling rate is much less than the oscillation frequency of the atoms in the trap (typically < 500 Hz).

For a harmonic potential, in the limit that the cooling rate is much less than the oscillation frequency of the atom in the trap $\Omega_{trap}/2\pi$, the potential energy is related to the total energy by,

$$U = E\cos^2(\Omega_{trap}t + \phi_o) \qquad (7.12)$$

The constant ϕ_o is determined by the potential energy of the atom at t=0.

Equation 7.11, 7.12 and the expression for the total energy E=T+U, can be combined to determine the time dependence of the energy of the atom in the magnetic trap.

We now look for the energy of the atom averaged over an oscillation period $\langle E \rangle$, in the limit as $t \rightarrow \infty$. In this limit, $\langle E \rangle$ approaches a constant value $\langle E \rangle_{lim}$ and $d\langle E \rangle/dt \rightarrow 0$. Figure 7.3 is a plot of the time averaged energy from equation 7.11 in this limit, as a function of cooling laser detuning. The detuning that minimizes $\langle E \rangle_{lim}$ occurs at $\Delta_L \approx -\Gamma/2$, with a corresponding $\langle E \rangle_{lim}$ ~400 μK. This energy is almost a factor of two larger than the corresponding limit for free atoms of 240 μK [WII79] reflecting that on average, only half the total energy of the atom is kinetic energy and Doppler cooling directly damps only the kinetic energy of the atom. The fact that the limiting energy for atoms in a magnetic trap is less than a factor of two larger than the limiting energy for free atoms is due to the confining magnetic potential which shifts the resonant frequency of the atom away from the frequency of the cooling laser as the motion of the atom in the trap converts kinetic energy into potential energy. This reduces the amount of heating that an atom will experience when it is at the turning point in its motion, i.e. when its kinetic energy is zero and the effect of the laser is only heating of the atom.

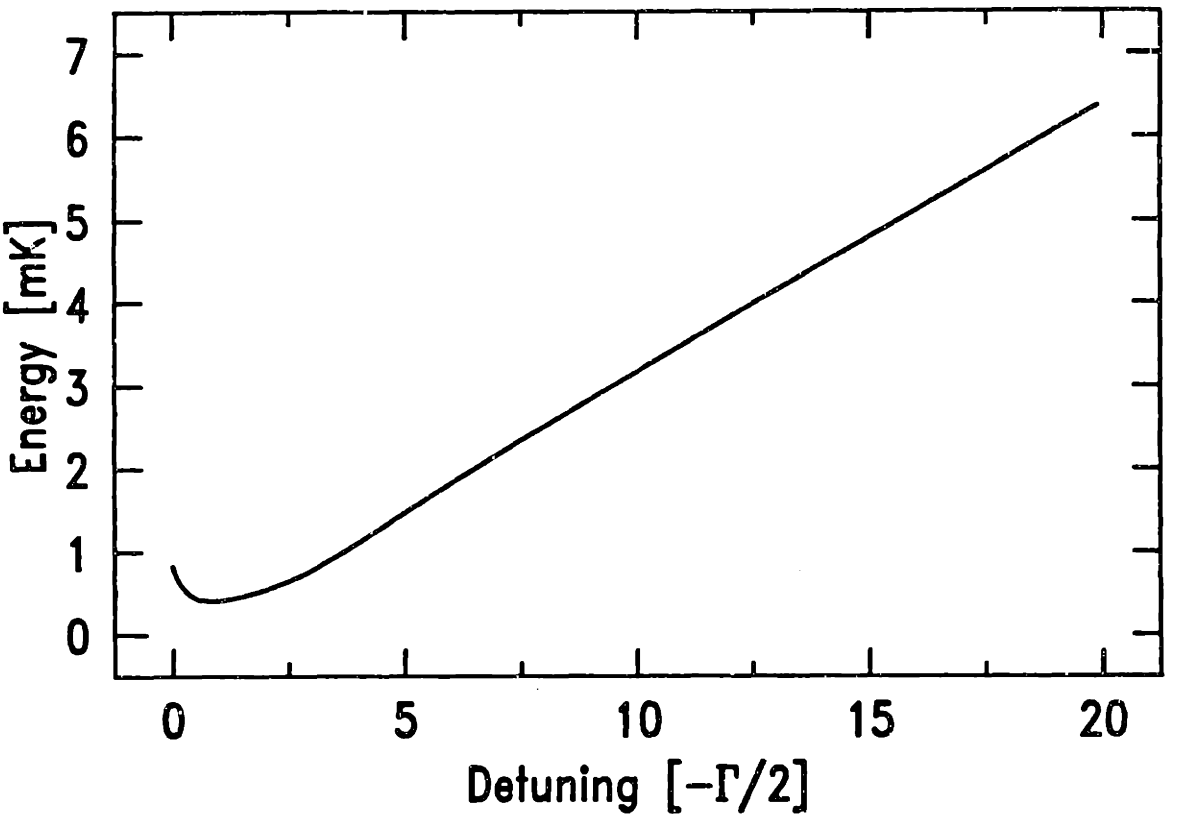

Figure 7.3: Plot of the energy of the atom averaged over one oscillation period of the trap in the limit as $t \rightarrow \infty$, as a function of cooling laser detuning.

Chapter VIII

Doppler Cooling in a Magnetic Trap - Experiments

One dimensional optical molasses was used to Doppler cool atoms in a magnetic trap. Coupling of the longitudinal and transverse motions of the atoms by the trap enabled the total energy of the trapped atoms to be cooled. A substantial narrowing of the line shape was observed in the laser absorption and rf resonance spectra obtained following Doppler cooling of the atoms. This led to an enhancement in the absolute density of trapped atoms, as observed in the absorption spectra.

8.1 GENERAL DESCRIPTION OF THE COOLING PROCESS

Doppler cooling is a powerful technique which allows trapped particles to be cooled to milliKelvin temperatures. Its effectiveness, demonstrated on trapped ions [WII87] and neutral atoms confined in light traps [RPC87] is impressive. This chapter describes the first experiments on Doppler cooling of magnetically trapped atoms. A reduction of more than a factor of 10 in the thermal energy of the trapped atoms was observed following the application of Doppler cooling.

Doppler cooling of the magnetically trapped atoms was performed in the following manner: A sample of atoms was loaded into the trap. The frequency of the standing wave laser beam, used for probing the trapped atoms (section 3.1), was detuned with

respect to the resonant frequency corresponding to atoms located at the minimum value of the magnetic field. The intensity of the laser beam was also set to a predetermined value. The laser beam was then applied to the trapped atoms for a fixed length of time. Laser fluorescence, absorption and rf resonance measurements were subsequently performed on the sample of trapped atoms.

The application of optical molasses in our magnetic trap was complicated by the fact that we had limited optical access. We were only able to apply the cooling laser along the longitudinal direction. This required the use of the trap itself to couple the transverse and longitudinal motions of the atoms so that the total energy of the sample of atoms could be reduced. In addition, the cooling laser beam diameter (~1 cm) was less than the radial extent of the trap (±2.4 cm). This reduced the amount of time the atom spent in the cooling laser to less than the amount of time the cooling laser was on.

In the absence of collisions, the typical time scale for the trap to transfer energy between the degrees of freedom τ_{trap}, is greater than or equal to the oscillation period of an atom in the trap which is ~0.1 seconds. From the discussion in the previous chapter, cooling is most effective when the characteristic cooling time τ_{cool}, is much greater than τ_{trap}. This is so that heating (due to the random nature of the spontaneously emitted photon [WII79]) of the motion orthogonal to the damped direction during the cooling process is kept to a minimum on a time scale τ_{trap}. In order to increase τ_{cool} to longer than 0.1 seconds, the cooling laser had to be detuned several

linewidths below resonance and attenuated several orders of magnitude below saturation intensity (see Eq. 7.6b). In addition, the cooling laser was applied for a time much longer than τ_{trap}. When $\tau_{cool} >> \tau_{trap}$, several coupling times are required to achieve an appreciable reduction of the energy of the trapped atoms.

8.2 ABSORPTION SPECTRA OF DOPPLER COOLED AND HEATED ATOMS

Absorption spectra of trapped atoms, following the application of the Doppler cooling laser, was obtained by recording the decrease in the intensity of a weak probe beam passing (twice) through the cloud of atoms as a function of the laser detuning. Figures 8.1(a), (b), and (c) are typical absorption spectra of trapped atoms for various Doppler cooling laser parameters. The absorption spectrum of figure 8.1(a) is for trapped atoms just after loading of the trap and before the application of Doppler cooling to the trapped atoms. The line shape is discussed at some length in chapter 3.

A typical absorption spectrum taken after applying one-dimensional optical molasses to the trapped atoms is shown in figure 8.1(b). In this case, the cooling laser was applied for 10 seconds at a detuning of -100 MHz and an intensity of 0.25 mW/cm^2 (τ_{cool} ~5 sec; computed from Eq. 7.6b). Substantial cooling of the trapped atoms is reflected by the narrower linewidth and increased maximum value of the absorption. From the simple arguments given in chapter 3 (figure 3.6), we see that the width of the absorption spectrum depends on the energy of the trapped atoms. For example, the second dip occuring at the high frequency end of the absorption

spectrum of figure 8.1(a) corresponds to absorption by atoms located around the top of the second slower magnetic field, which is ~25 mK higher in potential energy than the minimum of the trap. The absence of this second dip in the absorption spectrum of figure 8.1(b) indicates a substantial decrease in the number of atoms with energy large enough to reach this point. The increase in absorption, at the frequency corresponding to the minimum value of the magnetic field, implies that there is an enhancement in the number of atoms located near the minimum of the trap. From this, it is clear that the Doppler cooling process we applied to the trapped atoms, was not merely removing energetic atoms from the trap, but was reducing their energy.

Evidence of "Doppler heating" of the trapped atoms can be seen in figure 8.1(c). In this case, the laser beam was applied to the trapped atom sample for 5 seconds at a detuning of −10 MHz and an intensity of 0.025 mW/cm^2 (τ_{cool} ~3 msec). The substantial decrease in the first dip at the low frequency end of the absorption spectrum relative to the second dip indicates heating of low energy atoms in the minimum of the trap. The overall decrease in absorption implies that atoms have been heated out of the confining potential.

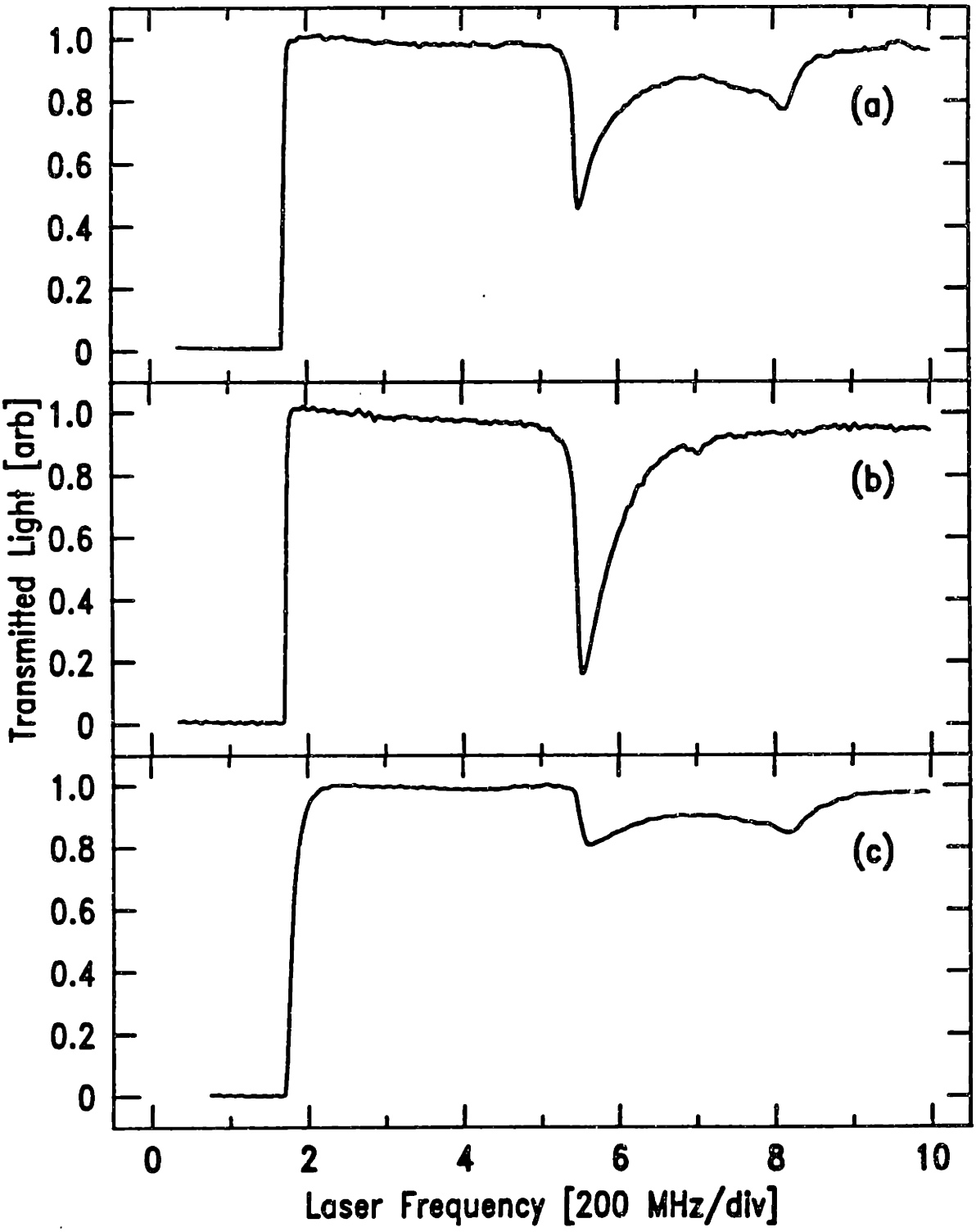

Figure 8.1: Absorption spectra of trapped atoms taken (a) just after loading the trap, (b) after Doppler cooling, (c) after "Doppler heating."

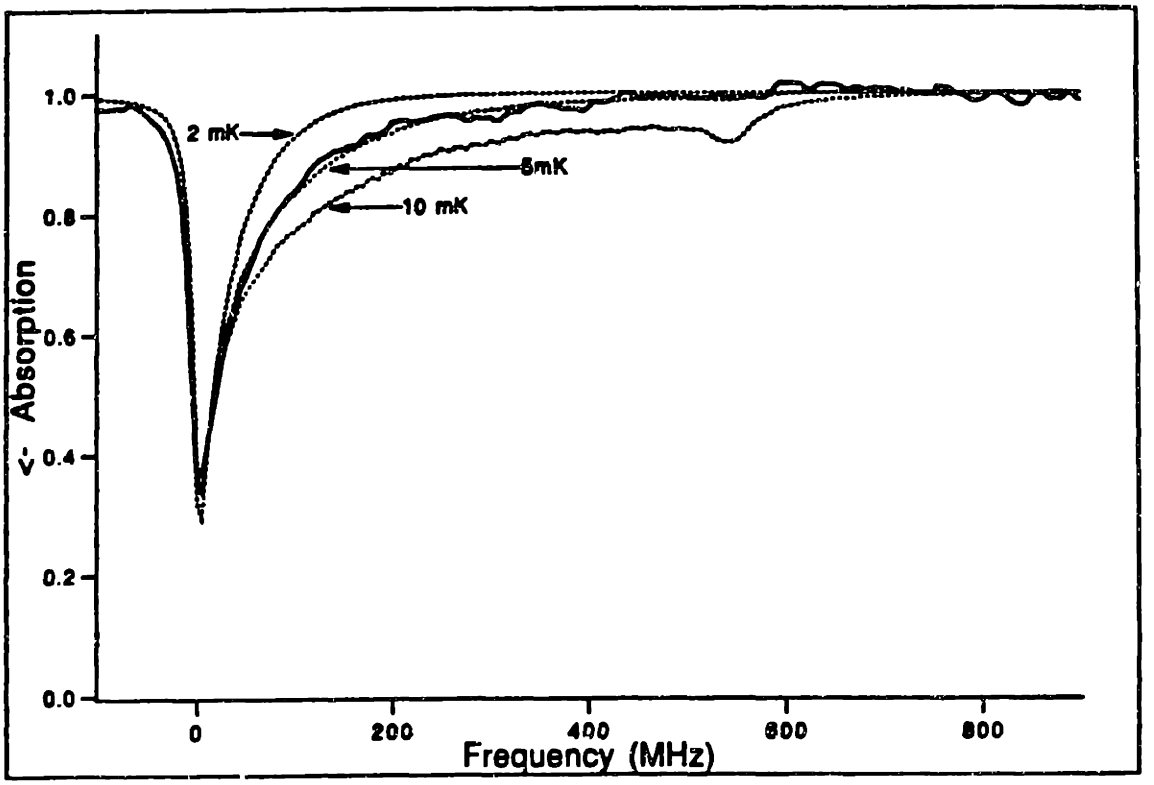

Figure 8.2: Absorption spectrum of Doppler cooled atoms and three calculated lineshapes (see chapter 4) for temperatures of 2, 5, and 10 mK.

Fit of the Absorption Spectrum of Doppler Cooled Atoms

We performed a fit of the model of the absorption lineshape, described in chapter 4, to a typical absorption spectrum of Doppler cooled atoms. Figure 8.2 shows the absorption spectrum and corresponding fit of the calculated lineshape. The absorption spectrum corresponds to trapped atoms after the application of the cooling laser for 30 seconds at a detuning of -120 MHz and an intensity of 2.5 $\mu W/cm^2$ (τ_{cool} ~33 seconds). A measured axial magnetic field profile corresponding to the axial "pinch" coils at 60 amps, the second slower coil at 28 amps, and the octopole magnet at +120 amps was used in the calculated lineshape. The best fit of the calculated line shape to the measured absorption spectrum was obtained with an $N=10^{11}$ for the total number of trapped atoms and a T=5 mK for the temperature in the Boltzmann distribution for the trapped atoms. This fit is quite good and for comparison, we include calculated lineshapes at 2 and 10 mK.

We can make a comparison of the minimum energy predicted by the simple model of the previous chapter for one-dimensional Doppler cooling of trapped atoms. The minimum energy is given by equation 7.9, and substituting equations 7.6a, and 7.6b for τ_{heat}/τ_{cool}, the minimum energy can be re-expressed as,

$$E_{lim} = \frac{3\hbar\Gamma}{8}\frac{\left(\delta^2 + 2I/I_{sat} + 1\right)}{\delta}\left[1 + \frac{2\tau_{trap}}{3\tau_{cool}}\right] \qquad (8.1)$$

Where Γ is the natural linewidth of the transition and δ is the detuning of the laser in units of $\Gamma/2$. For the laser cooling parameters used in the Doppler cooling of the sample of atoms corresponding to figure 8.2, δ=24 and $I/I_{sat} \sim 10^{-4}$. With $\hbar\Gamma \sim 1$ mK, we obtain $E_{min} \approx 6(1 + 2\tau_{trap}/3\tau_{cool})$ mK. The fit of the absorption spectrum of figure 8.2 produced a temperature of 5 mK for the distribution of Doppler cooled, trapped atoms. This is in agreement with the predicted temperature of the simple model and is consistent with $\tau_{cool} > \tau_{trap}$.

8.3 RF RESONANCE OF DOPPLER COOLED ATOMS

We performed rf resonance experiments on Doppler cooled atoms. One-dimensional optical molasses was applied to a sample of trapped atoms for 60 seconds. The cooling laser was detuned by ~-80 MHz and attenuated to an intensity of 20 $\mu W/cm^2$ ($\tau_{cool} \sim 12$ seconds). An rf resonance curve of the Doppler cooled atoms for the $|F=2, M=2\rangle$ to $|F=2, M=1\rangle$ ground state hyperfine transition was then obtained using the "semi-continuous scan" method, as described in chapter 5. Figure 8.3 shows an rf resonance curve obtained with Doppler cooled atoms. For comparison, we include the rf resonance curve of uncooled atoms from figure 5.4(a) (rescaled to 100%). A substantial narrowing of the resonance curve is observed for Doppler cooled atoms, reflecting that the sample of atoms have insufficient energy to reach the large values of magnetic field corresponding to the higher rf frequencies. In addition, we include a "best" fit of the rf lineshape model, as discussed in chapter 6. The inexact fit of the

model to the data could be due to a breakdown of the assumptions that went into the model. As discussed in chapter 6, these assumptions become less valid for distributions of trapped atoms at lower temperatures.

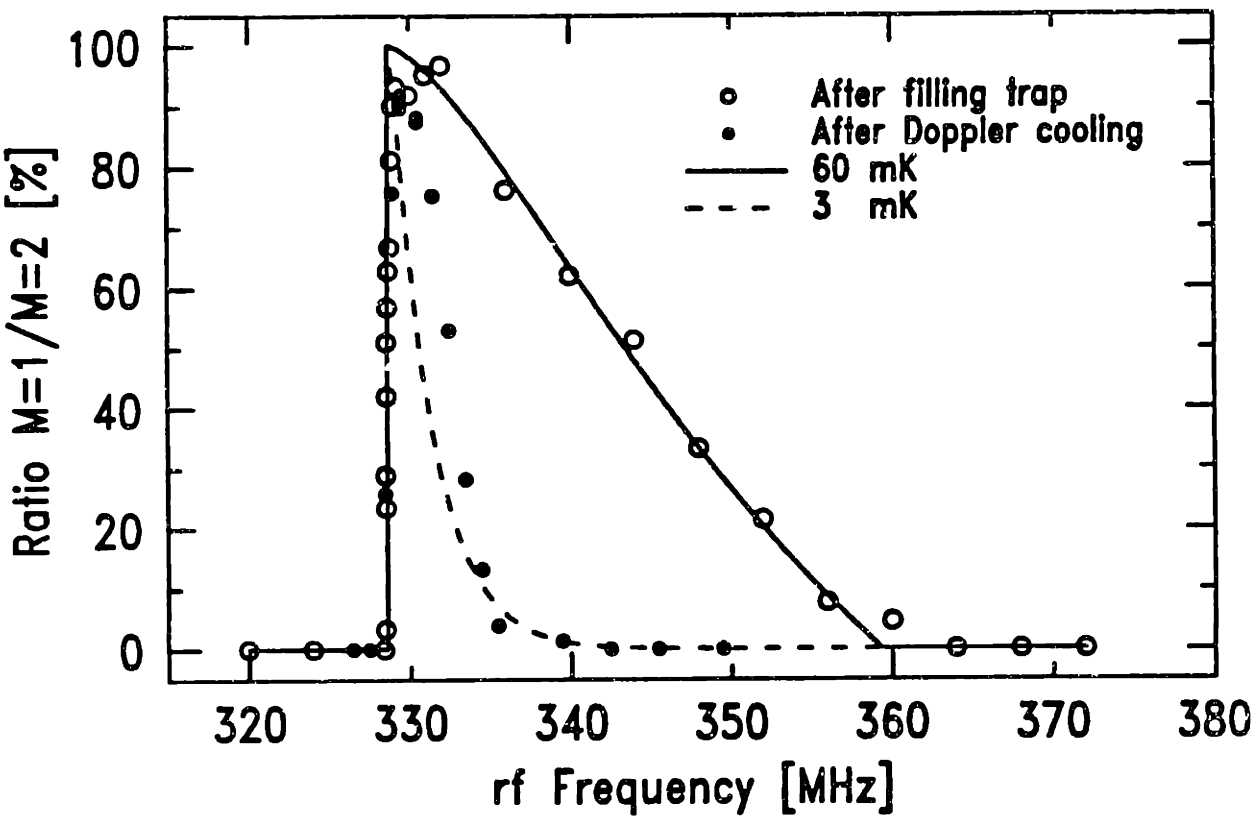

Figure 8.3: An rf resonance curve of Doppler cooled atoms, taken with the "semi-continuous scan" method (see chapter 5). The dashed line corresponds to the rf lineshape model, for a temperature of 10 mK. The rf resonance curve and calculated lineshape of figure 6.2, for uncooled atoms is included to emphasize the narrowing of the lineshape following Doppler cooling.

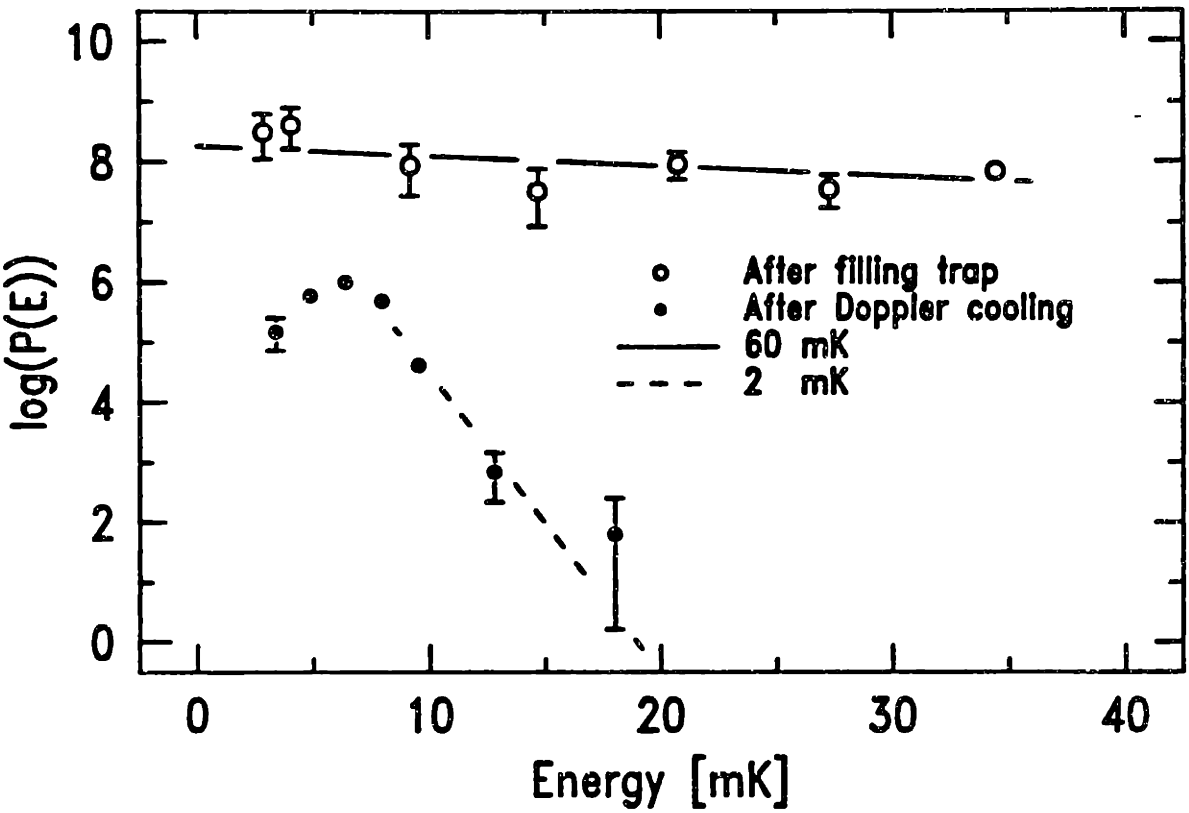

Figure 8.4: Logarithm of the energy distributions of trapped atoms extracted from the rf resonance curves of figure 8.3.

Extracted Energy Distribution of Doppler Cooled Atoms

The energy distribution P(E), of the Doppler cooled atoms can be extracted from the rf resonance curve using the procedure described in chapter 6. The procedure was performed and the logarithm of the extracted energy distribution (up to an overall normalization constant) is shown in figure 8.4. The dashed line corresponds to a Boltzmann distribution with a temperature of 2 mK. The deviation of the energy distribution from that of a Boltzmann distribution could be a result of Doppler cooling in only one dimension without sufficient thermalization of all the motions. More likely, it represents a breakdown of the assumptions made in the construction of the rf lineshape model from which the energy distribution is extracted. The assumptions become less valid for lower temperature distributions of atoms as was discussed in chapter 6.

8.4 ENERGY OF THE TRAPPED ATOMS VS. COOLING TIME

Measurements were made of the effective temperature of the trapped atoms as a function of the length of time the cooling laser beam was applied to the atoms. The change in the energy distribution of the trapped atoms was monitored by measuring the relative peak heights in the fluorescence spectra obtained from detectors 1 and 2, which are located at different values of the magnetic field. Due to their finite field of view, the height of the peak of the fluorescence spectrum from each detector reflects the

number of atoms resonant in a region in front of the detector. From figure 2.3, we see that detector 2 is located a an axial position corresponding to a magnetic field ~200 Gauss (~14 mK) higher than the value of the field where detector 1 is located. A measurement of the ratio of the peak height from detector 2 to that of detector 1 is therefore a measurement of the relative number of atoms with sufficient energy to reach the value of magnetic field in front of detector 2.

The cooling laser beam, at a fixed detuning and power, was applied to the trapped atoms for a predetermined length of time. A fluorescence spectrum of the trapped atoms was subsequently obtained from detector 1 and 2, from which the ratio of the height of the fluorescence peaks from detector 2 to that of detector 1 was extracted. Figure 8.5 is a series of plots of this ratio as a function of the length of time the cooling laser beam was applied to the trapped atoms, for two different values of laser detuning and two different laser intensities.

The decrease in the number of atoms with sufficient energy to reach detector 2 as a function of the length of time the cooling laser was on, is in qualitative agreement with the predictions from chapter 7. For $\tau_{cool} < \tau_{trap}$, the cooling process should be characterized by an initial rapid decrease in the energy of the trapped atoms, followed by a slower, more gradual decrease toward a minimum value of their energy. For $\tau_{cool} >> \tau_{trap}$, the decrease in the energy of the atoms

should be less abrupt and approach more slowly, a much lower value for the minimum energy.

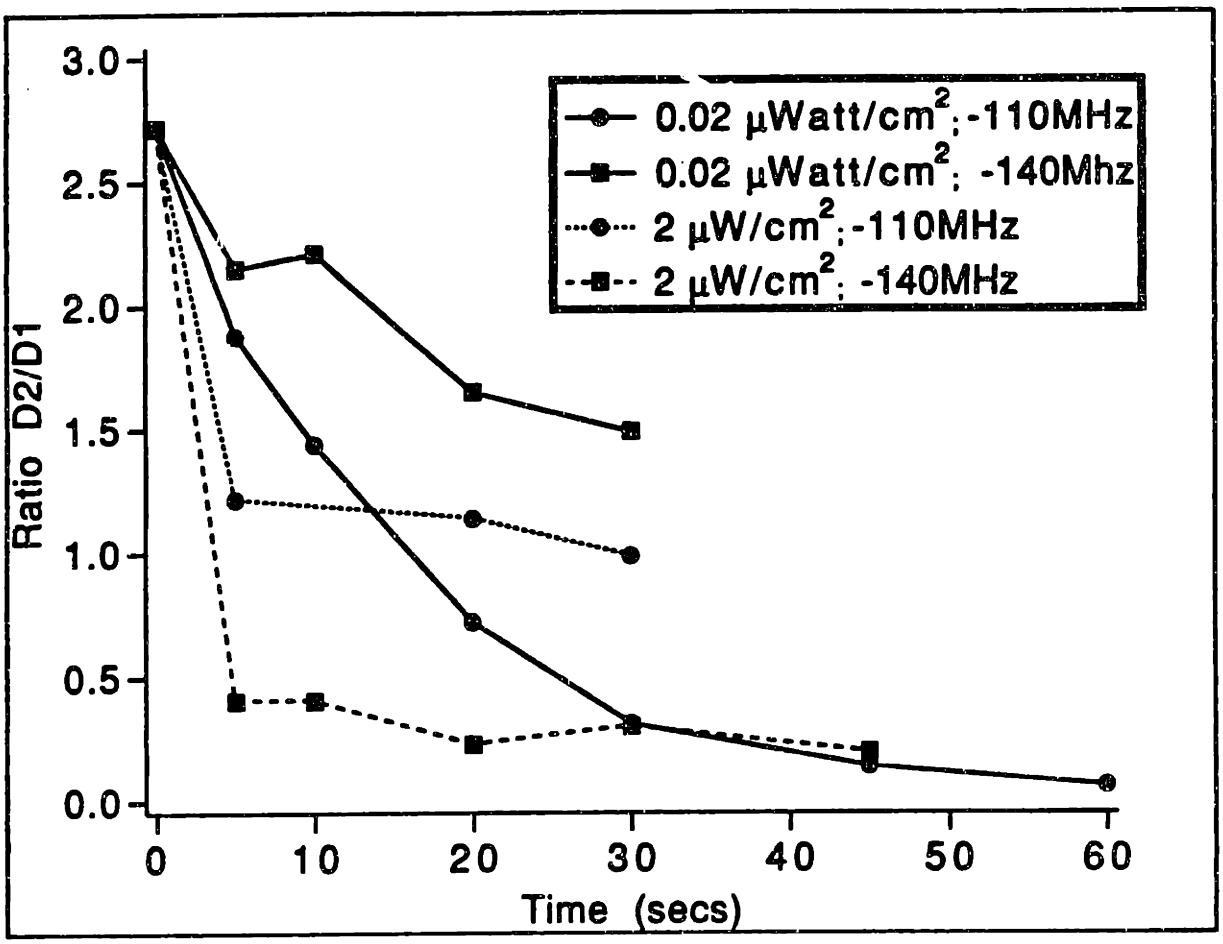

Figure 8.5: Ratio of the fluorescence peak heights from detectors 1 and 2 as a function of the length of time the cooling laser was applied to the trapped atoms, for various detunings and intensities. As detectors 1 and 2 are located at different values of the magnetic field, the ratio of the peak heights is a reflection of the energy of the trapped atoms.

This behavior of the cooling process can be seen in the data of figure 8.5. The curves showing a rapid decrease in the number of atoms reaching detector 2, correspond to the higher cooling laser intensity of 2 $\mu W/cm^2$ and detunings of −110 MHz and −140 MHz (measured with respect to the resonant frequency for atoms at the minimum value of the magnetic field). According to our calculations (equation 7.6b) we would expect values of 0.3 sec. and 0.5 sec for τ_{cool} respectively. As expected, the rapid decrease to a value close to the minimum energy occurs on a time scale τ_{cool}, after which the decrease in energy is much more gradual. This is consistent with the motion of the trapped atoms along the direction of the cooling laser beam being damped much faster than the rate at which energy in the other directions can be coupled into the cooling direction. After the initial rapid decrease in energy, the net cooling rate will be determined by the rate at which the energy in the transverse direction can be coupled back into the direction of the cooling laser beam and be damped.

The curves corresponding to the lower laser intensities of 2×10^{-2} $\mu W/cm^2$ and detunings of −110 MHz and −140 MHz display a much more gradual decrease of the energy of the atoms toward the minimum value. Our calculation would predict a τ_{cool} of 30 and 50 seconds, which is consistent with $\tau_{cool} >> \tau_{trap}$, so that the net cooling rate is basically determined by the cooling rate in the longitudinal direction.

When $\tau_{cool} >> \tau_{trap}$, the amount of excess heating (heating of the transverse direction without a corresponding amount of cooling in the longitudinal direction) is minimized, and the minimum energy achievable is correspondingly smaller. The curves of lower laser intensity (for a given detuning) have correspondingly larger τ_{cool}, and they would be expected to approach a lower value for their minimum energy. This is seen in the curves corresponding to laser intensities of 2 and 2×10^{-2} $\mu W/cm^2$ and detunings of -110 MHz, where the minimum effective temperature of the trapped atoms is observed for the lower laser power. Similarly, the curves of greater detuning (for a given intensity) have correspondingly larger τ_{cool}, and they would be expected to approach a lower value for their minimum energy. This is seen in the curves corresponding to a laser detunings of -110 and -140 MHz and intensities of 2 $\mu W/cm^2$, where the lower effective temperature of the cooled atoms is associated with the cooling laser detuned further from resonance. Unfortunately, insufficient confinement times for the trapped atoms prevented us from observing the asymptotic behavior of the curve corresponding to a laser detuning of -140 MHz and intensity of 2×10^{-2} $\mu W/cm^2$, therefore, a comparison of the minimum temperature attainable with these laser parameters cannot be made.

Conclusions

We have been able to perform both laser and rf spectroscopy on magnetically confined neutral atoms. In addition, we have been able to Doppler cool the atoms. The techniques presented in this thesis are of great utility for probing and cooling atoms confined in a magnetic trap and will most likely be used in future experiments with trapped atoms.

Unfortunately the magnetic trap is no longer working and the cost of resurrecting it is prohibitively high (both monetarily and in terms of graduate student lives). There are however, a few aspects of the apparatus that should be changed for "version II."

Clearly, the improved trapping time resulting from pumping on the liquid helium was a great benefit. Many more experiments could be performed (and cups of coffee consumed) with 30 minute trapping times. Experiments which require the trap to mix the motion of the trapped atoms, such as Doppler cooling in 1-D and rf spectroscopy, will necessarily require long confinement times as the typical oscillation frequency of atoms in a magnetic trap is on the order of 10 Hz. Thus obtaining long trapping times should be an important consideration.

It would have been nice to have optical access from other directions into the experiment. This would have enabled us to apply Doppler cooling in the transverse direction as well as allowing us to spatially select atoms along the longitudinal direction for laser excitation. Who knows, we may even have been able to video tape

the trapped atoms. (Always a crowd pleaser at colloquia and seminars.)

Perhaps the biggest problem in analyzing the lineshape of the spectra was in our knowledge of the magnetic field profile. The use of an octopole magnet for radial confinement added much uncertainty, especially in the contribution due to the end effects The use of a quadrupole magnet would simplify analysis as the end effects are at least an order of magnitude smaller than the octopole's, and a sufficiently strong quadrupole magnet would result in the minimum of the trap being located along the axis of the trap. The radial potential would also be harmonic (for small displacements) which would greatly enhance the density of the atoms as they are cooled. Of course, at the higher densities collisions become quite important and this may complicate the analysis of lineshapes.

As for the future, high resolution spectroscopy appears possible. However, it will most likely require the development of super-cooling schemes to cool magnetically trapped atoms to μK temperatures. This would would result in milli-Hertz linewidths for rf spectroscopy using field independent transition points [PRI86]. Optical spectroscopy with sub-Hz linewidths also appears possible. The use of an S-state to S-state transition would reduce much of the magnetic field broadening that we observed in our spectra for an S-state to P-state transition. The effect of gravity must also be considered in detail as it necessarily means that one cannot confine

atoms in a region of uniform magnetic field no matter how low the energies of the trapped atoms are.

As trapped atoms are successfully cooled to μK temperatures and the densities are increased, the observation of quantum collective phenomena such as Bose-Einstein condensation or a degenerate fermi gas should be possible. Most likely, a degenerate fermi gas will be observed first as the suppression of collisions at the low temperatures will make it easier to achieve the necessary densities.

Since we are on the subject of future experiments with magnetically confined atoms, we include several papers as appendices to this thesis which contain several ideas for experiments with magnetically trapped atoms. What follows is a brief description of the papers.

Appendix A is a paper presented at the 11th International Conference on Atomic Physics (ICAP). This paper is of particular relevance for two reasons: First, it contains a review of the field of neutral atom trapping up through 1988. Second, a cooling scheme involving the use of rf induced transitions is proposed. The scheme is called "radiative evaporation", a variation of evaporative cooling, in which rf induced transitions are used to remove the energetic atoms from the magnetic trap.

Appendix B is a paper presented at the Eighth International Conference On Laser Science (EICOLS). In this paper, we propose "phase space optical pumping." This is a novel scheme in which an rf induced transition can be used to select atoms of a certain class in phase space for laser excitation. This class of atoms will redistribute themselves in phase space upon spontaneously emitting a photon. In this manner, one can accumulate atoms in a particular area of phase space.

Appendix C is a paper presented at the International Quantum Electronic Conference (IQEC '90). In this paper, we discuss possible collective effects of densely confined neutral atoms. Specifically, we predict a suppression (enhancement) of the spontaneous decay rate for densely confined fermion (boson) atoms.

Appendix D is an article presenting our initial results on rf spectroscopy of trapped neutral atoms.

ICAP - Proceedings of the 11th International Conference on Atomic Physics
in Atomic Physics,, 11, eds. S. Haroche, J.C. Gay, and G. Grynberg
(Singapore: World Scientific, 1989), pp. 179-97.

ATOM TRAPS

D.E. Pritchard, K. Helmerson and A.G. Martin
Department of Physics and Research Laboratory of Electronics,
Massachusetts Institute of Technology
Cambridge, Massachusetts 02139

INTRODUCTION

Atomic physicists are well aware of the elegant and important measurements which have been made using charged particle traps. Now that neutral atoms have been trapped, the obvious question is, "will we succeed in doing such significant experiments with trapped atoms?" In this paper we present a review of the recent progress with atom traps and make projections for the future of the field. Our presentation is divided into the following sections: physics of atom traps, atomic collisions with cold trapped atoms, spectroscopy of trapped atoms, schemes for getting trapped atoms much colder, collective effects, and predictions for the future.

PHYSICS OF ATOM TRAPS

Confinement and Cooling

Two basic mechanisms have been proposed for supplying the force to confine neutral atoms: magnetic gradient forces and light forces. Magnetic gradient forces act only on atoms with magnetic dipole moments. Obviously atoms with net electronic spin are trapped $\sim 10^3$ times more strongly than atoms possessing only nuclear moments. Light forces are of practical interest for trapping atoms only if laser light is available near an allowed transition. However the force is supplied, a trap exists only if there is a point in space $\vec{r}_0$, towards which there is a restoring force, $\vec{F} = -k(\vec{r} - \vec{r}_0)$. Equivalently, there must be a minimum of the potential energy of

the particle at $\vec{r}_o$.

The existence of a local minimum in the potential energy of an atom is only one of the requirements for an atom trap — the other is that there be a mechanism to prevent atoms which enter one side of the trap from escaping out the other side. The requisite energy differential in the first atom trap (MPP85) was achieved by a pulse of near-resonant light which stopped some atoms, after which the trap was quickly turned on before they escaped. In all subsequent traps, the strength of the trap was held constant and some form of damping was provided to dissipate enough kinetic energy so that the atoms were unable to escape. For laser-excitable atoms, the damping force has been provided by optical molasses — light tuned roughly a linewidth below resonance. Optical molasses works because of the Doppler shift (HAS75, CHB85) and other more subtle phenomena (LWW88, SWU89, DAL89). In some traps molasses is simply alternated with the trapping light (CBA86, GLJ88); more elegantly it may be combined with the loading and/or confining light (BLM87, RPC87).

Another way of cooling trapped atoms is through evaporation: the top of the trapping potential is lowered until atoms in the high energy tail of the energy distribution can escape from the trap (HES86, TOM86). Since each escaping atom removes $\geq 10k_BT$ of energy, the fractional decrease in the thermal energy of the trapped atoms is many times the fractional decrease in the number of trapped atoms. Hence the remaining atoms are cooled.

Evaporation depends on having a trapped gas with enough collisions to repopulate the high energy tail of the energy distribution. Thus it is intrinsically suited to high density samples. In contrast, laser cooling is basically a single atom process for which collisions present serious problems in high density samples. While atoms are lost in evaporative cooling, roughly 20% to reduce the temperature by an order of magnitude, the process represents real cooling, and the density of particles in the bottom of the trap may be increased by evaporative cooling.

Magnetic Field Traps

The magnetic field trap was proposed a quarter century ago (HEE63, LEM80, PRI83), and was demonstrated for neutrons a decade ago (KPT78). The basic principle is that a local minimum in the magnitude of the magnetic field will

confine atoms whose potential energy, $U(\vec{r}) = -\mu_{eff}|\vec{B}|$, increases with increasing field — these are called weak field seekers in molecular beams parlance. Unfortunately, a min/max theorem (WIN85) allows only minima to exist for static electric or magnetic fields in a source-free region: this implies that it is impossible to trap the lowest energy state of any system using a static field trap, since the true ground state is always lowered by external perturbations. Although magnetic traps are weak for atoms and much weaker for neutrons (μ_{Bohr} B = 1 Kelvin for B = 1.5 Tesla), a magnetic trap for ultra-cold neutrons was demonstrated some time ago (KPT78). Demonstration of a magnetic trap for atoms had to await the development of techniques for slowing and cooling atoms to sub-Kelvin temperatures (PMP85, EBH85) — in fact the possibility of atom traps provided one of the principal motivations for atom slowing research.

The first trap for neutral atoms was a magnetic trap demonstrated by the N.B.S. group (MPP85). The magnetic field configuration was a spherical quadrupole, the field produced by two identical coaxial coils connected with opposing on-axis fields so as to produce a zero-field point midway between the two coils. This field configuration is simple, but has the disadvantage that the direction of the magnetic field reverses at the center of the trap, along with the direction of the spins of the trapped atoms. This makes it difficult to observe the trapped atoms using laser induced fluorescence without having some atoms decay to spin-down (ie. untrapped) states. It can also lead to loss of atoms which pass close enough to the origin to experience motion-induced spin flips.

These disadvantages may be overcome by employing a field configuration (PRI83) which has a local minimum in $|\vec{B}|$ where $\vec{B} = B_o \hat{z}$. This field configuration removes the problem of particle loss due to motion-induced spin flips, and has been used for Na (BLM87) and H (HKD87, VBJ88). The field is relatively uniform near this minimum (which may be split into several nearby minima in some field configurations (MHB88, BEM87)), allowing continuous irradiation of the trapped atoms by a laser whose polarization and frequency conspire to excite those excited states which decay only to trapped ground states. This not only generates fluorescence with which to monitor the spatial density of the trapped atoms, but it also allows continuous filling of the trap for at least several seconds (BLM87). Continuous filling has enabled us to accumulate enough atoms to absorb roughly half of a weak probe beam.

Light Traps

We now turn our attention to traps in which confinement is provided by light forces. Light forces are broken into two types: stimulated forces (also known as "gradient", "dipole" and "induced" force) and spontaneous forces (also called "scattering force" and "radiation pressure") (STE86). We consider stimulated force light traps first because of their conceptual similarity to magnetic field traps.

Because the electromagnetic fields of light oscillate, they are not constrained by the min/max theorem and may have a local spatial maximum, for example at the waist of a focussed laser beam. If the laser is just to the red side of a resonance, ground state atoms will be strongly attracted to regions of high field by the gradient forces. Thus the simplest light trap is the focus of a laser beam (ASH78); not surprisingly it was the first to be demonstrated (CBA86).

The other type of force due to light, the spontaneous or scattering force, results from the re-direction of the momentum of scattered photons. Early proposals to make optical atom traps using this force (MIN82, MIJ82) foundered on the rock of the optical Earnshaw theorem (ASG83) which forbids scattering force traps for particles whose light scattering cross section is constant. Once it was realized that the cross section for atoms depends on the magnitude and direction of the local magnetic field as well as the magnetic sublevel of the atom, several ways of making spontaneous force traps for atoms were proposed (PRB86). The first spontaneous force light trap to be demonstrated (RPC87) is simple and effective and has recently been applied to metastable Ne (SST89) and Cs (SWW89).

The two types of light forces lead naturally to qualitatively different traps: stimulated forces do not saturate at high laser intensities, making possible traps with small volume (10^{-9} cm^3) in which the atoms oscillate with relatively high frequencies; spontaneous force traps work best with light intensities near or below saturation, permitting traps with capture volumes ~ 1 cm^3 or larger. Various hybrid designs have been suggested (ASH78) and one has been built (GLJ88).

Traps for Hydrogen

Although not widely publicized in the atomic and laser physics communities, the atom traps which have held the most atoms at the highest density for the longest times use neither lasers for manipulating the atoms nor optical molasses for cooling

them. These are magnetic field minimum traps (PRI83) for spin aligned hydrogen H(↑) which are loaded by immersion in a cold dense hydrogen gas (HDK87, VBJ88). The loading gas may subsequently be removed, leaving behind trapped atoms which will cool further by evaporation.

Recently at MIT (MDS88) evaporative cooling of spin aligned hydrogen was demonstrated to reduce the temperature of the trapped gas from 38 mK to around 1 mK while maintaining the central density at $\sim 7.6\times10^{12}$ cm^{-3}. It is predicted that evaporative cooling should allow the production of hydrogen atoms with temperatures as low as 30 μK (HES86). At present the limitations are not in the achievement of these conditions, but rather in the detection of the remaining atoms in the trap and the measurement of their temperature. More sensitive diagnostics are being developed.

SUMMARY OF NEUTRAL ATOM TRAPS

In the following table we present a summary of all the neutral atom traps which we know about as of December 1988. Two features stand out: there has been dramatic improvement in all performance criteria since the first trap, and the emphasis has shifted from developing new types of traps towards trapping new species and refining trapping techniques.

Name	Ref.	N	V(cm^3)	n(cm^{-3})	$\tau_{1/2}$(sec)	T(mK)
magnetic: spherical quadrupole	MPP85	2×10^4	20	10^3	0.6	17
gradient light force	CBA86	500	10^{-9}	5×10^{11}	~1	.34
M.I.T. magnetic	BLM87	10^9	100	10^7	100	30
	recent	2×10^{10}	~10	10^9	1250	2
H(↑) magnetic M.I.T.	HKD87	5×10^{12}	76	10^{12}	1000	30
spontaneous light force (SLF)	RPC87	10^7	-10^{-4}	10^{11}	100	.6
hybrid light force	GLJ88	10^5	10^{-6}	10^{11}	~1	.75
H(↑) magnetic	VBJ88	4×10^{13}	-10^2	3×10^{14}	—	100
SLF for Ne*	SST89	4×10^7	$<10^{-3}$	10^{11}	.15	—
SLF for Cs	SWW89	2×10^8	10^{-3}	2×10^{11}	15	—

No compendium on traps is complete without noting possible conceptual and practical problems with light traps. There is reason to believe that magnetic traps work as advertised. The atoms have plenty of time to wander ergodically around the trap; indeed timescales of a few seconds are observed for coupling longitudinal and transverse motion in our magnetic trap. The current agreement of experiment and theory, at the 15% level for collision processes in trapped H (VBJ88), suggests the absence of strong filamentary structure (such structure increases the collision rate at

a given average density). For light traps, on the other hand, there is good reason to suppose that the traps do *not* operate as advertised. The first spontaneous force trap was observed to have irreproducible behavior (RPC87) with multiple density maxima, odd shapes, temporally unstable behavior, and fine filamentary structure (PCB88); similar irregularities have also been observed using this trap for Cs (SWW89). Also, the atom-atom collision rate reported in PCB88 would have produced strikingly observable non-linear decays in the optical molasses at densities reported by CBA86. Given the suprises which have been recently uncovered in optical molasses, the observation of strange structures and other inconsistencies in light traps is surely an indication that more understanding is needed (and possibly that more discoveries lie ahead).

COLD COLLISIONS

There have already been several observations of collisions of trapped atoms with themselves (HKD87, RPC87, GLJ88, VBJ88, PCB88), so the field of low temperature atomic collisions is already alive. Atomic collisions at low temperatures are qualitatively different from those occurring in the well-studied thermal and hyperthermal regime (PRI86). The most obvious difference is due to the large deBroglie wavelength: the number of partial waves involved in the usual partial wave expansion decreases with temperature, reaching unity around 1 mK for typical atoms. This has important consequences for completely spin aligned fermi atoms (eg. D, ^{6}Li) since they must have an anti-symmetric spatial wave function. Hence the lowest allowed partial wave is the p-wave (l=1). The p-wave phase shift goes to zero when the deBroglie wavelength exceeds the range of the potential, hence cross sections for *all* collisional processes for spin aligned fermions should go to zero as the temperature is lowered (PRI86, KSV87).

The most revolutionary aspect of cold collisions is the need to abandon the traditional viewpoint used to discuss excited state collisions - vis. that a collision involving an excited state atom is similar to a collision of ground state atoms except that it occurs on a different molecular potential curve. This view no longer applies because the duration of cold collisions (classically the distance at which the potential is a small fraction of the kinetic energy divided by the velocity) can be many nanoseconds — longer than the radiative lifetime — so that spontaneous emission becomes probable, thereby negating the assumption that only a single

potential curve is involved. If radiation is present, additional complexities arise: the radiation must be regarded as exciting predominately those atom pairs (i.e. molecules) whose separation brings them into resonance with the radiation. If the radiation is intense enough to induce transitions at a rate comparable to the spontaneous rate, then absorption by a quasi-molecule may well be followed by stimulated emission, suggesting that a dressed molecule viewpoint is helpful in treating the collision (JUL88). Both this dressed molecule picture and a forth coming classical treatment (GAP89) predict that the largest excited state collision rates occur when the laser is significantly detuned to the red side of the atomic transition. This prediction has been verified for associative ionization of sodium (GLJ88).

Some cold collision processes are detrimental to progress in atom trapping (PRI86). The worst is magnetic dipole-magnetic dipole depolarization (KVS81), in which two trapped spin up atoms collide to produce at least one spin down atom, which is expelled from a magnetic trap. This is the principal loss mechanism in the most recent H($\uparrow$) trapping experiments (MDS88, VBJ88); worse still, these collisions occur most rapidly near the center of the trap and consequently remove the coldest atoms, heating the remaining atoms. This process has been studied theoretically (SGV88, LSV86) for H, and agreement with experiment has been obtained. Calculations of the corresponding process for alkalis would be helpful, especially if they determined the reduction which occurs in high magnetic fields. Calculations in mixed (eg. H – Li) systems would be helpful in considering the possibility of sympathetic cooling of trapped H by laser cooled Li.

SPECTROSCOPY

While laser induced fluorescence is often used as a diagnostic of the number and spatial distribution of trapped atoms (other than hydrogen), only two experiments have actually demonstrated an optical spectrum of trapped atoms, one using fluorescence (BLM87) and the other absorption (RPC87). Recent experiments on Doppler cooled trapped atoms in both magnetic and spontaneous force light traps have showed linewidths of $\sim 2\Gamma_N$ where Γ_N is the natural decay rate of the Na D-line. Going to higher excited states (or forbidden transitions) should yield narrower linewidths due to the longer lifetime. In a magnetic trap, a very narrow line could be obtained by using a field-independent transition (eg. 3s→ns in Na $m_F=m_F'=2$);

in a light trap the trap must be turned off (or at least greatly weakened) to obtain a narrow transition.

r.f. Spectroscopy

Radio frequency resonance of trapped atoms is valuable for at least three reasons: as a high resolution diagnostic of the atoms' individual and collective behavior, as a tool to selectively manipulate the magnetic quantum state of the trapped atoms, and potentially for ultra high resolution spectroscopy of isolated atomic systems. We have recently demonstrated r.f. resonance experiments on Na atoms contained in our magnetic trap (MHB88) and now we describe our latest results in some detail.

Sequential r.f. pulses were applied to a sample of $\sim 2\times10^{10}$ Na atoms with the appropriate frequencies to transfer population between the four trapped magnetic substates. The relative populations of the magnetic substates were detected by sending a weak, narrowly collimated probe laser beam along the axis of the trap and monitoring the induced fluorescence with a photodiode (placed along the wall of the trap enclosure) located at the longitudinal magnetic field minimum. We demonstrated that population could be mixed among all four trapped magnetic sub-levels.

In order to diagnose the energy distribution of the trapped atoms, we measured the r.f. resonance curve for the |"F"=2, M=2>, to |"F"=2, M=1> transition by measuring the relative peak heights in the fluorescence spectrum for the two states as a function of the frequency of the applied r.f. pulse. Figure 1 is such an r.f. resonance curve for both "hot" atoms after initial loading of the trap and "cold" atoms after application of longitudinal doppler cooling. Doppler cooling of the sample was achieved with a standing wave laser beam, detuned ~80 MHz red of the minimum trapped atom transition frequency; it was applied for 60 seconds. It was necessary to reduce the intensity of the standing wave to $\sim10^{-3}$ saturation intensity to slow the transverse heating due to spontaneous recoil relative to the coupling rate of transverse to longitudinal motion provided by the trap; otherwise the transverse motion is not cooled efficiently.

In order to explain the shape of the spectrum, we note that the energy difference between the two levels increases monotonically with magnetic field (i.e.

d(E/h)/dB = 60 kHz/Gauss), hence each magnetic field value corresponds to only one point in frequency space. The r.f. pulses were of sufficient power and duration (number of Rabi flops: 5 secs x $\Omega_R/2\pi \approx 1\times10^4$) so that equilibrium was reached in the transfer of population between the two states of any atom which could reach the magnetic field at which it was resonant with the applied rf.

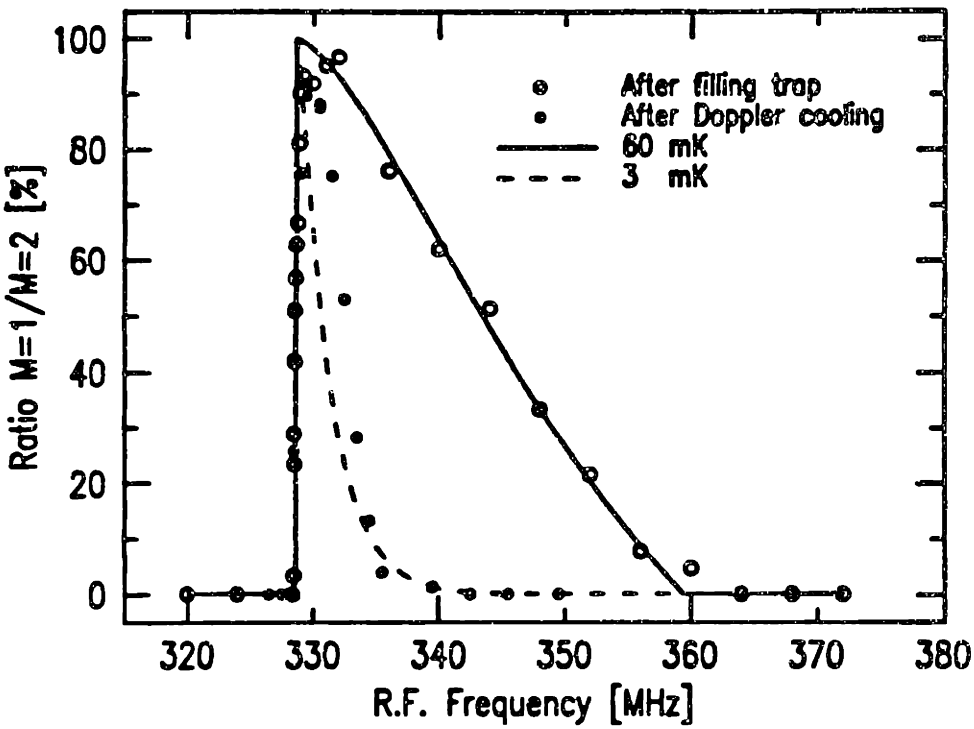

Figure 1: r.f. resonance curve for atoms after initial loading of the trap (open circles) and after application of doppler cooling (closed circles). The dashed and solid lines are theoretical fits using truncated Boltzmann distributions of 3 and 60 mK respectively.

The height of the resonance curve at each frequency is therefore determined by the fraction of atoms energetic enough to reach the corresponding magnetic field, and the lineshape of the high-frequency tail is therefore a direct measure of the energy distribution of the atoms in the trap. (We observe that our trap operates in the collisionless regime, consistent with our density and the expected ground state cross section for elastic scattering (PRI86).) Due to the configuration of probe laser and fluorescence detector our population ratio measurements of the various atomic states were made in a small volume element located at the magnetic field minimum of the trap, consequently there is no coordinate-space density of states factor in the

signal. This makes the shape of the spectrum a direct measure of the energy distribution, independent of the trapping potential. Thus it is possible to extract the energy distribution of the trapped atoms from the derivative of the resonance curves of figure 1.

Figure 2 is a plot of the logarithm of the energy distribution as a function of energy for the data of figure 1. If the energy distribution were a Boltzmann distribution, we would expect a straight line. The linear fits in figure 2 suggest that the "hot" atom distribution is a truncated Boltzmann distribution with a temperature of 60^{+40}_{-20} mK, while the "cold" atom distribution is approximately Boltzmann at higher energies with a temperature of ~2 mK. Deviations at low frequency may reflect lack of saturation of the r.f. resonance due to the small coordinate space volume in which the transition occurs (we verified saturation experimentally only at the peak of the curve), and can also result from the fact that we probe at the center of the trap, whereas the true field minimum occurs in a ring ~1 cm off axis which has ~4 Gauss lower field (MHB88, BEM88). Also, collisions could be a significant perturbation for the doppler cooled case.

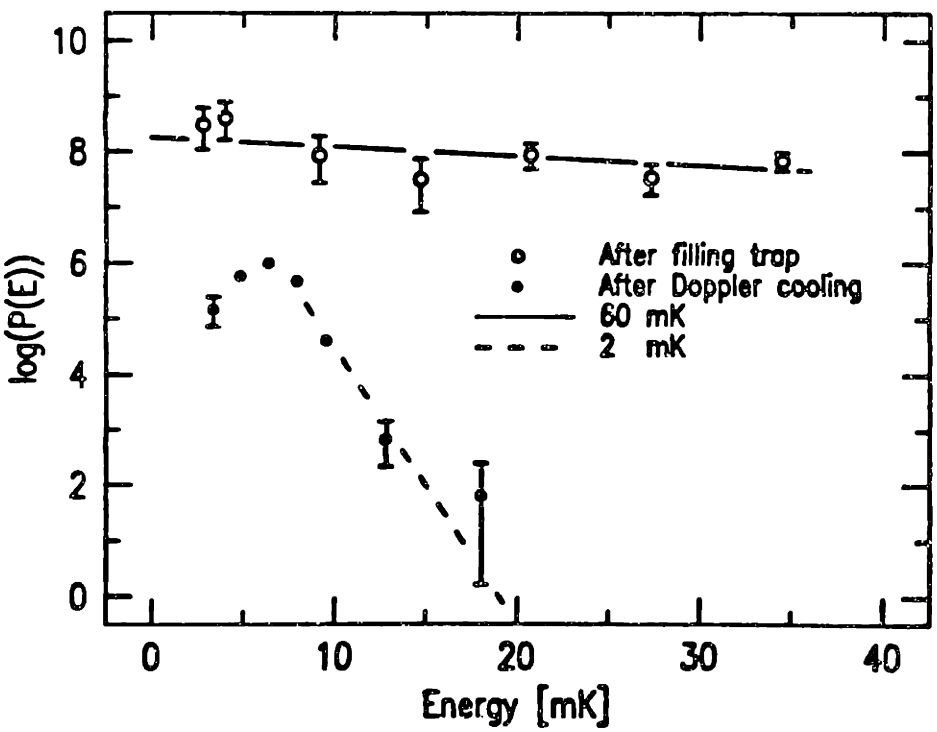

Figure 2: Logarithm of the energy distribution P(E), of the trapped particles vs. energy. The solid and dashed lines represent Boltzmann distributions of 60 and 2 mK respectively.

COOLING

High resolution spectroscopy, simplification of atomic collisions, and the observation of collective effects all demand cooling the atoms to much lower temperatures than the milli-Kelvin temperatures so far obtained with both doppler cooling and evaporative cooling. Recent work (LWW88) shows that carefully constructed optical molasses cools to a small fraction of the expected temperature for Doppler cooling, $k_B T_d = \hbar\Gamma_N/2$. Although recent explanations of this phenomenon (DAL89, CWS89) suggest that cooling to microKelvin temperatures may be possible using strong optical transitions, they depend on a degeneracy of the ground energy level which is destroyed by the application of static fields; thus these ideas are readily applicable to light traps, but not to static field traps (without creative generalization).

Cooling in a Magnetic Trap

Several schemes for laser cooling atoms in magnetic traps have been proposed, but none has yet been demonstrated. The earliest such proposal, called cyclic cooling (PRI83), involves a cycle in state space wherein an atom in a strongly trapped state makes an rf-induced transition to a less strongly trapped state at a spatial location where the magnetic field is high, and then is restored to the original state by optical pumping at a place where the field is low. Cooling occurs because net potential energy is removed by the stimulated and spontaneous emitted photons; they have a higher energy than the photons which are absorbed. A more modern, but equivalent, explanation is that cooling occurs due to "Sisyphus" optical pumping: the optical pumping consistently places the system in the most strongly bound state near the bottom of the potential well — hence the atom constantly finds itself traveling up the steepest available hill, losing kinetic energy as a result. (King Sisyphus was condemned to forever roll a big rock uphill.) Cyclic cooling, or some other variants of these basic ideas may well work to cool atoms in magnetic traps; if not we shall have to resort to more standard ideas: Doppler cooling on weakly allowed transitions, stark-induced transitions, or multiphoton transitions can all attain microKelvin temperatures without exceeding the usual Doppler limit, and evaporation is also projected to cool into this regime (TOM86, HES86).

Radiative Evaporation

We would like to point out the close connection between cyclic cooling and evaporative cooling and to suggest a new type of cooling which we term "radiative evaporation." Both cyclic and evaporative cooling work because the particles removed from the trapped state are located where they have a large potential energy, so that the average energy of the remaining trapped particles is reduced. The efficiency of both methods is increased if collisions repopulate the high energy tail of the energy distribution so that the removed particles take away the largest possible energy. In evaporative cooling these particles are lost; in cyclic cooling they are restored to the original trapped state with reduced total energy. In evaporative cooling the escaping particles must pass over the top of the potential barrier. This must be lowered as the particles are cooled in order to continue evaporative cooling, a process which normally weakens the confining potential. This causes adiabatic cooling and inconveniently slows the cooling process. In radiative evaporation, particles in the high energy tail do not evaporate, rather they undergo rf or optical transitions to an untrapped level (and are therefore lost from the trap). The advantages of this method are threefold: the trap does not have to be weakened to continue the cooling process, the rate and potential energy of atoms which escape are controlled by the amplitude and frequency (and possibly the position) of the applied radiation, and the space from which particles escape from the trap is "all points where the magnetic field equals the selected value" rather than the (sometimes spatially restricted) saddle point in the trapping potential.

Below the Recoil Limit

All optical cooling methods run into problems at the recoil limit, $k_B T_r = (\hbar k)^2/(2M)$, the energy imparted by the recoil from a single spontaneously emitted photon. In general, this last decay imparts a random amount of energy to the atom. This raises the possibility of cooling below this limit with a sufficiently selective interaction simply by recycling the "hot" atoms while leaving alone those which happen to decay to a final energy near zero (PHB87). Recently an elegant realization of this idea has been achieved in a one dimension using unconfined atoms (AAK88).

The preceding discussion really concerns optical pumping in phase space (PHB87) (velocity space for an unconfined system (PRI86, AAK88)). Indeed, this is

the analog of repopulation optical pumping familiar among discrete levels, in which atoms are reexcited until they spontaneously decay into a desired dark state from which further excitation is forbidden. In fact we should view cooling in the following perspective: the major objective of the particle trapping technology currently under development in atomic physics is to achieve the same degree of control over the translational degree of freedom as has been achieved over the internal quantum states of atoms during the half century since the development of resonance techniques. We should anticipate the preparation of trapped atomic systems in a single translational quantum state and we may eventually see systems deliberately prepared in superpositions of trap eigenstates; perhaps population inversion and an analog to laser action will ultimately be observed!

COLLECTIVE EFFECTS

Trapped atoms are ideal samples in which to observe several types of collective effects. This may seem surprising because present densities are about a billion times lower than typical solid state densities; the key characteristic which allows collective effects to occur in atom traps is that the atoms have very little kinetic energy available to disrupt an imposed or spontaneously arising long range order. We shall now discuss collective effects whose order arises due to radiative and quantum identity effects.

Radiative Effects

Collective spontaneous decay, called superfluorescence, can occur in extended samples (i.e. size $\gg\lambda$, the wavelength of light) — the system can spontaneously break the spatial symmetry and emit radiation in one particular direction or into a single mode of the radiation field. However, motion of atoms in the sample suppresses the buildup of superfluorescence if the atoms move a significant fraction of λ from their starting positions. In the trapped atoms this problem is enormously suppressed because of the low speed of the atoms — for example, sodium cooled to the doppler limit takes about sixty spontaneous lifetimes to move λ, much longer than timescales for superfluorescence. The interaction time is long enough to permit the study of systems in which spontaneous emission is inhibited (eg. by the action of a surrounding cavity) or the timescales are lengthened as would be the case if the trapped atoms were excited to Rydberg levels, or if only a very few

atoms were present.

Free-Bound Molecular Spectroscopy

When two atoms are closer than a wavelength of light, coherence arises in their interaction with radiation: both superradiant and subradiant states arise (DIC54). In the one-photon excited states the atoms share the excitation and experience the strongest interatomic force which can arise between the neutral atoms — the resonant dipole-dipole interaction which varies as the inverse cube of the separation. When this strong force is attractive (it can also be repulsive), it normally pulls the atoms close together to form a bound excited state molecule. In certain circumstances, however, shallow minima form at interatom separations on the order of 50 Å — these are pure long range molecules (SVP78). They have never been observed.

Trapped atoms make possible a new form of spectroscopy — high resolution free-bound spectroscopy. High resolution arises because the thermal broadening is reduced — in fact at the doppler cooling limit it is several times less than the natural linewidth of the molecular transitions! The low temperature also leads to large deBroglie wavelengths — longer than the minimum of the intermolecular potential. Therefore if two free atoms are close enough for the Franck-Condon factor to allow excitation to a bound excited state potential, their relative angular momentum is probably zero. Thus, although free, the initial energy and angular momentum of the atoms are both well defined — cold trapped atoms might be termed the "spectroscopically defined continuum." Free-bound spectroscopy in atom traps appears to be a feasible way to observe pure long range molecules.

Quantum Collective Effects

Quantum collective effects become significant when the thermal deBroglie wavelength becomes comparable to the interparticle spacing. Therefore, a group of trapped atoms with low temperature and high density is an attractive sample for their study. Indeed, attainment of Bose-Einstein condensation (BEC) of atoms was one of the original motivations for neutral atom trapping research, particularly of $H(\uparrow)$.

A recent theoretical study concerning BEC of trapped atoms (BPK87) showed that the critical density at which BEC begins is

$$n_c = 5 \times 10^{20} (AT)^{3/2}$$

where A is the atomic weight of the atoms and T the temperature. This density corresponds roughly to one particle per each cube, $\lambda_{dB}/2$ on a side. If this density is exceeded at the bottom of the trap, enough atoms condense into the $v_x=v_y=v_z=0$ vibrational level of the trap to lower the density back to exact criticality.

Although the local critical density for the onset of BEC is universal, independent of the trapping potential, a trap can be very helpful in achieving and observing BEC. The chief effect of the trap is to concentrate the particles so that BEC commences with a relatively small number of trapped particles. This effect is especially pronounced with a trapping potential $U(r)=r^n$ which has a low value of n, since the critical number of trapped particles varies as $N_c \propto T^{3/n+3/2}$. The trap can also change the thermodynamics of the transition to BEC, for example by giving rise to a discontinuity in the specific heat (BPK87).

For a 3 dimensional harmonic trap, N_c is just $(k_B T/\hbar\omega)^3$ where ω is the frequency of oscillation of atoms in the trap. Conventional low T_c superconducting technology would allow construction of a harmonic trap with a magnetic field of about 1 T at 1 cm, for which H would have an oscillation frequency of $\sim 10^4/2\pi$ Hz. Therefore, BEC would be reached with $N_c \approx 2\times10^3$ H atoms in such a trap if they were cooled to 1 μK. Since $N_c \propto$(Atomic mass·trap stiffness)$^{3/2}\times$(temperature)^3 it is clear that the simplist route to BEC in traps is to get to the lowest possible temperature.

Since many atoms (eg. D^6, Li) are fermions, our discussion of quantum collective effects must also consider the possibility of making a fermi gas of atoms. Such a gas has a markedly non-Boltzmann distribution only when $k_B T$ is smaller than the fermi energy; this occurs under roughly the same conditions of density and temperatures as BEC. Collective effects are considerably less dramatic with fermions, however, because the exclusion principle comes strongly into play only near the trap minimum. On the other hand, all collisional effects are suppressed in spin-aligned fermi systems as $T\to0$, including three body recombination. Hence, the chances of obtaining a reasonably degenerate fermi gas in an atom trap appear

much higher than those of obtaining BEC.

THE FUTURE

No review of a young field like atom trapping is completely responsible without an irresponsible prognostication of future results. Our first prediction is that the rate of trapping experiments will continue to grow in the next few years as different atoms are trapped in the existing traps and new light traps are demonstrated. (It would be very desirable to invent a light trap in which the atoms were completely polarized.) At the same time experiments involving collisions, spectroscopy, and new cooling techniques will be pursued by many of the groups active in the field. Li and Rb are good bets to be the next atoms trapped, almost certainly in experiments which will use diode lasers. Ultimately more exotic atoms possessing ultra-narrow optical transitions (EBH84) will be trapped.

Work on cold collisions will continue, especially collisions involving production of ions and/or excited state atoms. The dependence of effective collision rates on laser detuning will be an important issue which will prove to be a real challenge to theory, especially near line center.

Progress towards high resolution spectroscopy and the study of collective effects demands the development of new cooling schemes capable of cooling to a micro-Kelvin and below, especially in magnetic traps. The current ferment of new insights and ideas on super-cooling makes us optimistic that such success will be obtained. An important related development will be the application of laser cooling to the production of intense slow atomic beams, useful not only for loading traps but also in many other experiments.

Super-cooling raises the possibility of truly high resolution spectroscopy. r.f. spectroscopy with milli-Hertz linewidths is possible using field-independent transitions (PRI86), and sub-Hz optical spectroscopy is possible also, for example on the 1s-2s 2-photon transition in H. Several groups are currently pursuing the idea of laser spectroscopy of H, and it will certainly come to pass. A very interesting possibility is high resolution spectroscopy of anti-hydrogen made from anti-protons (which have already been trapped (GFH86)). This would serve as a stringent test of CPT invariance.

One final guess: if BEC is ever observed in an atom trap, it will be observed with H, but it will have to be cooled to 10 μK or below (to reduce collisional problems) — either by direct laser cooling or else by sympathetic cooling using a low mass laser-cooled atom (eg. Li) in the same trap. Observation of a fermi gas is more likely. Superfluorescence studies on trapped atoms appear feasible, and desirable, as do cavity QED experiments, possibly with single atoms.

In conclusion we return to the opening question: will atom traps produce as much good science as charged particle traps? Obviously it is too early to answer this definitively; only four years have passed since the demonstration of the first atom trap. But comparison of the current status of atom trapping with the status of ion trapping in 1940, (four years after the demonstration of the Penning trap (PEN36)) or even in 1963 (four years after the demonstration of the rf ion trap (FIS59)) provides a strong basis for optimistic projections.

ACKNOWLEDGEMENTS

Work in our lab on atom trapping has been supported by the ONR and the AFOSR through grant #N00013-83-K-0695 and seminal early support was provided by the Joint Services Electronics Program (grant DAAL03-86-K-0002). Major equipment was provided by a DOD instrumentation grant. Trapping experiments described here were carried out with many gratefully acknowledged valuable contributions from R. Ahmad-Bitar, V. Bagnato, G. Lafyatis, E. Raab, Ke-Xun Sun and R. Stoner.

REFERENCES

AAK88 A. Aspect, E. Arimondo, R. Kaiser, N. Vansteenkiste and C. Cohen-Tannoudji, Phys. Rev. Lett. 61, 826 (1988), see also the proceedings of this conference.

ASG83 A. Ashkin and J.P. Gordon, Opt. Lett. 8, 511 (1983).

ASH78 A. Ashkin, Phys. Rev. Lett. 40, 729 (1978).

BEM87 T. Bergeman, Gidon Erez and Harold J. Metcalf, Phys. Rev. A 35, 1535 (1987).

BLM87 V.S. Bagnato, G.P. Lafyatis, A.G. Martin, E.L. Raab, R.N. Ahmad-Bitar and D. E. Pritchard, Phys. Rev. Lett. 58, 2194 (1987).

BPK87 Vanderlei Bagnato, David E. Pritchard and Daniel Kleppner, Phys. Rev. A 35, 4354 (1987).

CBA86 Steven Chu, J.E. Bjorkholm, A. Ashkin and A. Cable, Phys. Rev. Lett. 57, 314 (1986).

CHB85 Steven Chu, Leo Hollberg, John E. Bjorkholm, Alex Cable and Arthur Ashkin, Phys. Rev. Lett. 55, 48 (1985).

CWS89 Steven Chu, D.S. Weiss, Y. Shevy and P.J. Ungar, post-deadline paper ICAP.

DAL89 J. Dalibard, see the proceedings of this conference.

DIC54 R.H. Dicke, Phys. Rev. 93, 99 (1954).

EBH84 W. Ertmer, R. Blatt, J.L. Hall and M. Zhu, Prog. Quantum Electron. 8, 248 (1984).

EBH85 W. Ertmer, R. Blatt, J.L. Hall and M. Zhu, Phys. Rev. Lett. 54, 996 (1985).

FIS59 E. Fischer, Z. fur Physik 56, 1 (1959).

GAP89 A. Gallahger and D.E. Pritchard, to be published.

GFH86 G. Gabrielse, X. Fei, K. Helmerson, S.L. Rolston, R. Tjoelker, T.A. Trainor, H. Kalinowsky, J. Haas and W. Kells, Phys. Rev. Lett. 57, 2504 (1986).

GLJ88 P.L. Gould, P.D. Lett, P.S. Julienne, W.D. Phillips, H.R. Thorsheim and J. Weiner, Phys. Rev. Lett. 60, 788 (1988), see also the proceedings of this conference.

HAS75 T. Hänsch and A. Schawlow, Opt. Commun. 13, 68 (1975).

HEE63 C.V. Heer, Rev. Sci. Instrum. 34, 532 (1963).

HES86 Harald F. Hess, Phys. Rev. B 34, 3476 (1986).

HKD87 Harald F. Hess, Greg P. Kochanski, John M. Doyle, Naoto Masuhara, Daniel Kleppner and Thomas J. Greytak, Phys. Rev. Lett. 59, 672 (1987).

JUL88 Paul S. Julienne, Phys. Rev. Lett. 61, 698 (1988).

KPT78 K.J. Kugler, W. Paul and U. Trinks, Phys. Lett. 72B, 422 (1978).

KVS81 Yu. Kagan, I.A. Vartanyants and G.V. Shlyapnikov, Zh. Eksp. & Teor. Fiz. (USSR) 81, 1113 (1981).

KVS87 J.M.V.A. Koelman, H.T.C. Stoof, B.J. Verhaar and J.T.M. Walraven, Phys. Rev. Lett. 59, 676 (1987).

LEM80 V.S. Letokhov and V.G. Minogin, Opt. Commun. 35, 199 (1980).

LSV86 A. Lagendijk, I.F. Silvera and B.J. ver Haar, Phys. Rev. B 33, 626 (1986).

LWW88 Paul D. Lett, Richard N. Watts, Christoph I. Westbrook, William D. Phillips, Phillip L. Gould and Harold J. Metcalf, Phys. Rev. Lett. 61, 169 (1988).

MDS88 N. Masuhara, J.M. Doyle, J.C. Sandberg, D. Kleppner, T.J. Greytak, H.F. Hess and G.P. Kochanski, Phys. Rev. Lett. 61, 935 (1988).

MHB88 A.G. Martin, K. Helmerson, V.S. Bagnato, G.P. Lafyatis and D.E. Pritchard, Phys. Rev. Lett. 61, 2431 (1988).

MIJ82 V.G. Minogin and J. Javanainen, Opt. Comm. 43, 119 (1982).

MIN82 V.G. Minogin, Kvant. Electron. (Moscow) 9, 505 (1982) [Sov. J. Quantum Electron. 12, 299 (1982)].

MPP85 Alan L. Migdall, John V. Prodan, William D. Phillips, Thomas H. Bergeman and Harold J. Metcalf, Phys. Rev. Lett. 54, 2596 (1985).

PCB88 M. Prentiss, A. Cable, J.E. Bjorkholm, Steven Chu, E.L. Raab and D.E. Pritchard, Opt. Lett. 13, 452 (1988).

PEN36 F.M. Penning, Physica 3, 873 (1936).

PHB87 D.E. Pritchard, K. Helmerson, V.S. Bagnato, G.P. Lafyatis and A.G. Martin, in Laser Spectroscopy VIII, w. Persson and S. Svanberg eds. (Springer, Berlin, 1987).

PMP85 John Prodan, Alan Migdall, William D. Phillips, Ivan So, Harold Metcalf and Jean Dalibard, Phys. Rev. Lett. 54, 992 (1985).

PRB86 D.E. Pritchard, E.L. Raab, V.S. Bagnato, C.E. Wieman and R.N. Watts, Phys. Rev. Lett. 57, 310 (1986).

PRI83 David E. Pritchard, Phys. Rev. Lett. 51, 1336 (1983).

PRI86 David E. Pritchard, in Electronic and Atomic Collisions, D.C. Lorents, W.E. Meyerhof, J.R. Peterson, editors (Elsevier, B.V., 1986).

RPC87 E.L. Raab, M. Prentiss, Alex Cable, Steven Chu and D.E. Pritchard, Phys. Rev. Lett. 59, 2631 (1987).

SGV88 H.T.C. Stoof, L.P.H. de Goey and B.J. ver Haar, private communication.

SST89 Fujio Shimizu, Kazuko Shimizu, and Hiroshi Takuma, in preparation.

STE86 Stig Stenholm, Rev. Mod. Phys. 58, 699 (1986).

SVP78 W. Stwalley, Y.H. Vang and G. Pichler, Phys. Rev. Lett. 41, 1164 (1978).

SWU89 Y. Shevy, D.S. Weiss, P.J. Ungar and Steven Chu, submitted to PRL.

SWW89 David Sesko, Thad Walker and Carl Wieman, private communication.

TOM86 T. Tommila, Europhys. Lett. 2(10), 789 (1986).

VBJ88 R. van Roijen, J.J. Berkhout, S. Jaakkola and J.T.M. Walraven, Phys. Rev. Lett. 61, 931 (1988).

WIN85 W.H. Wing, Prog. Quantum Electron. 8, 181 (1985).

Proceedings of the Eighth International Conference, Åre, Sweden, June 22-26, 1987.

Optical Pumping in Translation Space

D.E. Pritchard, K. Helmerson, V.S. Bagnato, G.P. Lafyatis, and A.G. Martin

Department of Physics and Research Laboratory of Electronics, Massachusetts Institute of Technology, Cambridge, MA 02139, USA

Introduction

Perhaps the broadest overall trend in the art of experimental atomic spectroscopy has been the steady development of techniques to obtain more control of the atoms under study. After the discharge was replaced by the molecular beam to improve the control over the translational degrees of freedom, the Stern-Gerlach magnet was developed to select the internal degrees of freedom. This led immediately to the demonstration that the internal degrees of freedom were discretely quantized, and eventually to the discovery of resonance techniques. In the context of this discussion resonance may be viewed as a tool to change the internal quantum state. The development of the separated oscillatory field method opened (prematurely) the field of coherent spectroscopy, which allows, in principle, the preparation of any coherent superposition of the internal states. In addition, the coherences between internal states of different atoms may depend on the atom's spatial coordinate or velocity.

Although we can prepare the internal state as desired (and indeed are learning to slow the ravages of spontaneous decay which destroy our handiwork), we are just beginning to develop techniques to achieve comparable control of the translational degree of freedom of atoms. This explains the great amount of interest in slowing, cooling, and trapping atoms — all techniques to master the translation. In spite of this interest, only one good method has so far been demonstrated — Doppler cooling. This has been applied to both atoms and ions where milli-Kelvin temperatures have been achieved. This closely approaches the theoretical limit of Doppler cooling, $k_B T_l = 1/2\,\hbar\,\Gamma$, for strong transitions with $\Gamma \sim 10$MHz. We can anticipate significant improvement when weaker transitions are used (this requires greater than current commercial dye laser stability). Unfortunately, T_l cannot be reduced arbitrarily by the use of increasingly narrow transitions: the finite momentum imparted in the last cycle of velocity selective absorption and subsequent spontaneous decay limits the temperature and velocity to the so-called recoil limit:

$$k_B T_r = E_r = (\hbar k)^2/m \,, \qquad (1)$$

$$v_r = \hbar k/m \,.$$

This paper explores the application of optical pumping techniques to cool the translational degrees of freedom below the recoil limit. The key idea is simple: since the final spontaneous decay of the cooling cycle has a random direction, there is a finite probability for the atom to decay to a translational state whose energy is less than $\varepsilon^2 E_r$, where ε is less than unity. If there exists a mechanism which can selectively recycle

only those atoms with translational energy above $\varepsilon^2 E_r$, those may decay inside $\varepsilon^2 E_r$ on a subsequent recycling. Thus after many cycles a large fraction of the atoms will have been cooled below $\varepsilon^2 E_r$. In the following sections we shall discuss this idea more fully, derive the limits imposed by imperfections in the selectivity of the excitation, discuss solutions to the problems of systematic heating due to the repeated cycling, and give results from a computer simulation of one example of this general idea, velocity space optical pumping.

Translation Optical Pumping of Trapped Particles

Consider the case of an atom in a trap. We consider first the cooling mechanism called cyclic cooling [1], then show how this may be altered to cool below the recoil limit using translation state optical pumping. The translational degree of freedom is now quantized, as shown in Fig. 1; atoms in internal states U or L move in different potentials each with its own set of translational states. These states are densely packed, and we will have to introduce the density of states $\rho(E)$ later on. Imagine that the system starts in eigenstate $U,1$. An RF transition to internal state L provides an extremely energy selective excitation to eigenstate state $L,1'$. Let us assume that optical excitation followed by spontaneous decay now provides optical pumping back into U and a translational state in the vicinity of 2. The uncertainty results from the uncertainty of the momentum transfer in the optical pumping cycle, and is reflected in the spectrum of the fluorescence. Note that the spontaneous decay is *essential* in order to make the system cycle in the desired direction; more fundamentally it is the mechanism which removes entropy from the system and permits real cooling. The scheme described above obviously lowers the translational energy of atoms in internal state U. If the frequency of the RF is lowered slowly, atoms near translational state 2 will come into resonance and will be lowered further in translational energy [1].

A limit for this cooling process is reached as the RF frequency approaches the transition frequency at the bottom of the well. There the recoil energy becomes comparable to the amount of energy removed in the cycle and the atoms returning to state 2 after a cooling cycle are sometimes hotter than when they started!

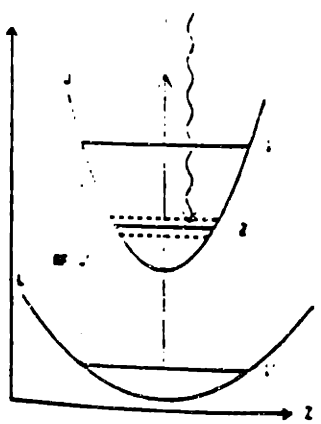

Fig. 1. Schematic diagram of translation space optical pumping mechanism. (Note: optically excited state not shown.)

The idea of optical pumping in translation space is now implemented by the following procedure. If the RF transition frequency is lowered only to a limit just above the transition frequency at the well bottom, atoms with energies very close to the well bottom (we call this region of phase space the *target zone)* will never come into resonance and will not be cycled (and possibly heated by the recoil). If the RF is repeatedly swept down to this limit, additional atoms will decay into the target zone so that they will not be excited again by subsequent sweeps. By repeating the sweep enough times, an arbitrarily high fraction of the atoms may be accumulated in the target zone, whose maximum energy is $\varepsilon^2 E_r$ with $\varepsilon < 1$.

Limit to pumped fraction due to finite resolution

In the preceding section we ignored the fact that the RF transition must have a finite linewidth with Lorentzian wings. Therefore atoms pumped into the target zone may possibly be excited again by the wings of this line and removed from the target zone by the recoil, even though the RF is never again in exact resonance with them. Consequently it will not be possible to pump all of the atoms into the target zone, but only that fraction for which the removal rate due to line wing excitation less than or equal to the optical pumping rate. We now calculate this fraction as a fraction of the limiting energy of the target zone, $\varepsilon^2 E_r$. This, in turn, determines the fraction which can be optically pumped into the target zone as a function of the size of this zone.

If we denote the fraction of atoms in the target zone by f_o, then

$$\frac{df_o}{dt} = + \text{ optical pumping flux in} - \text{off-resonant excitation out} . \qquad (2)$$

If the excitation rate is R for resonant atoms and $R(\Gamma/\delta)^2$ for off-resonant atoms where δ is the detuning from resonance, then we approximate the rate out as the off-resonant rate for atoms with zero energy when the excitation frequency is at its lowest (where $\delta = \varepsilon k v_r$, assuming the Doppler shift dominates the shift due to the trapping potential). The rate out is then $f_o R(\Gamma/\varepsilon k v_r)^2$ ignoring the small fraction of off-resonantly excited atoms which happen to decay back inside the target zone.

In order to calculate the optical pumping flux in we need to know the integral of the density of states

$$P(E) = \int_0^E \rho(E)dE .$$

If we assume that the atoms excited resonantly have initial energy $-E_r$, then the excitation rate per atom is $R(\hbar\Gamma/E_r)$, because only a bandwidth Γ is excited. Assuming that the spontaneous decay distributes them evenly in phase space, a fraction $P(\varepsilon^2 E_r)/P(E_r)$ will decay into the target zone and Eq. (2) becomes

$$\frac{df_o}{dt} = (1-f_o) R(\frac{\hbar\Gamma}{E_r}) \frac{P(\varepsilon^2 E_r)}{P(E_r)} - f_o R(\frac{\Gamma}{\varepsilon k v_r})^2 .$$

At equilibrium $df_o/dt = 0$ and this equation becomes (taking $P(E) \propto E^n$)

$$0 = R\left[(1-f_o)\frac{\pi\Gamma\varepsilon^{2n}}{E_r} - f_o\left(\frac{\Gamma}{\varepsilon k v_r}\right)^2\right].$$

Thus if it is desired to cool a fraction f_o of the atoms, they can be cooled to

$$E_{limit} = \varepsilon^2 E_r = \left[\left(\frac{f_o}{1-f_o}\right)\left(\frac{\Gamma}{k v_r}\right)\right]^{\frac{1}{n+1}} E_r .$$

For a three-dimensional harmonic potential $n = 3$, hence if the R.F. transition width is 10^5 times less than the Doppler shift due to the recoil velocity (i.e. $\Gamma/k v_r = 10^{-5}$), then 90% of the atoms can be pumped to $E_{limit} = 0.1\ E_r$. This is rather disappointing considering such good selectivity, but it nevertheless represents a substantial improvement over the recoil limit.

Velocity Space Optical Pumping

Velocity space optical pumping is another example of phase space optical pumping. It would be appropriate for particles confined to a trap with very steep walls. It is more favorable than harmonically confined atoms since the phase space exponent is only $n = 3/2$. (so that E_{limit} would be 0.02 E_r in the example above).

We have run a computer simulation of a velocity space optical pumping. Our objective was to study a simple version of the above scheme in which there were two discrete pumping frequencies rather than a continuous sweep. (It can be shown that a single frequency which excites particles inside the recoil velocity will heat the atoms; two frequencies therefore appears to be the simplest workable scheme.) Since our

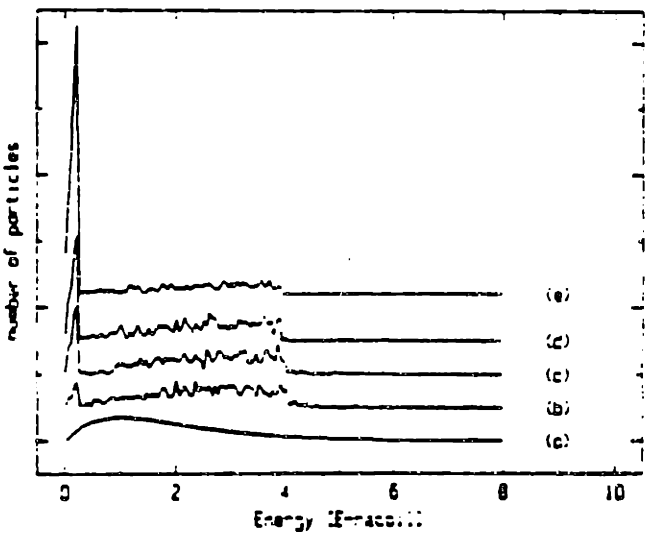

Fig. 2. Plots of energy distribution of atoms undergoing velocity space optical pumping. (Lasers tuned to 0.5 v_r and 2.0 v_r with widths 0.1 v_r and 1.0 v_r and relative intensity 1:10.) (a) Original distribution. After (b) 3,100, (c) 15,600, (d) 24,700, (e) 66,200 laser excitations.

objective was to verify that a two frequency scheme could work, as well as to study the rate of accumulation of atoms in the target zone. we did not use Lorentzian excitation functions, but rather square profile functions. This should not affect the overall feasibility or the initial accumulation rate — only the ultimate fraction (as calculated above). Figure 2 shows the results of the computer simulation where a laser tuned to 0.5 v_r is used to pump atoms into the region of energy less than 0.25 E_r, while a second laser at 2.0 v_r rescues those atoms heated by the first laser and cools them to the recoil limit.

Note. This material was not presented in the talk at EICOLS, which covered material reported in [2] and [1] on the magnetic atom trapping experiment at M.I.T.

References

[1] D.E. Pritchard, Phys. Rev. Lett. 51, 1336 (1983).
[2] V.S. Bagnato, G.P. Lafyatis, A.G. Martin E.R. Raab, R.N. Ahmad-Bitar and D.E. Pritchard, Phys. Rev. Lett. 58, 2194 (1987).

Radiative Decay of Densely Confined Atoms

K. Helmerson, M. Xiao and D. Pritchard
Massachusetts Institute of Technology
Department of Physics/Research Laboratory of Electronics
Cambridge, MA 02139
(617)253-6812

Abstract

When an excited atom decays in a region of densely confined atoms, the spontaneous radiation may be significantly altered. For bosons, the rate is increased and the radiation is blueshifted leading to cooling, fermions behave oppositely.

Radiative Decay of Densely Confined Atoms

K. Helmerson, M. Xiao and D. Pritchard
Massachusetts Institute of Technology
Department of Physics/Research Laboratory of Electronics
Cambridge, MA 02139
(617)253-6812

The decay rate of an excited state atom into a ground state atom and a photon of momentum k depends on the photon mode structure [1,2] and also on the number of photons present in those modes [3]. We consider the extent to which the rate of spontaneous emission may be altered by the mode structure of the atom (caused eg. by a trap), and in particular by the presence of other ground state atoms in the modes. We predict that this rate is enchanced in the presence of occupied atom modes for boson atoms and strongly suppressed for fermi atoms.

For a system of densely confined atoms, we must necessarily use a multiparticle atomic wavefunction that is symmetric for bosons and antisymmetric for fermions. Such wavefunctions, together with the Golden Rule, result in a decay rate for an excited state atom in mode ϕ_i of the trap

$$\Gamma_i = \frac{2\pi}{\hbar} |\langle \psi_{A^*} | \hat{\varepsilon}^* \cdot \vec{er} | \psi_A \rangle|^2 \sum_j (1 \pm N_j) \rho(\hbar c k_{ij}) |\langle \phi_j(\vec{R}) | e^{i\vec{k}\vec{R}} | \phi_i(\vec{R}) \rangle|^2,$$

where the sum is over all ground state modes, N_j is the initial number of atoms in ground state mode j, and the positive and negative signs in the sum correspond to bosons and fermions, respectively. $\rho(\hbar c k_{ij})$ is the density of radiation field modes at momentum $\hbar k_{ij}$, and the first matrix element is the electronic dipole matrix element.

Radiative Decay of Densely Confined Atoms

K. Helmerson, M. Xiao and D. Pritchard

In general, the $e^{i\vec{k}\cdot\vec{R}}$ term in the trap matrix element, M_{ij}, strongly couples only those trap states differing in momentum by roughly $\hbar k_{ij}$. [4] Thus, if the excited state is the zero state ($i = 0$), then M_{0j} will be big only where j corresponds to a trap state with energy roughly equal to the recoil energy.

To estimate the amount of suppression or enhancement of the radiative decay rate, we consider atoms confined in a spherically symmetric, harmonic potential. The energy levels in such a trap are given by $E_n = \hbar\omega_t(n+3/2)$ where ω_t is the trap oscillation frequency; the degenerancy of level n is $g_n = 1/2(n+1)(n+2)$. The fermi energy is $E_f = \hbar\omega_t(6N)^{1/3}$ where N is the total number of atoms ($N \gg 1$) (with $\omega_t/2\pi = 100$ Hz and $N = 10^9$, $E_f = 8.7\,\mu K$).

For lithium atoms (^6Li) cooled to on the order of their recoil energy ($E_{recoil} = 2.8\,\mu K$) a reasonably degenerate fermi gas results. Since the trap matrix element favors transitions between trap states that differ in energy by roughly the recoil energy, absorption followed by spontaneous emission will most often place the atom in a state with energy well within $2E_{recoil}$ of the initial state. Since $2E_{recoil}$ is less than E_f, we expect that most atoms excited from within the fermi sea will want to decay back within it, leading to suppression of the decay rate by a factor of order E_f/E_{recoil}. There will also be a red shift of the spontaneous emission relative to the excitation light, which may heat the atoms. Of course, the narrowing of the linewidth makes Doppler cooling a correspondingly more powerful cooling mechanism.

Radiative Decay of Densely Confined Atoms

K. Helmerson, M. Xiao and D. Pritchard

A densely confined system of Bose atoms (eg ^{7}Li) will experience an increase in the spontaneous emission rate of comparable magnitude when $k_B T \approx E_f$. As the temperature of Bose condensation is approached, the population of the lowest trap states becomes substantial ($\sim N^{1/3}$), and the spontaneous emission will therefore be shifted to the blue. This represents a new cooling mechanism. This work is supported by ONR Contract No. N00014-90-J-1642.

[1] E.M. Purcell, Phys. Rev. 69, 681 (1946).

[2] D. Kleppner, Phys. Rev. Lett. 47, 233 (1981).

[3] A. Einstein, Phys. Zeits. 18, 121 (1917).

[4] D.J. Wineland and W.M. Itano, Phys. Rev. A 20, 1521 (1979).

rf Spectroscopy of Trapped Neutral Atoms

A. G. Martin, K. Helmerson, V. S. Bagnato,[a] G. P. Lafyatis,[b] and D. E. Pritchard
Department of Physics and Research Laboratory of Electronics, Massachusetts Institute of Technology, Cambridge, Massachusetts 02139
(Received 17 February 1988)

We report the first observation of rf-induced transitions of trapped neutral atoms. An rf resonance curve for a sample of trapped Na atoms has been obtained by measuring the relative population of two trapped magnetic substates as a function of applied rf frequency. The shape of the resonance curve has been used to determine the energy distribution of the trapped atoms.

PACS numbers: 32.80.Pj

Recent progress in the field of neutral-atom trapping has been very rapid; in the last year three new traps have been developed with orders of magnitude improvements in the number of trapped atoms and confinement times.[1-4] At present, the emphasis is on applying the traps to new scientific measurements, such as the study of ultracold collisions,[4,5] and developing new techniques to monitor and/or manipulate the trapped atoms. This paper reports the first demonstration of rf-induced transitions and rf spectroscopy of a sample of trapped neutral atoms. rf spectroscopy is an important development for neutral-atom traps because it not only provides a powerful high-resolution probe of trap conditions, but also may be used to manipulate the atoms, and may ultimately lead to high-resolution spectroscopy. Our present experiments demonstrate the use of rf transitions to measure the energy distribution of a sample of trapped atoms; this can lead to interesting applications, such as the identification of a Bose condensate, which would have a very narrow spike in its rf spectrum. We also demonstrate the use of rf transitions to selectively change the magnetic-sublevel population of the trapped atoms; in this context its use has been proposed as part of a "cyclic" cooling scheme[6] which may permit cooling of the trapped atoms to μK temperatures.

In our present experiments, we have applied resonant rf pulses to samples of trapped neutral Na atoms confined in a magnetic trap. We have been able to populate all four of the trapped magnetic substates, and have obtained a resonance curve for one of the rf transitions by measuring the relative populations of the initial and final magnetic substates using laser-induced fluorescence. Modeling of the trapped atoms has allowed us to reproduce the measured rf line shape and extract from it their energy distribution.

The experiments were performed on a gas of $\sim 2\times 10^{10}$ Na atoms confined in a volume of ~ 100 cm^3 by a superconducting magnetic trap.[1] The trap consists of a local, nonzero, minimum of the magnetic field in free space which confines "weak-field seeking" atoms, i.e., atoms in a state whose energy increases with magnetic field. For Na in its ground state there are four trapped levels: $|F=2,M=2,1,0,-1>$ (which adiabatically join the $F=2$ hyperfine multiplet as the magnetic field approaches zero, see Fig. 1). dE/dB, and therefore the trapping potentials, are the same for the four trapped states to within $\sim 5\%$ for the range of magnetic fields used in this trap. Atoms in the other four levels of the ground-state manifold are repelled from the field minimum and expelled from the trap.

The minimum of the magnetic field (~ 1500 G) is produced between two "pinch" coils in the trap's longitudinal (vertical) direction, and by a superposed octupole field in the radial (horizontal) direction. The trapped atoms experience a confining potential with a predominantly r^6 radial dependence, and an axial dependence which is approximately quadratic at the minimum of the trap. The trap depth is limited radially to ~ 600 G (~ 60 mK for Na) where the octupole field meets the trap enclosure. The radial octupole field and the small radial component of the pinch field combine to give an

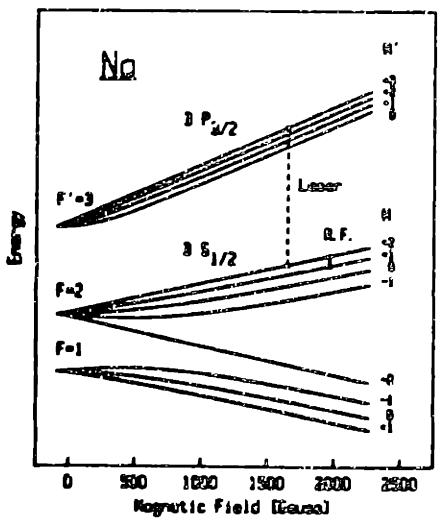

FIG. 1. Relevant energy levels of Na $3^2S_{1/2}$ and $3^2P_{3/2}$ in a magnetic field (not to scale).

off-axis annular trap minimum which is ~8 G lower than the field at the center.[7] Low-order multipole "contaminants" in the radial field will further split this into several small local minima of a few gauss, and produce "lumpy" equipotentials. The atoms follow complex trajectories within the trap, with oscillation frequencies in the $\geq$ 10-Hz range, with mixing of the radial and axial motions on the $\gtrsim$ 1-sec time scale (i.e., angular momentum is not conserved on this time scale).

An ~40-cm-long, shorted, two-wire transmission line, ~0.3 cm from the wall of the trap, was used to produce an oscillating rf magnetic field. The rf signal was generated by a Fluke model 6060A frequency synthesizer followed by a 3-W rf amplifier, and fed to the transmission line via a coaxial cable. At this power level, the rf magnetic field in the trap region was ~10 mG, inducing magnetic dipole transitions amongst the trapped magnetic substates with a Rabi frequency $\Omega_R/2\pi$ of ~2 kHz.

The trap is loaded from a thermal atomic beam of sodium with use of lasers to slow and cool the atoms (see Ref. 1). After the loading of a sample of atoms into the trap, the loading lasers and atomic beam are blocked, and measurements are performed on the isolated, trapped atoms. A typical fluorescence spectrum for trapped atoms near the field minimum is shown in Fig. 2, scan *a*. The fluorescence was induced by a weak probe laser beam (~1 μW/cm^2 and 1 cm in diameter) and monitored with use of a 2.5-cm-long photodiode placed on the wall of the trap enclosure. The trap loading process leaves the atoms in the $|F=2,M=2\rangle$ magnetic substate,[1] and hence only one peak is observed, corresponding to the $|F=2,M=2\rangle \rightarrow |F'=3,M'=3\rangle$ transition (which must decay back to the $|F=2,M=2\rangle$ state to conserve angular momentum).

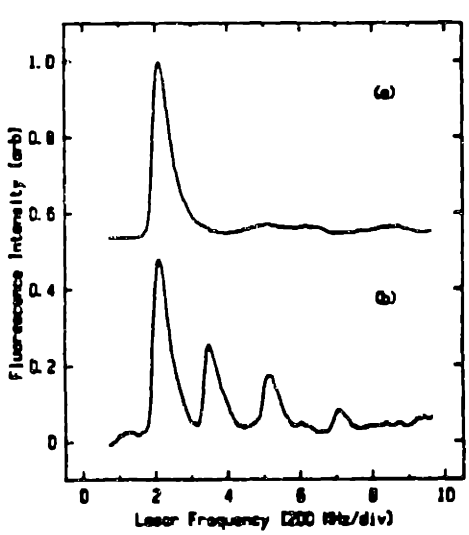

FIG. 2. Fluorescence spectrum for trapped Na atoms induced by a weak circularly polarized probe laser beam. Scan *a*, before the application of the rf pulses, with all the atoms in the $|F=2,M=2\rangle$ state; scan *b*, after the rf pulses, showing population in all four trapped magnetic substates, $|F=2,M=2,1,0,-1\rangle$.

rf transitions transfer populations between the four trapped magnetic substates $|F=2,M=2,1,0,-1\rangle$ (see Fig. 1), which have fluorescence peaks at different laser frequencies. Figure 2, scan *b* shows a fluorescence spectrum after repeated application of rf pulses at 330, 378, 455 MHz. These frequencies correspond to the three possible $\Delta M=\pm 1$ magnetic dipole transitions among the four trapped substates at the minimum magnetic field in the trap. These frequencies are the most effective for transferring population, as all the trapped atoms, regardless of their total energy, eventually pass close to the field minimum during their motion in the trap. The applied rf pulses were of sufficient power ($\Omega_R/2\pi$ ~2 kHz) and duration (~5 sec) to ensure that the populations of the four magnetic substates were approximately equalized. [The difference in the four peak heights in Fig. 2(b) is mainly due to optical pumping by the circularly polarized probe laser and disappears at low enough laser power. The branching ratios for decay of the various excited states determine the number of times each atom can be cycled, and therefore the height of the peak.]

An rf resonance curve (Fig 3) for a sample of trapped atoms for the $|F=2,M=2\rangle$ to $|F=2,M=1\rangle$ transition was obtained by inducing rf transitions, and subsequently measuring the relative peak heights for the two states in the fluorescence spectrum as a function of the frequency of the applied rf pulse. As the energy difference between the two levels increases monotonically with magnetic field [$d(E/h)/dB$ ~60 kHz/G], the rf frequency is resonant only with atoms at one value of the magnetic field. At low rf frequencies, no transitions are induced, since no trapped atoms can be in a magnetic field below the trap minimum (B_{min}=1520 G). The sharp rise of the curve at ~328.5 MHz corresponds to atoms at the trap minimum. As the frequency is further increased, the rf resonates with atoms at higher magnetic fields; since it will never resonate with atoms whose total energy is insufficient to allow them to reach this value of the field, the height of the curve decreases monotonically at higher fields. At approximately 360 MHz the lowest edge of the trap is reached (~2300 G); nearly all atoms energetic enough to reach this value of the field escape from the trap within the time scale of these measurements (tens of seconds), and so the signal is essentially zero above this value.[8]

The applied rf pulses were of sufficient power and duration [number of Rabi flops: (5 sec) $\times \Omega_R/2\pi \sim 1 \times 10^6$] so that equilibrium was reached in the transfer of population between the two states. At the peak of the resonance curve, a reduction in rf application time by a factor of 5 resulted in only a ~5% decrease in the ratio of the measured peak heights. Our calculations indicate

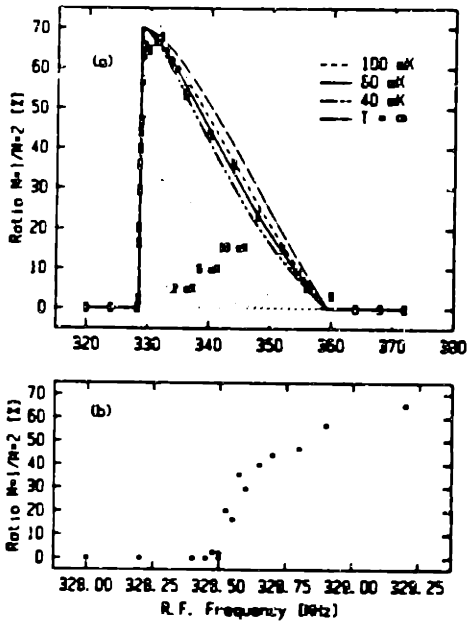

FIG. 3. rf resonance line shape (points) for the $|F=2,M=2>$ to $|F=2,M=1>$ transition. The calculated line shapes (curves) allow us to estimate the temperature of the trapped atoms to be 60^{+30}_{-20} mK. A $T=\infty$ curve is also included for comparison. The calculations for 2, 5, and 10 mK show the greatly increased sensitivity to temperature for colder samples. The sharp rise at 328.5 MHz, expanded in (b), corresponds to atoms at the minimum magnetic field of the trap (error bars are about the size of the points).

that the transition was also saturated away from the trap minimum. The height of the resonance curve at each frequency is therefore determined by the fraction of atoms energetic enough to reach the corresponding magnetic field, and line shape becomes a direct measure of the energy distribution of the atoms in the trap.[9]

The rf line shape has been modeled by assuming a truncated Boltzmann distribution for the atoms in the trap (i.e., all atoms with $E > E_{escape}$ are assumed to have left the trap), and assuming saturation in the transfer of population between the two states for all atoms energetic enough to come into resonance. Figure 3(a) shows results for three different temperatures (100, 60, and 40 mK), from which we obtain an estimate of 60^{+30}_{-20} mK for the temperature of the atoms in the trap. (Some lack of saturation away from the trap minimum could lower the apparent temperature.)

As $kT \gtrsim E_{escape}$, the atoms are close to being uniformly spread over all possible states within the trap, and the energy distribution is mainly characterized by the truncation at E_{escape} [as is evident by the $T=\infty$ curve of Fig. 3(a)]. This measurement of the energy distribution is in poor agreement with our previous estimate of 4–20 mK for the temperature of the atoms,[1] which was based on a combination of relative fluorescence intensity measurements for different photodetectors in the trap, and estimates of cooling-laser detuning.[10]

The main point is that the atoms are much hotter than the usual Doppler-cooling limit[11] of ~240 μK for Doppler-cooled Na. We attribute this to heating in the transverse direction by the 10 mW/cm^2 standing-wave laser beam, detuned ~80 MHz to the red for atoms at the bottom of the trap, used to stop the atoms in the trap.[1] This beam rapidly cools the longitudinal motion of the atoms in the trap[12–14]; cooling of the transverse motion is achieved only through the coupling of the transverse and longitudinal motions of the atoms by the trap, and occurs over time scales of $\gtrsim 1$ sec.

If the intensity of the standing wave were reduced to make the transverse heating rate slow compared to the coupling rate of transverse to longitudinal motion, and the application time correspondingly extended, sample temperatures a few times the usual Doppler limit should be achievable. Figure 3(a) shows the rf line shapes that would be obtained for sample temperatures of 2, 5, and 10 mK. The rf line shape is obviously much more sensitive to temperature variations at these lower temperatures, which will make rf spectroscopy an accurate thermometer in future experiments where these lower temperatures are achieved.

A detailed scan of the rising edge of the resonance curve was performed [Fig. 3(b)], showing a width of ~250 kHz. This width may be a reflection of a lack of saturation in the process of population transfer in this region of the curve: The atoms may not have time, within the time scales of these measurements, to find the trap minimum. Other sources of broadening also exist, such as power broadening due to the rf field, and transit-time broadening due to the motion of the atoms through the resonance region. These effects could contribute ~100 kHz to the width of the edge. The magnetic field irregularities discussed earlier will also contribute to the width, and may possibly be the origin of the apparent structure in the leading edge of the curve. These field irregularities may be overcome in future experiments by the use of a quadrupole radial field in the trap.

To perform high-resolution rf spectroscopy of the trapped atoms, one must use field-independent transition points, where to first order the transition frequency is independent of magnetic field. For example, at ~1 mK the linewidth of the $|F=2,M=2> \rightarrow |F=2,M=1>$ transition at ~13.3 kG is ~20 Hz. Further cooling of the sample to μK temperatures by currently demonstrated[15] or proposed[6,16] cooling schemes would yield much narrower linewidths, making magnetic traps a promising candidate for high-resolution rf spectroscopy.

In summary, this Letter reports the first rf spectroscopy of trapped neutral atoms. All four trapped magnetic substates of a sample of trapped Na atoms have been populated, and we have obtained an rf resonance curve

by measuring the relative population of the $M=1$ and $M=2$ magnetic substates as a function of applied rf frequency. We have used the technique to determine the energy distribution of a sample of trapped atoms by fitting the measured resonance line shape with that of a model of the atoms in the trap. The demonstration of rf resonance on samples of trapped neutral atoms offers an important diagnostic on the atoms as well as a way to selectively alter their magnetic sublevels. It also opens the way for demonstration of proposed supercooling schemes,[6] which if successful, offer possibilities in high-resolution trapped-neutral-atom spectroscopy and in the study of collective effects such as Bose condensation.

We are grateful for support by the Office of Naval Research and the Air Force Office of Scientific Research through ONR Grant No. N 00014-83-K-0695. Acknowledgement is made of partial support for two of us (A.G.N. and G.P.L.) by the Donors of the Petroleum Research Fund, administered by the American Chemical Society. We gratefully acknowledge helpful conversations with H. Hess and G. Kochanski during early phases of this work.

---

[a]Present address: Instituto de Fisica e Quimica de São Carlos, Universidade São Paulo, 13560 São Carlos, São Paulo, Brazil.

[b]Present address: Department of Physics, The Ohio State University, Columbus, Ohio 43210.

[1]V. S. Bagnato, G. P. Lafyatis, A. G. Martin, E. L. Raab, R. N. Ahmad-Bitar, and D. E. Pritchard, Phys. Rev. Lett. 58, 2194 (1987).

[2]H. F. Hess, B. P. Kochanski, J. M. Doyle, N. Masuhara, D. Kleppner, and T. J. Greytak, Phys. Rev. Lett. 59, 672 (1987).

[3]E. L. Raab, M. Prentiss, A. Cable, S. Chu, and D. E. Pritchard, Phys. Rev. Lett. 59, 2631 (1987).

[4]P. L. Gould, P. D. Lett, P. S. Julienne, W. D. Phillips, H. R. Thorsheim, and J. Weiner, Phys. Rev. Lett. 60, 788 (1988).

[5]M. Prentiss, A. Cable, J. E. Bjorkholm, S. Chu, E. L. Raab, and D. E. Pritchard, Opt. Lett. 13, 452 (1988).

[6]D. E. Pritchard, Phys. Rev. Lett. 51, 1336 (1983).

[7]T. Bergeman, G. Erez, and H. J. Metcalf, Phys. Rev. A 35, 1535 (1987).

[8]Similar asymmetric line shapes, due to thermal motion, have been seen in the cyclotron-resonance curves of trapped electrons. See R. S. Van Dyck, P. B. Schwinberg, and H. G. Dehmelt, Phys. Rev. D 34, 722 (1986).

[9]Since our population ratios are measurements of atomic density in a restricted volume element of the trap over which the magnetic field varies by only ± 10 G, there is no coordinate-space density-of-states dependence, making the shape of the spectrum independent of the trap potential.

[10]The temperature of the trapped atoms seems to depend on experimental parameters such as the loading-laser detuning. We have seen temperatures as low as ~ 25 mK in other rf scans, closer to the values reported in Ref. 3, but not in the ~ 1-mK regime as reported in Science 237, 26 (1987) and D. E. Pritchard, Phys. Today 41, No. 1, 8-32 (1988). Observation of gravitational effects at the observed temperatures is precluded.

[11]D. J. Wineland and W. M. Itano, Phys. Rev. A 20, 1521 (1979).

[12]S. Chu, L. Hollberg, J. E. Bjorkholm, A. Cable, and A. Ashkin, Phys. Rev. Lett. 55, 48 (1985).

[13]D. J. Wineland, R. E. Drullinger, and F. L. Walls, Phys. Rev. Lett. 40, 1639 (1978).

[14]W. Neuhauser, M. Hohenstatt, P. Toschek, and H. Dehmelt, Phys. Rev. Lett. 41, 233 (1978).

[15]P. D. Lett, R. Watts, C. Westbrook, W. D. Phillips, P. L. Gould, and H. J. Metcalf, Phys. Rev. Lett. 61, 169 (1988).

[16]D. E. Pritchard, K. Helmerson, V. S. Bagnato, G. P. Lafyatis, and A. G. Martin, in *Laser Spectroscopy VIII*, edited by W. Persson and S. Svanberg, Springer Series in Optical Sciences Vol. 55 (Springer-Verlag, New York, 1987).

REFERENCES

BAG87 V. Bagnato, Ph. D. Thesis (1987), (unpublished).

BLM87 V. Bagnato, G. Lafyatis, A. Martin, E. Raab, R. Ahmad-Bitar and D. E. Pritchard, Phys. Rev. Lett. **58**, 2194 (1987).

BLM89 V. S. Bagnato, G. P. Lafyatis, A. Martin, K. Helmerson, J. Landry, and D. E. Pritchard, JOSA B **6**, 2171 (1989).

CBA86 S. Chu, J. Bjorkholm, A. Ashkin, and A. Cable, Phys. Rev. Lett. **57**, 314 (1986).

CPB90 A. Cable, M. Prentiss, N. P. Bigelow, Opt. Lett. **15**, 507 (1990).

CWD89 Y. Castin, H. Wallis, J. Dalibard, JOSA B **6**, 2046 (1989).

DEH90 H. Dehmelt, Rev. Mod. Phys. **62**, 525 (1990).

DSM89 J. M. Doyle, J. C. Sandberg, N. Masuhara, I. A. Yu, D. Kleppner, T. J. Greytak, JOSA B **6**, 2244 (1989).

EBH85 W. Ertmer, R. Blatt, J. L. Hall, and M. Zhu, Phys. Rev. Lett. **54**, 996 (1985).

GLJ88 P. L. Gould, P. D. Lett, P. S. Julienne, W. D. Phillips, H. R. Thorsheim, and J. Weiner, Phys. Rev. Lett. **60**, 788 (1988).

HAS75 T. Hänsch and A. Schawlow, Opt. Comm. **13**, 68 (1975).

HKD87 H. Hess, G. Kochansky, J. Doyle, N. Masuhara, D. Kleppner and T. J. Greytak, Phys. Rev. Lett. **59**, 672 (1987).

HLS89 T. W. Hijmans, O. J. Luiten, I. D. Setija, and J. T. M. Walraven, JOSA B **6**, 2235 (1989).

IBW87 W. M. Itano, J. C. Bergquist, D. J. Wineland, Science **237**, 612 (1987).

JOS89 Special issue, JOSA B **6**, No.11 (1989).

KRC89 M. A. Kasevich, E. Riis, S. Chu, R. G. DeVoe, Phys. Rev. Lett. **63**, 612 (1989).

KSS88 Y. Kagan, B. V. Svistunov, and G. V. Shlyapnikov, JETP Lett., **48**, 56 (1988).

LBB79 D. J. Larson, J. C. Berquist, J. J. Bollinger, W. M. Itano, and D. J. Wineland, Phys. Rev. Lett. **57**, 70 (1986).

MAN79 L. Mandel, J. Opt. (Paris) **10**, 51 (1979).

MDS88 N. Masuhara, J. Doyle, J. Sandberg, D. Kleppner, T. Greytak, H. Hess, and G. Kochanski, Phys. Rev. Lett. **61**, 935 (1988).

MHB88 A. Martin, K. Helmerson, V. Bagnato, G. Lafyatis, and D. E. Pritchard, Phys. Rev. Lett. **61**, 2431 (1988).

MPP85 A. Migdall, J. Prodan, W. D. Phillips, T. Bergeman and H. Metcalf, Phys. Rev. Lett. **54**, 2596 (1985).

MSR90 C. Monroe, W. Swann, H. Robinson, and C. Weiman, Phys. Rev. Lett. **65**, 1571 (1990).

PCB88 M. Prentiss, A. Cable, J. E. Bjorkholm, S. Chu, E. L. Raab, and D. E. Pritchard, Opt. Lett. **13**, 452 (1988).

PHB87 D. E. Pritchard, K. Helmerson, V. Bagnato, G. Lafyatis, and A. Martin, in *Advances in Laser Spectroscopy* VIII, W. Persson and S. Svanberg, eds. (Springer, Berlin, 1987), p.72.

PHM89 D. E. Pritchard, K. Helmerson, and A. Martin, in *Atomic Physics* XI, S. Haroche, J. C. Gay, G. Grinberg, eds. (World Scientific, Singapore, 1989), p.179.

PMP85 J. Prodan, A. Migdall, W. D. Phillips, I. So, H. Metcalf, and J. Dalibard, Phys. Rev. Lett. **54**, 992 (1985).

PRI83 D. E. Pritchard, Phys. Rev. Lett. **51**, 1336 (1983).

PRI86 D. E. Pritchard, in *Electronic and Atomic Collisions*, D. C. Lorents, W. E. Meyerhof, J. R. Peterson, editors (Elsevier, B.V., 1986).

RPC87 E. L. Raab, M. Prentiss, A. Cable, S. Chu, D. E. Pritchard, Phys. Rev. Lett. **59**, 2631 (1987).

SEW89 D. W. Sesko and C. E. Wieman, Opt. Lett. **14**, 269 (1989).

SST89 F. Shimuzu, K. Shimuzu, and H. Takuma, Phys. Rev. A **39**, 2758 (1989).

SWM89 D. Sesko, T. Walker, C. Monroe, A. Gallagher, and C. Weiman, Phys. Rev. Lett. **63**, 961 (1989).

WID75 D. Wineland and H. Dehmelt, Bull. Am. Phys. Soc. **20**, 673 (1975).

WII79 D. Wineland and W. Itano, Phys. Rev. A **20**, 1521 (1979).

WII87 D. Wineland and W. Itano, Physics Today, 2 (June 1987).

WIN85 W. Wing, Prog. Quantum Electron. **8**, 181 (1985).

WSW90 T. Walker, D. Sesko, and C. Weiman, Phys. Rev. Lett. **64**, 408 (1990).

Acknowledgments

This is it, this must mean that I'm finally finished. I know I'll accidently forget to acknowledge somebody who has helped me get through graduate school so I will apologize ahead of time.

I'd like to thank my advisor, Dave Pritchard for allowing me to do research in the field of neutral atom trapping and for teaching me his style of approaching problems in physics. Although Dave may think that often I wasn't paying attention, I did learn a lot from him.

A very big "thank you" goes to Alex Martin. When I first started working in Dave's lab, Alex said (rather jokingly) that his job was to get me through graduate school. Little did I (and maybe he) realize the truth in that statement. Alex is one of those rare individuals you can truly count on. It's been a great pleasure working with Alex and I wouldn't hesitate to do it again.

I'd also like to thank others who directly and indirectly helped to make the magnetic trap a success. Those who worked on the experiment: Vanderlei Bagnato, Greg Lafyatis, Ke-Xun Sun and Min Xiao, and those who were there to lend a hand, piece of equipment, technical advice, or moral support at one time or another: Kevin Boyce, Rick Stoner, Chris Ekstrom, Michael Ioffe, David Keith, Eric Cornell, Joe Landry, Pete Magill, Brian Stewart, Scott Paine, Peter Chang, Robert Lutwak, Barbara Hughey, Tom Gentile, Chun-ho Iu, George Welch, Mike Kash, John Doyle, Jon Sandberg, Bruce Oldaker, Robert Weisskoff, Vasant Natarajan, and Wolfgang Ketterle.

Finally, I wish to thank my parents to whom I have dedicated this thesis.